ASSESSING THE INTERACTIONS BETWEEN RED SNOW ALGAE AND BLACK CARBON FROM FOREST FIRE SOOT USING A FIELD EXPERIMENT AND REMOTE SENSING METHODS IN WESTERN CANADA

by

Charlie Bourque

B.Sc., University of Northern British Columbia, 2021

THESIS SUBMITTED IN PARTIAL FULFILLMENT OF
THE REQUIREMENT FOR THE DEGREE OF
MASTER OF SCIENCE
IN
NATURAL RESOURCES AND ENVIRONMENTAL STUDIES

UNIVERSITY OF NORTHERN BRITISH COLUMBIA

June 2025

Abstract

My thesis investigates the relationship between snow algae and black carbon from forest fire aerosols. In Chapter One, I discuss the motivation and objectives of this thesis, followed by a background on the importance of glaciers in Western Canada, processes of glacier surface darkening, and a review of the ecology of snow algae and forest fire aerosols. In Chapter Two, I describe and analyze the results from a field experiment conducted on Place Glacier, in which I fertilized snow with wood ash. I observed no difference in snowmelt from the treatment, and due to a loss of data from early snowmelt on the last field visit, the wood ash impact on red snow algae growth was inconclusive. At the beginning of the field experiment, I measured snow reflectance, which I then converted to instantaneous radiative forcing. The average instantaneous radiative forcing for the snow algae at Place Glacier on June 3 was 192 ± 12 W m^{-2} with a maximum of 274 ± 16 W m^{-2}. This radiative forcing translated to a melt potential of up to 27.8 mm w.e. d^{-1}. In Chapter Three, I use remote sensing data from the Harmonized Landsat Sentinel (HLS) project and reanalysis products from MERRA-2 and ERA-5 Land to model the occurrence of red snow algae on glaciers in British Columbia and Alberta for the summer seasons of 2015 to 2023. I modelled the red snow algae using the random forest regressor and XGBoost algorithms, and used the permutation feature importance and SHAP to evaluate the variables' influence on the model output. The model explained 60% of the variance in the data and the three most important variables were longitude, black carbon and temperature. These results suggest that black carbon may promote red snow algae growth. Finally, in Chapter Four I conclude with the major findings, limitations and recommendations for future research.

Table Of Contents

List of Tables

Appendix Tables

List of Figures

Appendix Figures

Acknowledgement

1   Chapter 1: Introduction

This research sought to improve our understanding of processes of glacier surface darkening by investigating the relationship between black carbon from wildfire soot and blooms of red algae using a field experiment and remote sensing methodologies. This thesis focuses on fire emissions, which are commonly referred to by a range of terms (smoke, ash, soot, etc) and are typically made up of a complex mix of constituents, including black carbon, organic carbon, char, trace metals, and mineral dust, among others. In this thesis, an assumption is being made that black carbon is the dominant aerosol, and the most important fire emission aerosol for impacting snow cover, and therefore, for simplicity, is being used as the primary term for aerosols originating from fire

1.1 Motivations and Objectives

The formation of snow algae blooms and black carbon deposition from forest fire activity during the snowmelt season represent two processes that diminish glacier albedo. Yet, the interaction between snow algae and forest fire soot remains uncertain. My research objective was to examine the interaction between black carbon from forest fires and snow algae on glaciers in western Canada. In the following chapters, I:

A) Describe the field experiment during which I quantify the snow algae response to the application of wood ash on the mid-elevation bench of Place Glacier, British Columbia, Canada for the 2023 melt season (Chapter two);

B) Use remote sensing imaging from the Harmonized Landsat Sentinel datasets and reanalysis data from MERRA-2 and ERA5-Land to investigate the interaction between

snow algae and black carbon and produce a regional analysis of glaciers in BC and

Alberta using machine learning (Chapter 3), and;

C) Synthesize and discuss the research limitations and recommendations for future work

(Chapter 4).

1.2 Importance of glaciers

Snow and ice account for about 70% of the global storage of freshwater (Stephens et al., 2020). Loss of snow and ice cover will thus have major ramifications on accessibility to water worldwide. In western Canada, glacier mass loss has great implications for society and the ecosystem, as glacier runoff provides an integral source of freshwater to regional inhabitants (Bonsal et al., 2020a), freshwater ecosystems (Moore et al., 2009a; Schoen et al., 2017), and supply water for agriculture and hydropower purposes (Hock et al., 2019a). Glaciers deliver cold, ample flows to many streams during late summer when conditions are typically hot and dry (Bonsal et al., 2020b; Jost et al., 2012). Glacial contributions to streamflow, even for drainages with glacier cover as low as 1 or 2%, are crucial during this period (Huss, 2011; Jost et al., 2012) as they provide needed inputs of cold water. Yet, due to anthropogenic climate change, glacier extents are rapidly declining (Hugonnet et al., 2021). As glaciers shrink and lose mass, runoff contributions to streamflow are reduced (e.g. Huss, 2011; Moore et al., 2020; Stahl & Moore, 2006). For example, Anderson & Radić (2020) models predict unprecedented low streamflow for many communities established along glacier-fed rivers in Alberta as glaciers disappear.

1.3 Glacier Darkening

Since the turn of the twenty-first century, rates of glacier mass loss accelerated (Hugonnet et al., 2021). While increased global temperatures are largely responsible for accelerated mass loss, there are other factors that may explain regional variations (Cook et al., 2020). Numerical models based on increased global mean temperature project Western Canadian and US glaciers to lose 60 to 100% of their mass by 2100, supporting that glaciers are highly sensitive to temperature changes and that every degree of warming will have significant impacts on glacier mass loss (Clarke et al., 2015; Rounce et al., 2023). Recent studies also suggest that changes in glaciers' albedo – the index measuring the proportion of reflected light at the Earth's surface ranging for 0 (full absorbance) to 1 (full reflectance)– is an important factor influencing surface melt in the ablation season, along with air temperature (Box et al., 2012; Dumont et al., 2012; Skiles et al., 2018). Thus, improving our understanding of the physical processes that drive glacier darkening could provide insight into factors that could explain observed accelerated mass loss in western Canada.

The energy balance at a glacier's surface controls melt (Hock, 2005). Darker surfaces absorb more solar radiation, increasing glacier melt (Box et al., 2012). Changes in the density and snow grain size of snow and ice during melt season (Warren, 1982) and the deposition of light-absorbing particles (LAPs), such as mineral dust, black carbon, and microbial growth, darken glacial surfaces. The excess energy absorbed from solar irradiance due to surface darkening from LAPs is characterized as radiative forcing and is measured in W m^{-2}. LAPs lower the albedo in the visible wavelength, the part of the light spectrum where snow is the most reflective (Flanner et al., 2007; Benning et al., 2014; Biagio Di Mauro, 2020; Aubry-Wake et al., 2022). During the melt season, LAPs can accumulate on the snow surface if not entrained by the

melt runoff, increasing the darkening process and further decreasing the albedo. Similarly, the bare ice surface on glaciers accumulates LAPs over the year, contributing to the ongoing darkening process (Di Mauro, 2020; Flanner et al., 2007). Dust deposition on glaciers is mainly due to the aeolian transport from arid and semi-arid landscapes (Clow et al., 2016), land-use changes and from local lithology. Black carbon, the optically absorbing portion of soot, is produced by incomplete combustion of fossil and biofuels and is emitted from anthropogenic sources and forest fires (Kang et al., 2020). Finally, biological darkening is mainly caused by blooms of snow algae (*Chloromonas*, *Chlainomonas* and *Chlamydomonas* sp.) and ice algae (*Mesotaenium* and *Ancylonema* sp.) (Williamson et al., 2019).

On average, alpine glaciers albedo is 0.80 in the spring prior to the onset of melt (Marshall & Miller, 2020), and typical summer snow albedo is about 0.5 due to changes in snow grain sizes (Wiscombe & Warren, 1980). Blooms of red snow algae alone can further reduce the albedo to 0.38, increasing snowmelt by 40% (Cook et al., 2017). In Western North America, snow algae blooms are estimated to occur on 5% of the total glaciated area (Engstrom & Quarmby, 2024). Similarly, on the western margin of the Greenland Ice sheet, studies found biological darkening from ice algae to be the main albedo-reducing agent of the conspicuous dark area known as the "dark zone" (Ryan et al., 2018; Cook et al., 2020; McCutcheon et al., 2021). Meanwhile, Williamson & Menounos (2021) show that albedo for Western North American glaciers is declining due to rising temperatures and propose that this decline might also be linked to an increase in black carbon deposition from forest fires, as suggested by the change in aerosol optical depth in MODIS global aerosol product.

1.4 Life on Snow

Glaciers and perennial snow patches worldwide support microbiological life, such as algae, bacteria, and fungi (Hoham & Remias, 2020). During melt season, blooms of snow algae colour the snow surface red, green and sometimes orange. Blooms of algae have been observed on the Greenland Ice Sheet (Uetake et al., 2010; Williamson et al., 2018; Cook et al., 2020) and glaciers in Antarctica (Fujii et al., 2010; Huovinen et al., 2018; Khan et al., 2021), Europe (Remias et al., 2009; Di Mauro et al., 2020), Asia (Yoshimura et al., 2000; Takeuchi et al., 2006; Tanaka et al., 2016; Nakashima et al., 2021), Chile (Takeuchi & Kohshima, 2004) and North America (Painter et al., 2001; Takeuchi et al., 2006; Ganey et al., 2017; Hamilton & Havig, 2017; Engstrom et al., 2020).

Organisms that subsist on the cryosphere are restricted to periods when liquid water is available (Laybourn-Parry et al., 2012). Thus, algal blooms typically appear following surface melt and will remain on the surface for the duration of the ablation season (Ganey et al., 2017). Liquid water limits snow algae growth; therefore, algae bloom typically appears near the transient snow line (Jones et al., 2001; Takeuchi, 2001; Takeuchi et al., 2013). Some studies speculate that snow algal cells, during the incipient of snow melt, undergo a motile, haploid, vegetative stage that allows them to 'swim' up to the surface (Laybourn-Parry et al., 2012; Davey et al., 2019; Matsumoto et al., 2024). Using a collection of cell types from *Chlainomonas* species, Matsumoto et al. (2024) hypothesized a life cycle for snow algae (Fig. 1.1). The life cycle includes large quadriflagellate swarmers (A) in the early season that develop into large non-motile red cells (F) that will remain on the snow surface during the melt season and have the potential for asexual cell division through a protoplast exclusion process (K). The large red immobile cells then transition into spores (I) when in wet snowpacks and will settle in the

snowpack or other surface, typically at the end of the melt season. At this stage, sporangia (L, M) will develop from the spores. Pill cells (O) are then released from the sporangia and will develop as flagellated pill cells (O+) to start the life cycle again.
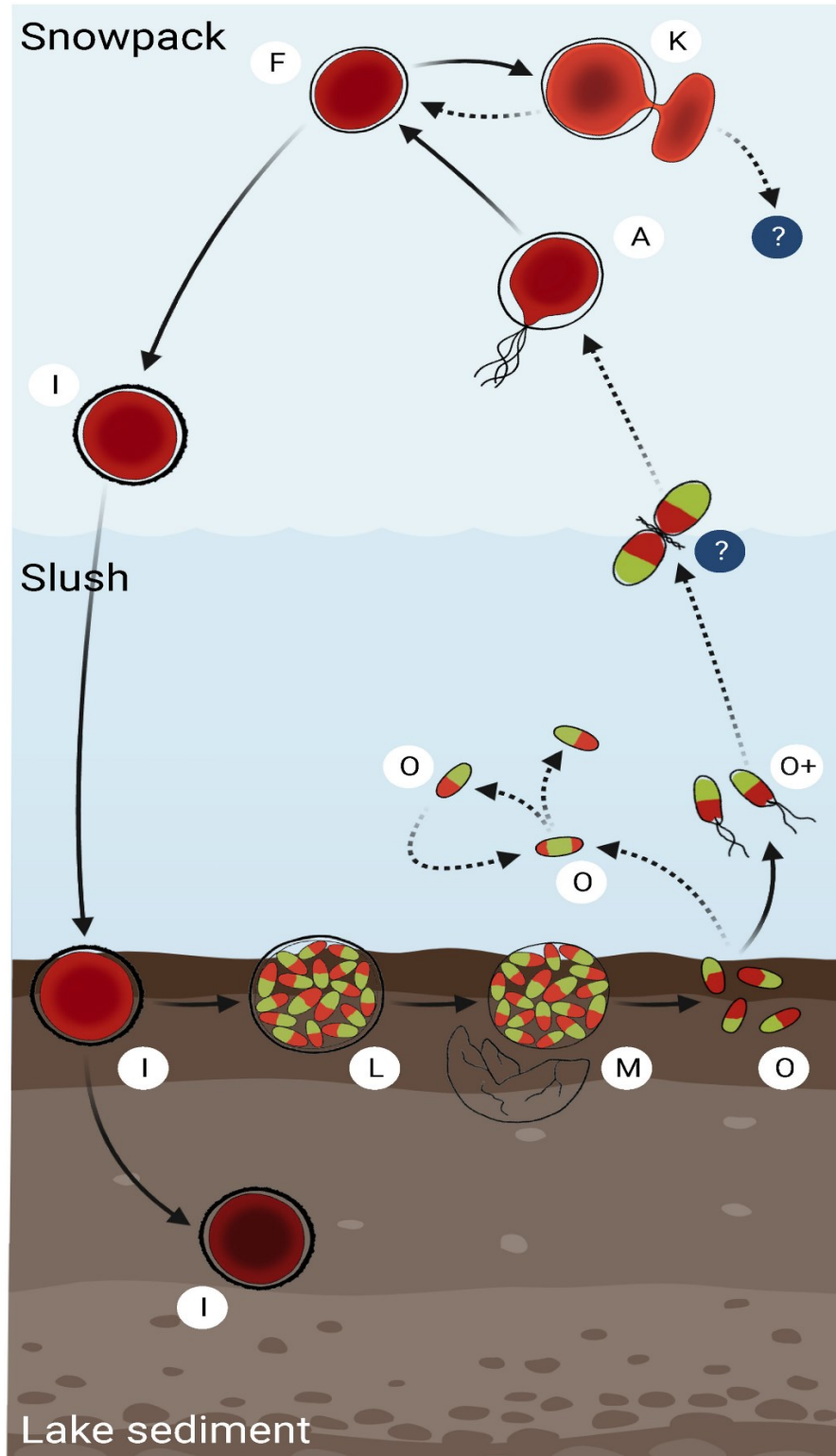
Figure 1-1: Hypothesized *Chlainomona*s sp. life cycle in Bagley Lake Habitat (Matsumoto et al., 2024). Phases denoted with a letter on a white background were observed in the field. Phases not observed in the field are denoted with a "?" on a dark background. The dotted lines represent the transition process that remains unknown.

Snow and ice surfaces present challenging conditions for life as they are subject to high levels of irradiance, low nutrients, and freezing temperatures (Laybourn-Parry et al., 2012). Organisms that live on snow and ice surfaces require many adaptations to cope with this harsh environment. Multiple snow algae species from the genera *Chlamydomonas* and *Chloromonas* produce secondary carotenoid pigment (mainly astaxanthin) that protects them against strong solar radiation, freezing temperatures and as a response to low nitrogen levels (Remias et al., 2005; Laybourn-Parry et al., 2012). The algal cells accumulate cytoplasmic secondary carotenoids around the chloroplast, which attenuates the light travelling through their internal photosynthetic apparatus and protects the cell against damage from overheating and photodamage (e.g. Bidigare et al., 1993; Leya et al. 2009). Healy & Khan (2023) analyzed the pigment composition of snow algae collected over an early and late season survey. They observed an increase in photoprotective pigment, astaxanthin, to the detriment of photosynthetic pigment such as chlorophyll α in snow algae cells in the late survey. The photoprotective pigment absorbs part of the solar radiation and dissipates it into radiant energy as heat. The added heat melts the surrounding snow and ice crystals and increases the local liquid water content, promoting algae growth (Dial et al., 2018; Williamson et al., 2020). Secondary carotenoid production also offers protection against freezing temperatures and is linked to nitrogen starvation (Bidigare et al., 1993; Remias et al., 2012). When deprived of nitrogen, the algae redirect their energy to produce nitrogen-free metabolites, such as fatty acids and secondary carotenoids. The increase of production in secondary carotenoids often parallels a decrease in cellular chlorophyll and primary carotenoids, leading to the colour change from green to red (Müller et al., 1998). The presence of unsaturated fatty acids, which can be esterified with astaxanthin, a hydroxyl member of secondary carotenoids (Leya et al., 2009), lowers the

water content in the alga cell and reduces damage from crystalline ice formation, providing protection against freezing temperatures (Bidigare et al., 1993; Dial et al., 2018).

The production of secondary carotenoids results in red pigmentation of the snow algal blooms, which darkens the snow and ice surface. Snow algae blooms have the potential to significantly reduce glacier albedo and, thus, increase melt. A study looking at snow algae blooms in all Western North America glaciated areas found that glaciers with blooms covering up to two-thirds of their surface have an estimated increase of snow meltwater of 3 cm across the entire glacier surface (Engstrom & Quarmby, 2024). On average, glacier and snow algae accounted for 9 to 13% of surface melt on the south-western edge of the Greenland Ice Sheet (Cook et al., 2020), 17% of snow melt on the Harding Icefield in Alaska (Ganey et al., 2017), and 13% of surface albedo reduction in the Arctic (Lutz et al., 2016).

A few studies measured the radiative forcing of red snow algal blooms on glaciers. They found that red snow algae's maximum instantaneous radiative forcing was 175 W m^{-2} in Alaska (Ganey et al., 2017), 185 W m^{-2} in Antarctica (Khan et al., 2021), 295 W m^{-2} in the Purcell Mountains, British Columbia (Engstrom et al., 2022), and 235.56 W m^{-2} in the North Cascade, US (Healy & Khan, 2023). The cell density was higher in the Purcells than in Alaska, with a maximum algal cross-sectional cell area of 1779 cm^2 mL^{-1} compared to ~360 cm^2 mL^{-1} (Ganey et al., 2017; Engstrom et al., 2022), suggesting that high cell density at the snow surface has greater impacts on the albedo than low cell density. In addition, higher radiative forcing from snow algae in the mid-latitudes suggests that algal blooms' influence on snowmelt is greater in the mid-latitudes compared to the high latitudes (Healy & Khan, 2023).

The parameters controlling snow algal spatial distribution and bloom intensity are poorly understood, although the presence of nutrients has been linked to increased algae growth.

Previous studies found that nitrogen limitation, among other factors, often triggers the synthesis of secondary carotenoids (Muller et al. 1998; Leya et al. 2009). On the Harding Glacier, Alaska, snow algae blooms are more predominant on the continental side of the Icefield. Researchers speculate that inputs of nutrients from terrestrial aerosols are higher on the continental than the coastal side, promoting increased growth of algae blooms on the continental side (Takeuchi et al., 2006). Likewise, experiments on red snow show that algae growth increased following the addition of nitrogen, phosphorous and potassium (NPK) fertilizer in Alaska (Ganey et al., 2017). On the Greenland Ice sheet, phosphorus-rich mineral dust from the local lithology promotes ice algae growth (McCutcheon et al., 2021). Another study suggests that algae growth increased in the presence of Fe-rich minerals (Phillips-Lander et al., 2020). Finally, photosynthetic activity on glaciers from algal blooms was linked to a decrease in nutrient concentration in the meltwater, especially nitrogen (Holland et al., 2019; Jones et al., 2001). Those studies suggest that the presence of nutrients in the snow and ice is likely to be linked with the spatial distribution of snow and ice algae.

1.5 Remote Detection of Snow Algae

Previous studies used remote sensing to map the spatial and temporal distribution of red snow algal blooms. The first detection of red snow algae from remote sensing used airborne hyperspectral images to map the algae distribution from a snowfield in the Sierra Nevada, California (Painter et al., 2001). They observed a linear relationship between the spectral reflectance depth of the chlorophyll absorption feature at 680 nm and algae abundance collected on the field. Painter et al. (2001) created a model using the integral of the scaled chlorophyll absorption feature and cell concentration from field observations and applied the model to the hyperspectral image to map snow algae. Several studies used satellite optical remote sensing

such as SPOT, Landsat and Sentinel to map the extent and duration of red snow algae blooms (e.g. Engstrom et al., 2022; Ganey et al., 2017; Takeuchi, 2013). Due to the coarse spectral resolution of the sensors, the 680 nm chlorophyll absorption feature cannot be detected by satellite. Takeuchi et al. (2006) used satellite images from SPOT-3 and targeted the broad carotenoids absorption feature at 400-600 nm to estimate the spatial distribution and abundance of red snow algae on the Harding Icefield in Alaska. They found a correlation between snow algae abundance and the reflectance ratio of the red (610-680 nm) and green (500-590 nm) SPOT satellite bands and used this ratio to estimate the distribution and abundance of algae blooms on the icefield. Similarly, Ganey et al. (2017) utilized a normalized-difference spectral index between the red and green Landsat-8 bands to target the carotenoid absorption feature to estimate algae abundance over the Harding Icefield. The advantage of normalization that ratio is that it considers varying light intensity between the different images. Others successfully used the red-green normalized difference (RGND) index to map the extent of snow algae blooms from satellite in Antarctica (Gray et al., 2020) and in British Columbia (Engstrom et al., 2022). Healy & Khan (2023) used a multispectral camera mounted on an uncrewed aerial vehicle (UAV) to map snow algae near Mt. Baker in Washington, US. They used a principal components analysis and an optimized RGND to map the abundance of snow algae under differing bloom states. They found that the RGND yields better distinction between snow and snow algae during early season, likely due to clean early snowpack being more spectrally distinct from the algae patches than aged snow filled with other impurities. A few studies pointed out that mineral dust and dirt have a similar spectral signature to snow algae when using a ratio between the red and green bands, which can potentially lead to an overestimate of algae abundance if other impurities are present in the snow (Di Mauro et al., 2015; Di Mauro et al., 2024; Huovinen et al., 2018). A new spectral

11

index between the green and blue bands was developed to distinguish mineral dust from snow algae when both are present (Di Mauro et al., 2024) and could be used to mask mineral impurities when using the RGND index.

1.6 Forest Fire & Black Carbon

Prolonged summer dry seasons and reduced moisture in vegetation due to climate change are leading to more frequent forest fires with increased duration, size and severity (Hanes et al., 2018; Westerling et al., 2006). Forest fires in 2017, 2018, 2021 and 2023 in British Columbia, exceeded the 10-year average in hectares of forest and land burned. Notably, over 2,800,000 hectares were burned in 2023 (Government of British Columbia, 2024). Forest fires release large amounts of aerosols into the atmosphere, including black carbon (Kondo et al., 2011). Through wet and dry processes, black carbon gets deposited on snow and ice surfaces, accelerating melt due to increased radiative forcing and reduced surface albedo (Flanner et al., 2007; Skiles et al., 2018). Additionally, the excess warmth released by the black carbon particles in snow increases snow grain size, further reducing the snow albedo (Hadley & Kirchstetter, 2012a). Williamson and Menounos (2021) observed that declining albedo from mountain glaciers in the last two decades in western North America correlated with increasing air temperatures and deposition of aerosols from forest fires. Similarly, in the North Cascade Mountains, Washington, USA, black carbon and dust deposition from the Big Hump forest fire in 2012 was linked to the observed increased glacier melt from that year compared to other years (Kaspari et al., 2015).

As forest fire aerosols can be transported over long distances, the impact of black carbon has regional impacts beyond the sources of emission (Kim et al., 2005). On the Greenland ice sheet, observations from shallow ice cores (Keegan et al., 2014) and snow pits (Thomas et al.,

2017) linked black carbon deposition to forest fire activity in North America. In the Himalayas, black carbon concentration reached high levels (20-25 ng mL^{-1}) in southeastern Tibetan glaciers following episodes of wildfires, increasing melt (You et al., 2016). Glaciers in New Zealand experienced unprecedented snow-darkening and melting from smoke plumes from the disastrous forest fires in Australia in 2019 – 2020 (Pu et al., 2021).

Forest fire smoke has been linked to aerosol optical depth (AOD) (Barnaba et al., 2011), providing a means for remote sensing detection of atmospheric black carbon flux. The AOD is a parameter used to determine the aerosol load distributed within a column of air in the atmosphere. In other words, it indicates how much light is blocked by aerosols in the atmosphere. Thomas et al. (2017) used the Cloud-Aerosol Lidar with Orthogonal Polarization (onboard CALIPSO) and Moderate Resolution Imaging Spectroradiometer (MODIS) Aqua instrument to detect aerosols from the forest fires while moving from Canada to Greenland, linking black carbon deposition on the Greenland Ice sheet to forest fires. Williamson and Menounos (2021) used AOD at wavelengths 550 nm to quantify forest fire-generated aerosols from the two MODIS sensors, Terra and Aqua, to assess the importance of black carbon in altering glaciers' albedo.

NASA's latest reanalysis dataset, the Modern-Era Retrospective Analysis for Research and Applications, version 2 (MERRA-2), uses the Goddard Earth Observing System, version 5 (GEOS-5), to assimilate field observation and modelled datasets to provide aerosols' surface mass concentration amongst other datasets (Randles et al., 2017). MERRA-2 assimilates bias-corrected AOD from MODIS and the Advanced Very High-Resolution Radiometer (AVHRR) instruments, and non-bias-corrected AOD retrievals from the Multiangle Imaging SpectroRadiometer (MISR) over bright surfaces and ground-based Aerosol Robotic Network

(AERONET) observations. MERRA-2 then uses the GEOS-5 radiatively coupled to the Goddard Chemistry, Aerosol, Radiation and Transport model (GOCART) to simulate five types of aerosols, including dust, sea salt, sulphate and black and organic carbon. The black carbon aerosol surface mass concentration dataset has been used to characterize the historical trends and contributing sources of black carbon in Beijing, China (Qin et al., 2019). The MERRA-2 black carbon dataset was also used to analyze the spatiotemporal variation of black carbon over Northern Eurasia during the 2016 Siberian forest fires (Sitnov et al., 2020) and to assess and quantify atmospheric black carbon contribution from forest fires in the circum-Artic in 2019 and 2020 (X. Chen et al., 2023).

1.7 Research Gap

Glaciers are critical sources of freshwater but are rapidly melting due to rising temperatures. Several studies found that a reduction in albedo from LAPs, including dust, black carbon and snow algae, accelerates melt (Di Mauro, 2020; T. H. Painter et al., 2013; Skiles et al., 2018). While the impact of LAPs has been widely studied, as presented above, the interaction among them remains poorly understood. In particular, the interaction between red snow algae and black carbon from wildfire soot has yet to be studied. The chapters below seek to address this knowledge gap through a field experiment and by leveraging remote sensing and machine learning techniques.

2 Chapter 2: Quantifying the interaction between wood ash and snow algae on Place Glacier, British Columbia

2.1 Introduction

Western Canada's glaciers are retreating at an accelerated rate (Bevington & Menounos, 2022), having consequences on the regional hydrology, ecosystem (Moore et al., 2009b), and hydroelectric power generations due to changes in runoff (Hock et al., 2019b). Air temperature and albedo - an index measuring the proportion of reflected light at the Earth's surface - largely influence glacier surface melt during the ablation season (Box et al., 2012). Albedo reduction occurs due to changes in snow and ice grain sizes (Wiscombe & Warren, 1980) and the accumulation of LAPs such as mineral dust (Di Mauro et al., 2015), black carbon (Flanner et al., 2007), and microbial growth (Healy & Khan, 2023). Many studies investigated the impact of red snow (e.g. Engstrom et al., 2022), mineral dust (e.g. Di Mauro et al., 2015), black carbon (e.g. (Flanner et al., 2007; Hadley & Kirchstetter, 2012b) and the combination of dust and black carbon (e.g. Nagorski et al., 2019) on snow and glacier albedo, but research focused on the interaction between snow algae and black carbon is lacking.

Unlike inorganic LAPS, red snow algae forms perennial populations that resurface in the spring and summer, following overwintering burial by snow when sufficient interstitial water is available (Jones et al., 2001). While snow algae blooms can cover up to 65% of an individual glacier surface, they display a high degree of interannual variability in intensity and spatial extent (Engstrom & Quarmby, 2024), which is not fully understood. It is well known that snow algae are both nutrient- and water-limited (e.g. Anesio & Laybourn-Parry, 2012; Ganey et al.,

15

2017; Jones et al., 2001); however, the provenance of these nutrients for Western Canadian glaciers remains poorly documented.

Glaciers are oligotrophic environments, meaning that they have a low nutrient content. Most nutrient input on glaciers comes from precipitation and airborne material (Hodson et al., 2008; Anesio & Laybourn-Parry, 2012). On the 'Dark Zone' of the Greenland Ice Sheet, a nutrient addition experiment indicates phosphorous from mineral dust from local lithologies to be a limiting nutrient for ice algae blooms (McCutcheon et al., 2021). In the Arctic, snow algae preferentially grow in the snow with high concentrations of dust, which is believed to provide input of nutrients for the snow algae population (Lutz et al., 2015), and on North American stratovolcanoes, increased carbon dioxide concentrations promoted snow algae growth (Hamilton & Havig, 2020). A field experiment in Alaska demonstrated that adding aqueous nitrogen, phosphorous and potassium nutrients increased snow algae concentration by fourfold (Ganey et al., 2017). Similarly, snow algae in Antarctica bloomed in greater populations in coastal regions than inland regions, likely due to the input of nutrients from local minerals and marine fauna on the coast (Hodson et al., 2021). Red snow algae nutrient limitations generally stem from local mineralogy and the environment, suggesting that those limitations are not global; rather, they are driven by regional geology and environmental processes.

In Western North America, forest fires are common between spring and autumn, releasing large amounts of aerosol and black carbon into the atmosphere (Kondo et al., 2011). Black carbon is a light-absorbing particle and short-lived aerosol emitted from the incomplete combustion of carbon-based fuels such as fossil fuels, biofuels, and wood. It absorbs solar radiation across all wavelengths in the visible spectrum and impacts the radiation budget through positive radiative forcing, increasing melt when deposited on snow and ice (Kang et al., 2020).

This enhanced radiative forcing is expected to increase liquid water at the glacier surface. Black carbon also has the potential to nourish snow algae. In the Arctic Ocean, forest fire aerosol deposition was linked to increased summertime phytoplankton bloom in 2014 (Ardyna et al., 2022). The study suggests that aerosol from Siberian forest fires in the summer of 2014 led to N-enrichment of the sea surface, resulting in increased phytoplankton activity.

The deposition of black carbon on snow and ice can accelerate total glacier melt by up to 20% and reduce snow cover duration by several days (Kang et al., 2020). Following large forest fires and intense forest fire seasons, several field and model observations found an increased deposition of black carbon on snow and ice (e.g. Kaspari et al., 2015; Marshall & Miller, 2020; Williamson & Menounos, 2021). As forest fire activity and aerosols intensify, increased snow water and nutrients from the black carbon may enhance snow algae growth, further impacting glacier albedo and melt. However, little is known about the interaction between snow algae and black carbon, despite mentions made about this potential feedback (Aubry-Wake et al., 2022).

In this study, I conducted a field experiment on Place Glacier, British Columbia, Canada [50.42°, -122.6°], where I fertilized snow with wood ash and quantified the treatment effect on snow algae growth and melt. I measured snow algae cell abundance, melt and surface spectral reflectance in the field during three field visits conducted in the summer of 2023. I estimated the radiative forcing and associated snowmelt potential of snow algae using the spectral measurements taken on the first field visit and compared it to previous studies.

2.2. Methods

2.2.1 Study Site

I selected Place Glacier for the field experiment due to its ease of access via helicopter from Pemberton and field observation of snow algae blooms in 2022. Place Glacier is a small (3 km^2) glacier located in the southern Coast Mountain range (Fig. 2.1), northeast of Pemberton, British Columbia, Canada (50.42°, -122.6°). The glacier extends from ~2610 m a.s.l. (above sea level) in the accumulation zone to ~1900m a.s.l at the toe (Mukherjee et al., 2022). Winter accumulation at Place Glacier results in a deep snowpack that covers the glacier ice late into the summer ablation period.
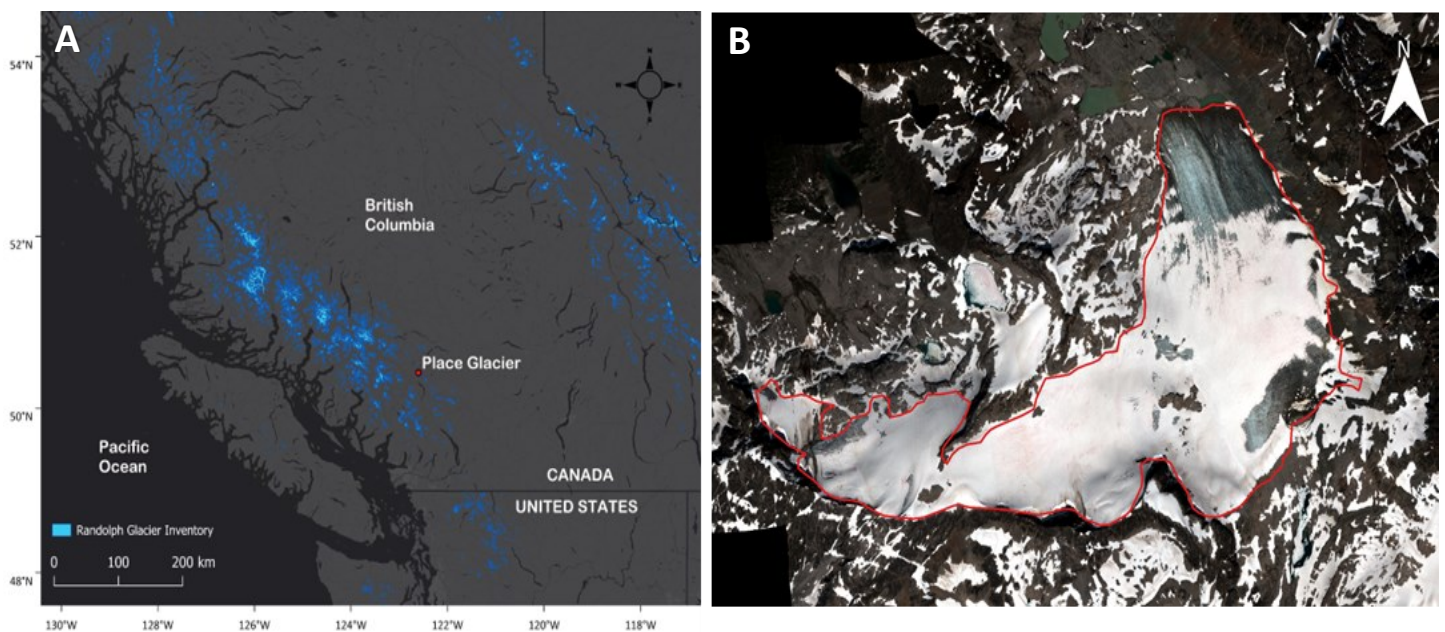
Figure 2-1 A. Map showing the location of Place Glacier in the southern Coast Mountains of British Columbia, Canada. Blue polygons are glaciers from the Randolph Glacier Inventory V. 7 (RGI Consortium, 2023). B. Hyperspectral mosaic RGB of Place Glacier on 22 August 2022 produced by the Airborne Coastal Observatory. The glacier boundary is outlined in red.

2.1.1 Snow algae and black carbon experiment

I conducted a replicated (10 blocks x 4 plots block $^{-1}$ = 40 plots total), manipulative field experiment to quantitatively measure the interaction between snow algae and black carbon from wood ash (Fig 2-2). The experiment occurred on the mid-elevation bench of Place Glacier (approx. 2000m a.s.l.) from 3 June to 2 July 2023. Each experimental block consists of four circular plots, each plot being 2.0 m^2 in area. In each block, I selected two plots with an established bloom (colonized) and two plots with no visible bloom (uncolonized), spacing the plots by at least 2 meters. One of the colonized and one of the uncolonized plots received a treatment of 0.4 g of wood ash, with particles filtered to 50 μm, and the other two plots remained as control. In the absence of a perfect experimental treatment for emissions from fire, wood ash was used as a proxy. I replicated this plot setup ten times, spacing each block by at least 15 m.
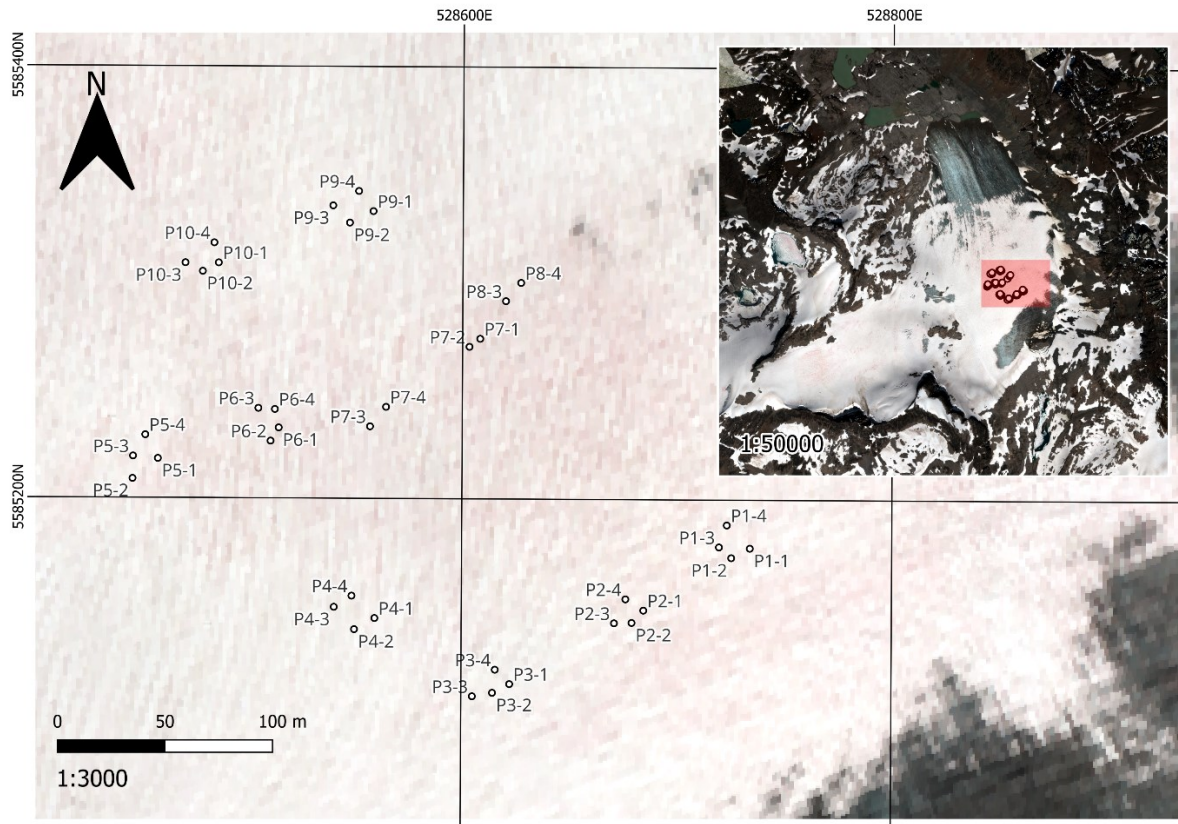
Figure 2-2: Map of the experiment plots and their location on Place Glacier, BC, Canada. Location for P8-2 and P8-1 missing.

I used three measurements to quantify the effect of wood ash on the snow algae: snow melt, algae cell abundance and spectral reflectance. I measured snow melt and algae abundance during our three field visits on 3-4 June, 11 June, and 2 July. I only collected optical properties on 3-4 June for all plots and for four of the blocks on 11 June due to rapidly changing atmospheric conditions. The field logistics on July 2 were not conducive to collecting optical properties, as I accessed the glacier by foot. Elemental metal and total carbon and nitrogen concentrations were determined for half of the treated and non-treated plots, randomly selected. This allowed to understand the metal concentration present in the snow that did not receive treatment and in the snow that received the ash treatment. Table 2-1 shows which plots on which dates receive reflectance, cell count and nutrient measurements.

Table 2-1: Description of measurements conducted per dates on the experiment plots. Snowmelt is not included, as each plot on each field visit was measured. No*: Data loss due to human error during processing of the sample.

Test	Reflectance			Cell Count			Nutrient
ID	June 3	June 4	June 11	June 4	June 11	July 2	June 4
P1-1	Yes	Yes	Yes	Yes	Yes	No	Yes
P1-2	Yes	Yes	Yes	No	Yes	Yes	No
P1-3	Yes	Yes	Yes	Yes	Yes	Yes	Yes
P1-4	Yes	Yes	Yes	No	Yes	Yes	No
P2-1	Yes	Yes	Yes	Yes	Yes	Yes	No
P2-2	Yes	Yes	Yes	No	Yes	Yes	Yes
P2-3	Yes	Yes	Yes	Yes	No*	Yes	No
P2-4	Yes	Yes	Yes	No	Yes	No	No
P3-1	Yes	Yes	Yes	Yes	Yes	Yes	No
P3-2	Yes	Yes	Yes	No	Yes	No	No
P3-3	Yes	Yes	Yes	Yes	Yes	Yes	No
P3-4	Yes	Yes	Yes	No	No*	Yes	Yes
P4-1	Yes	Yes	Yes	Yes	Yes	Yes	No
P4-2	Yes	Yes	No	No	Yes	Yes	Yes
P4-3	Yes	Yes	No	Yes	Yes	No	Yes
P4-4	Yes	Yes	No	No	Yes	Yes	No
P5-1	Yes	Yes	No	Yes	Yes	Yes	Yes
P5-2	Yes	Yes	No	No	Yes	No	No
P5-3	Yes	No	No	Yes	Yes	No	Yes
P5-4	Yes	No	No	No	Yes	No	No
P6-1	No	Yes	No	Yes	Yes	Yes	No
P6-2	No	Yes	No	No	Yes	Yes	Yes
P6-3	No	Yes	No	Yes	Yes	No	No
P6-4	No	Yes	No	No	Yes	No	No
P7-1	No	Yes	No	Yes	Yes	Yes	Yes
P7-2	No	Yes	No	No	Yes	No	Yes
P7-3	No	No	No	Yes	Yes	No	No
P7-4	No	No	No	No	Yes	No	Yes
P8-1	No	Yes	No	Yes	Yes	No	Yes
P8-2	No	Yes	No	No	Yes	No	Yes
P8-3	No	No	No	Yes	Yes	No	Yes
P8-4	No	No	No	No	Yes	Yes	No
P9-1	No	Yes	No	Yes	Yes	No	Yes
P9-2	No	Yes	No	No	Yes	No	No
P9-3	No	No	No	Yes	Yes	No	Yes
P9-4	No	No	No	No	Yes	No	No
P10-1	No	Yes	No	Yes	Yes	No	No
P10-2	No	Yes	No	No	Yes	No	Yes
P10-3	No	No	No	Yes	Yes	No	Yes
P10-4	No	No	No	No	Yes	No	Yes

I measured snow melt in each plot using ablation stakes drilled in the centre of each plot. I measured the length of the stake extending above the snow surface, with the depth of snow calculated as the difference in the current and previous measured lengths. To avoid introducing errors from snow cups and local melt around the stake, I measured the snow height from an ice axe set perpendicularly to the base of the stake. On 3 June and 4 June, I also measured the depth of the snowpack using an industrial gridded steel probe. Using 3 hours near-surface air temperature for Place Glacier collected at 1924 m.a.s.l. shared from the Geological Survey of Canada (appendix A), I calculated the melt factor using a simple degree day model as follows:

$$M = K_I PDD + K_S PDD \tag{2.1}$$

Where M is the depth of snow melted in millimetres water equivalent w.e., PDD is the positive degree day sum for the specific period and K_I and K_S are the degree day melt factors for ice and snow respectively. For this study, I calculated the K_S only and converted the height of snow melt to mm w. e. using a snow density of 500 kg m^{-3}. I then compared the melt factor (K_S) to the annual melt factor modeled by Shea et al. (2009) for Place Glacier from 1965 to 1995.

I sampled snow algae abundance from snow cookies in all plots three times during the experiment. At the time of our last visit on 2 July, the snow had already melted out over the location of the experimental blocks, but I sampled wet snow when present. I collected snow cookies of 7.62 cm (3 inches) in diameter and approximately 2 cm thick in each plot using a short segment of PVC tube labelled with a 2 cm depth line. I chose to sample the top 2 cm of the snow based on previous studies observing the majority of the red snow algae located at or near the snow surface (Engstrom et al., 2022; Ganey et al., 2017) and because the optical properties of snow are mainly affected by the top 2 cm layer (Di Mauro et al., 2024). Using a clean spatula to cut the snow at the base of the PVC tube, I carefully transferred the snow cookie into a Whirl-

Pak® bag upon collection. The samples were kept frozen on snow in the field and transported in coolers from Pemberton to the University of Northern British Columbia in Prince George, where they were stored at -20ºC.

2.2.3 Cell abundance

I conducted cell count at the University of Northern British Columbia using a Nikon FN1 microscope and a hemacytometer. The samples were thawed at room temperature, then preserved in glutaraldehyde. The melted samples were homogenized, and a 10 mL aliquot subsample was fixed with 50% glutaraldehyde to 1% final concentration. I measured algae abundance as cell count per unit of volume via microscopy. I performed algal cell count with an Improved Neubauer Hemacytometer cell counting chamber under a 40x objective. I counted individual algal cells, measured cell diameter, and cell surface area using the *NIS Elements* software. All nine 1x1 mm grids of the hemacytometer were used for the count. For each algae count, I sub-sampled 1 mL from the preserved preparation and performed four cell and dimension counts over 0.1 mL each. The surface area and diameter of the cells were averaged for each count, and the mean of the four counts was retained. All cells were considered in each count due to the low population number per 0.1 mL. The averaged cells per volume were scaled per unit of area using the following formulas to allow for comparison with other studies.

$$N\ Total = \frac{Average\ number\ of\ cells \times 10^4}{Number\ of\ square\ counted\ on\ hemocytometer} \left(\frac{cells}{mL} \right) \times sample\ volume \qquad (2.2)$$

$$Cells\ m^{-2} = \frac{N\ total}{Snow\ cookie\ area\ (m^2)} \qquad (2.3)$$

2.2.4 Empirical measurement of snow reflectance

I measured spectral reflectance from 350 to 2500 nm over the plots using the Spectral Evolution RS-5400 portable spectrometer, which has a spectral resolution of 2.7 nm from 350 to 700 nm, 5.5 at 1500, and 5.8 at 2100 nm. I collected spectra with the bare optic pointing directly downward, held 15 to 30 cm above the snow surface. I conducted the measurements at ±2h from solar noon. Reference scans were taken approximately every 15 minutes over a 99% clean white 5x5 inch Spectralon board to account for changing atmospheric conditions.

2.2.5 Radiative Forcing and Red Snow Algae Melt Estimate

To compare with previous studies, I estimated the snow algae instantaneous radiative forcing (IRF) from the reflectance data over the visible spectrum on 3 and 4 June for the estimated snow grain size, following similar method used by Engstrom et al. (2022), Ganey et al.(2017) and Healy & Khan (2023). I calculated the IRF of the snow algae over the visible spectrum as follows:

$$\text{IRF} \approx \sum_{350}^{850} I(\lambda) \, (\alpha_{white}(\lambda) - \alpha_{red}(\lambda)) \, \Delta\lambda \qquad (2.4)$$

Where IRF is calculated as the sum of the spectral solar irradiance (I), multiplied by the wavelength interval ($\Delta\lambda$) and the difference between clean snow albedo (α_{white}) and the snow algae reflectance (α_{red}) over the wavelengths 350 to 850 nm. The field spectrometer measurements (α_{red}) were collected on flat grounds of < 5° slope, and thus, the error due to the anisotropy factor is considered negligible (C. Donahue, personal communication, 2024), allowing the use of the reflectance data without conversion. Downwelling irradiance was measured at Place Glacier on 3 June and 4 June using a calibrated cosine diffuser attached to the

field spectrometer. I obtained clean snow albedo (α_{white}) from SNICAR-ADv3 (Flanner et al., 2021) using the following parameters. The solar zenith angle was estimated to be 34º for Place Glacier on 3 June and 4 June 2023 at 18:30 UTC (11:30 local time) using the 'pvlib' open-source Python tool (Jensen et al., 2023). The snowpack thickness was derived from the snowpack depth measured on the field (~2m), and snowpack density was set to 500 Kg/m^3. The snow grain shape was set to spheroids. Multiple effective grain sizes were input based on the nearest 50 nm as modelled from the measured spectra ice absorption feature centred at $\lambda = 1030$ nm (Nolin & Dozier, 2000). I calculated the effective snow grain size from the field spectra based on the continuum-removed depth rather than integrating the area to reduce uncertainty introduced by wet snow, which can shift the location of the continuum minimum (Donahue et al., 2023).   All the other parameters in SNICAR were set as the default or zero. The model outputs the albedo at 10 nm intervals ($\Delta\lambda$).

From the IRF calculated for the red snow algae, I calculated a first-order estimate of the glacier and snow melt rate by applying a simple energy analysis, similar to the method used in Donahue et al. (2023), Kaspari et al. (2015) and Painter et al., (2013). For this calculation, I assumed that the snow and ice are at the melting point (0°C) and that the additional energy is used entirely for melting and is not contributing to raising the temperature of the snow and ice. The assumption that isothermal snow and ice are at 0°C is reasonable, as from the interpretation of the air temperature sensor at Place Glacier, the snow temperature is very close to 0°C when the snow begins to melt and is isothermal between May 1st and May 15th, 2023, before the sensor is snow free on May 17th (Appendix A, Fig. A1). Additionally, I did not consider the amount of energy utilized for the photosynthesis process by the algae in this calculation, as suggested by Cook et al. (2020), and assumed that all of the absorbed energy is used for melting.

I obtained hourly instantaneous radiative forcing (HRF) as described in equation 2.3, using incoming irradiance simulated for Place Glacier on June 3rd, 2023 from the PVSystem solar irradiance program (https://pvlighthouse.com.au) acquired at hourly intervals from sunrise to sunset. The radiative forcing is assumed to remain constant during each 1h time step; therefore, the total hourly energy supplied by the radiative forcing is equivalent to HRF multiplied by 3600 s h^{-1}. To calculate the red snow algae contribution to melting, I divided the total hourly energy by the latent heat of fusion of water at 0°C ($0.334x10^6$J kg^{-1}), returning melt in terms of millimetres water equivalent per hour (mm w.e hr^{-1}). I then summed the hourly melt to obtain the estimated daily melt caused by the red snow algae.

2.2.6 Total metals, carbon and nitrogen content

The Northern Analytic Laboratory Service (NALS) at the University of Prince George tested the wood ash and randomized snow samples for total metals. The randomized snow samples represented samples from ten control plots and ten treated plots with the wood ash, all without snow algae as per visual inspection. The total metals test conducted by NALS followed the United States Environment Protection Agency (USEPA) method 200.7 (U.S. Environmental Protection Agency, 1994a) for assessing metals in the snow samples (liquid) and method 200.2 (U.S. Environmental Protection Agency, 1994b) for digesting the wood ash (solid) with an Agilent 5100 ICP-OES on the wood ash digestates. The statistical difference in nutrients between the treated plots and control plots was assessed using t-tests.

To identify which total metals most strongly influence algae growth, I applied a forward stepwise feature selection model using linear regression. The forward stepwise feature selection is a method that uses machine learning and statistics to build a model in which the most relevant

variables, nutrients in this case, are added iteratively until no further improvement is achieved or a predetermined number of variables is reached. I used the mlextend Python library to perform the algorithm and selected the top three nutrients. I then used the three selected nutrients in an ordinary least squares (OLS) regression model to estimate their individual contributions to algae cell count from June 11.

NALS performed a total carbon and nitrogen element test on the wood ash. They used a Costech 4010 Elemental Analyzer to combust the samples via the standard sequential combustion/reduction setup recommended by Costech with a flow rate of 100 mL min^{-1} of helium 5.0 as the carrier gas. The combustion oven was set to 1000°C, the reduction oven to 650°C, and the GC oven to 70°C. Gases were then separated on a standard 3m column and quantified with the built-in thermal conductivity detector (TCD).

2.2.7 Statistical Test

Statistical differences in the snowmelt and snow algae concentration and diameter among the different groups were assessed using the ANOVA and Kruskal-Wallis test based on the distribution of the dataset. I used the Shapiro-Wilk test to determine the normality of the snowmelt and snow algae concentration and diameter data. The Shapiro-Wilk test quantifies how well the data fit the normal distribution with the test statistic (W), ranging from 0 (deviation from normality) to 1 (normally distributed), and provides a ρ-value that indicates whether the data follows a normal distribution. A ρ-value < 0.05 indicates that the data do not follow a normal distribution. Based on the Shapiro-Wilk test results (Table 2-2), all the snowmelt data were normally distributed ($\rho > 0.05$), and only part of the cell concentration and diameter data followed a normal distribution; therefore, I conducted the ANOVA test on the snowmelt data and the Kruskal-Wallis on the cell concentration and diameter data. For test results where the

ANOVA or Kruskal-Wallis was significant (p-value < 0.05), I applied a post-hoc test to identify

which pairs of groups are significantly different through pairwise comparisons. Since only one of

the Kruskal-Wallis tests indicated a significant difference, I used Dunn's test with Bonferroni

correction to determine which group pairs are significantly different. Due to the small sample

size on July 2 for the cell concentration (n=17) and diameter (n=15), I also applied the non-

parametric Mood's Median test to compare the cell concentration medians to verify for Type II

error in the Kruskal-Wallis test (failing to detect a real difference).

Table 2-2: Shapiro-Wilk Test results for the snowmelt and cell concentration data and sample size (n).

		Colonized Treated	Uncolonized Treated	Colonized Control	Uncolonized Control
Snowmelt June 11	W-stats	0.843	0.953	0.889	0.959
	ρ-Values	0.313	0.279	0.744	0.249
	n	10	10	10	10
Snowmelt July 2	W-stats	0.914	0.91	0.956	0.905
	ρ-Values	0.313	0.279	0.744	0.249
	n	10	10	10	10
Cell concentration June 11	W-stats	0.859	0.804	0.842	0.791
	ρ-Values	0.0745	0.0163	0.0607	0.0162
	n	10	10	10	10
Cell concentration July 2	W-stats	0.921	0.957	0.75	0.927
	ρ-Values	0.513	0.759	0.000	0.576
	n	6	4	3	4
Cell diameter June 11	W-stats	0.665	0.899	0.818	0.943
	ρ-Values	0.001	0.406	0.033	0.690
	n	9	5	9	5
Cell diameter July 2	W-stats	0.942	0.964	NA	0.931
	ρ-Values	0.672	0.807	NA	0.601
	n	6	4	1	4

According to the Shapiro-Wilk test, the radiative forcing for clean snow (stat = 0.922, ρ = 0.334), snow colonized with snow algae (stat = 0.881, ρ = 0.133), and snow darkened with ash (stat = 0.946, ρ = 0.674) are normally distributed. I assessed the statistical difference in radiative forcing between clean snow with the ANOVA test and used the post hoc Dunn's test to determine which groups are significantly different.

2.3. Results & Discussion

2.3.1 Wood ash effect on snow algae abundance and melt

Snow algae blooms in the Coast Mountains typically appear in late June or early July and can last late into the summer (Engstrom & Quarmby, 2024). Snow algae bloomed approximately one month early in 2023, with observations in the Olympic Peninsula and on Place Glacier of snow algae as early as late May. Temperatures in May 2023 were higher than normal, with temperatures in the Coast Mountains near Place Glacier reaching 4-5°C above normal (Zhang et al., 2023). Snow algae typically bloom when sufficient liquid water is available within the snowpack. Thus, the higher-than-normal temperatures in May likely triggered the early bloom. Compounded with snowpack that was 20% below normal for the area around Place Glacier (B.C River Forecast Centre, 2023), early snow loss, as observed on 2 July, resulted in a reduced snow algal growth season on the Place Glacier bench, providing a short window for the field experiment.

Cell abundance and diameter

The statistical tests provide no evidence that wood ash had an impact on snow algae cell concentration during the experiment (Fig. 2-3). The Kruskal-Wallis test performed on the cell abundance on June 11 indicated a significant difference in the data (Stats = 16.93, ρ = 0.0007, n

= 40). The post-hoc Dunn's test, however, showed that the significant differences in algae cell median concentration were between the colonized and uncolonized plots, and no significant differences were identified between the treated and control plots. The colonized treated cell concentration was significantly higher than the uncolonized treated ($\rho = 0.0029$, n = 40) and the uncolonized control ($\rho = 0.031$, n = 40), and the colonized control cell concentration was significantly larger than the uncolonized treated ($\rho = 0.0272$, n = 40). These results suggest that plots that were already colonized during the first field visit support a higher cell concentration than the plots that had no visible red snow algae (uncolonized plots). This difference is likely because the cells in the colonized plots had undergone cell reproduction during the seven days between the two field visits, leading to a higher cell concentration. Whereas the algae cells in the uncolonized plots were possibly just starting to emerge. The microscopy, however, provided no evidence for this hypothesis. All cells observed in the microscopy were red, and no specific observations were conducted to discriminate among the cell types, as presented in Figure 1-1. At the end of the experiment, no significant difference was detected among the plots' concentration in the Kruskal-Wallis test (Stats= 3.033, $\rho = 0.387$, n = 17) and in the Mood's Median test (Stats = 0.830, $\rho = 0.841$, n =17). The cell abundance results, therefore, show that experimental additions of wood ash had no effect on cell abundance during the field experiment.
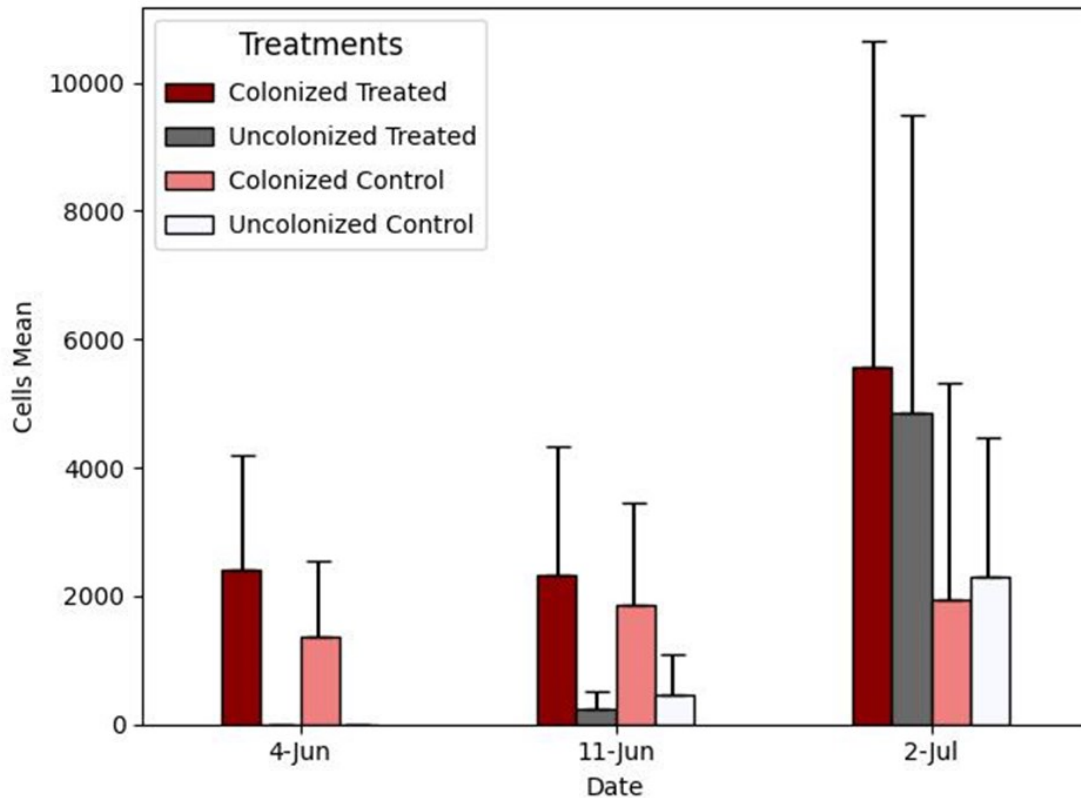
Figure 2-3: Mean cells per mL for the 4 plot settings from 4 June, 11 June and 2 July 2023 on Place Glacier, British Columbia, Canada

Algal cells per square meter during the field experiment varied from a minimum of 4.9 $\times$ 10^6 to a maximum of 8.0×10^7 on June 4, and 2.9×10^6 to 8.8×10^7 on June 11. The algae sample collected on 2 July consisted of firn and slushy snow, making it difficult to collect consistent volume. For this reason, I did not convert the cells ml^{-1} to cells m^{-2}. The maximum algal cell concentrations are comparable to those previously observed in the Eastern Alaska Mountains [5.1×10^7 (Takeuchi et al., 2013) and in the Sierra Nevada Mountains, California [1.3 $\times 10^7$] (Painter et al., 2001).

The wood ash treatment did not impact cell diameter during the field experiment. The Kruskal-Wallis test on June 11 (Stats = 2.878, ρ = 0.411, n = 28) and July 2 (Stats = 2.896, ρ =

0.408, n = 15) indicated no significant difference in the cell diameter among the plot types. The Mood's Median test indicated the same lack of statistical difference among the cell diameter on July 2 (Stats = 2.946, ρ = 0.400, n = 15). The averaged cell diameter during the experiment varied from 13 ± 4 µm to 41 ± 3 µm with a mean of 27 ± 9 µm. Cell diameter from algae samples collected in the Southern Coast Mountains had similar dimensions, with a diameter ranging from 20 to 30 µm (Engstrom et al., 2022).

Snowmelt over experimental plots

Snowmelt on Place Glacier over the field experiment from 3 June to 2 July, 2023 averaged 135.1 ± 7.1 cm or 675.5 ± 35.5 mm w.e (Fig. 2-4). I observed no significant difference in the measured melt between the plot treatments and the colonized versus non-colonized plots on June 11(ρ_{anova} = 0.18) and July 2 (ρ_{anova} = 0.23), as calculated by the ANOVA statistical test. The melt factors for snow from June 3 to June 4, June 4 to June 11 and June 11 to July 2 are respectively 3.5, 4.5 and 3.7 mm w.e $+ºC^{-1}$ d^{-1}, and is 3.8 mm w.e $+ºC^{-1}$ d^{-1} for the entire experiment period. In comparison, Shea et al. (2009) modelled a melt factor of 2.71 mm $+ºC^{-1}$ d^{-1} for Place Glacier.
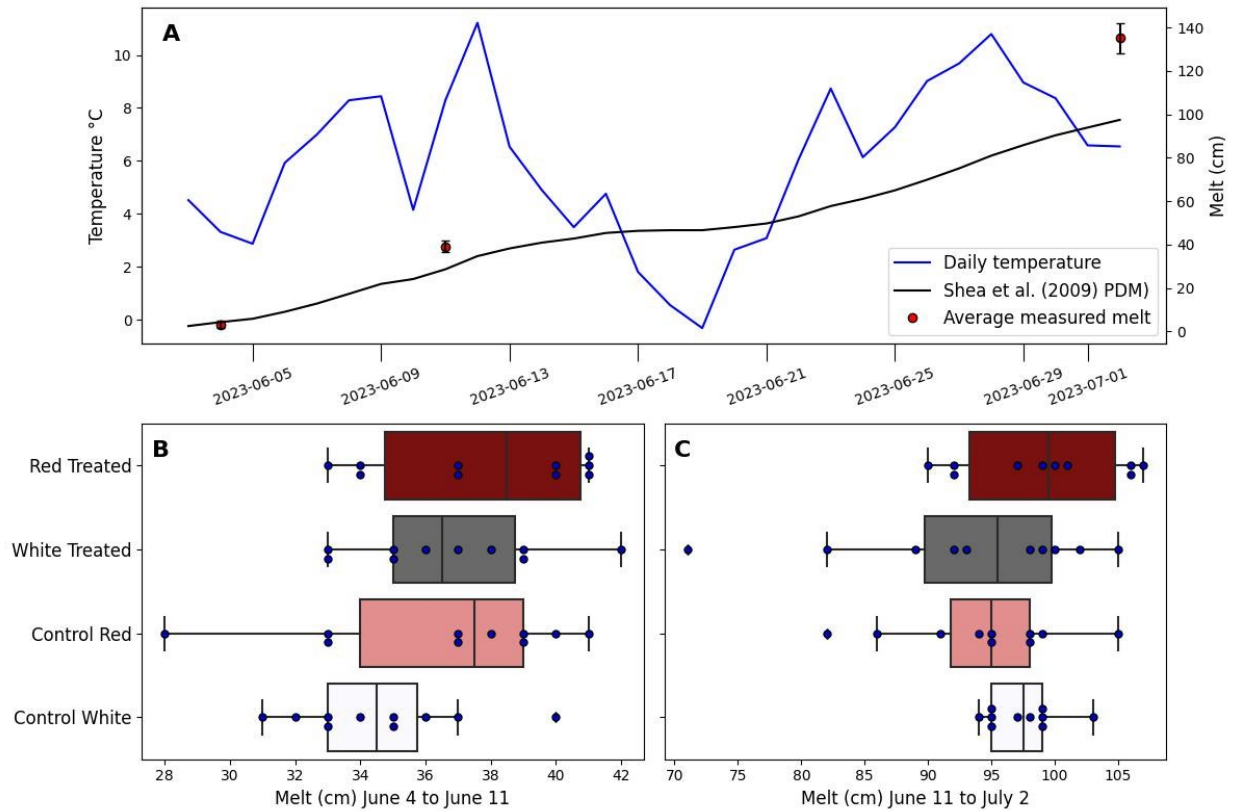
Figure 2-4: Snowmelt and temperature trends on Place Glacier, British Columbia, Canada. A. Daily temperature, average measure melt and positive degree day melt model (PDM) from Shea et al. (2009) B. Melt per plot setting from 4 June and 11 June 2023. C. Melt per plot setting from 11 June and 2 July 2023.

The average melt consistently trends higher for the treated colonized plots during the experiment. However, the difference is not large enough to be significant and only varies by a few centimetres from the other averages. I expected to observe higher snow melt in the treated and colonized plots from the increased radiative forcing and reduced albedo from the algae and ash. A few factors may explain why no significant difference was observed between the plot settings. First, I recorded snowmelt as a point measurement taken in the middle of the plot, as described in section 2.2.2. The algae blooms typically did not cover the entire plot area and were rather concentrated in heterogeneous snow cup patches. Therefore, it is possible that the measurement did not capture melt induced by the algae if they were not taken directly within the

33

immediate bloom area. Second, the melt caused by the algae during the 30-day experiment in June was possibly too little to be detected by statistical tests. Engstrom et al. (2022) estimated 16 cm of melt from snow algae over a two-month period (July and August) for two glaciers in the Purcell Mountains. Based on this estimate, the bloom observed on Place Glacier during our 30-day field experiment would have produced approximately half the melt (8 cm). Compared to an average total melt of 137 cm, the melt induced by the snow algae might have been too small to be detected in statistical tests and may explain the lack of statistical differences between the colonized and non-colonized plots.

In comparison to the Shea et al. (2009) melt model, the calculated melt factor for the field experiment was 3.6 mm w.e $+^{\circ}C^{-1}$ d^{-1}, compared to 2.71 mm w.e $+^{\circ}C^{-1}$ d^{-1}. This discrepancy could be explained by the fact that the melt factor calculated for the field experiment is over a much shorter period compared to Shea et al. (2009), which was modelled for the entire ablation seasons (May 15 to September 30) from 1965 to 1995. In contrast, the melt factor measured during this experiment was calculated from June 3 to July 2, around peak insolation. The difference between the two melt factors may also be due to surface albedo, as glaciers in the decades have become darker (Williamson & Menounos, 2021). This difference supports the concept that sensible heat alone is not the only factor that enhances melt on glaciers and that radiation heat from aging snow grain and light absorbing particles contribute to glacier melt via radiative forcing.

2.3.3 Wood ash Nutrients

Previous field studies and laboratory observations suggest that algae's response to nutrients is study-dependent. For example, a study on North American volcanoes (Hamilton &

Havig, 2017) and in the Arctic (Lutz et al., 2015) found no correlation between nutrient and snow algae abundance, whereas several other studies linked nutrients to algae abundance. In Alaska, for example, a field addition of nitrogen-phosphorous-potassium fertilizer promoted algae growth (Ganey et al., 2017). On Harding Glacier, Alaska, researchers observed more prominent algae blooms on the continental side than on the coastal side of the glacier. They speculated that the input of terrestrial nutrients from aerosols is higher on the continental side than on the coastal side, promoting the algae bloom (Takeuchi et al., 2006). On the Greenland Ice Sheet, McCutcheon et al. (2021) found that phosphorous from the local mineral dust increased algal blooms, and Holland et al. (2019) observed a decrease in nutrient concentration in the glacier meltwater surrounding areas of algal blooms.

In this study, nutrient levels of aluminium, barium, calcium, chromium, iron, potassium, magnesium, manganese, nickel and phosphorous were significantly higher in the treated plots with wood ash than in the control plots (Appendix B: Table B.1). The wood ash contains 0.05% of total nitrogen and 5.7% of total carbon. The forward stepwise feature selection indicates that Chromium, Iron and Lead have the most significant impact on snow algae abundance. Overall, the OLS model is statistically significant (F statistic = 7.138, $\rho = 0.0076$), and explains about 58.6% of the variation, as per the adjusted R-squared, indicating a moderately strong model. All three nutrients have a statistically significant influence on algae abundance. Iron (coefficient = 16 170, $\rho = 0.001$) has a positive impact on algae abundance and chromium (coefficient = -1631000, $\rho = 0.033$) and lead (coefficient=-1199000, $\rho = 0.048$) have a negative impact on algae abundance. This suggests that red snow algae are likely inhibited by heavy metal contamination, such as chromium and lead, and iron may be a limiting nutrient that supports algae growth. This

supports the relationship observed in Phillips-Lander et al. (2020) which observed that Fe-rich minerals increased red snow algae growth.

2.3.4 Reflectance and Radiative Forcing

Spectral reflectance

Spectral reflectance from the different plot settings varied consistently according to the plot composition, but the ash treatment did not impact the spectral reflectance (Fig 2-5. A-D). The reflectance of the uncolonized plots ('clean snow' and 'clean snow + ash') is spectrally flat in the visible wavelengths with values above 75% reflectance, as expected for white snow and decreases in the near-infrared typical for snow spectra (Wiscombe & Warren, 1980). The colonized plots ('red snow') reflectance varies between 40% and 80% in the visible wavelength, in accordance with other observations of red snow algae reflectance (e.g. Khan et al., 2021; Painter et al., 2001). The red snow spectra depict the uniquely biological chlorophyll absorption feature located around 680 nm used by Painter et al. (2001) to map snow algae from hyperspectral images, and the concave carotenoid absorption feature from 400 to 600 nm used in the RGND to map snow algae extent from satellite multispectral sensors (e.g. Ganey et al., 2017; Takeuchi et al., 2006).
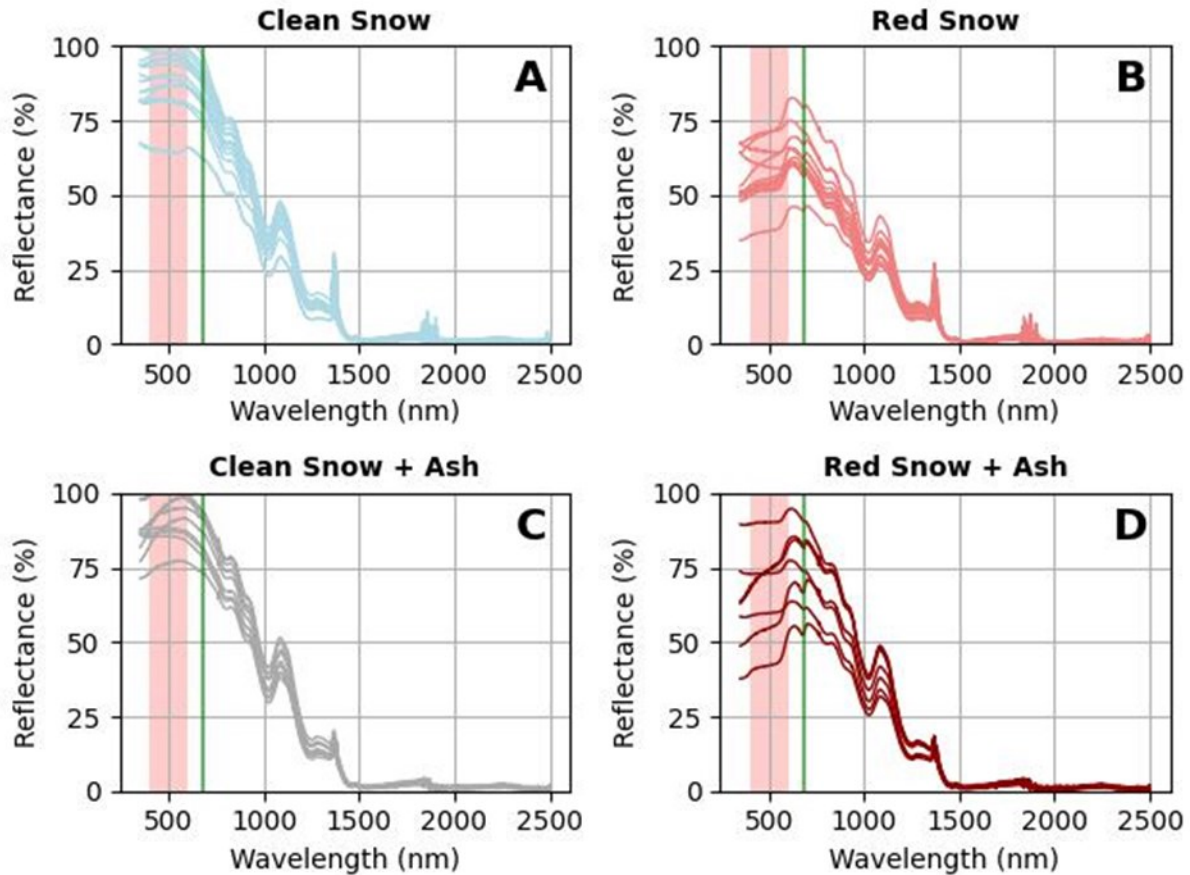
Figure 2-5: Spectral reflectance measured on 3 and 4 June coloured according to the different plot settings A. Uncolonized and untreated [Clean snow], B. Colonized and untreated [Red snow], C. Uncolonized and treated [Clean snow with wood ash], and D. colonized and treated [Red snow with wood ash]. The green lines point out to the chlorophyll absorption feature (680 nm), and the red rectangles point out to the carotenoid absorption feature (400-600 nm)

To assess the impact of ash and red snow algae on snow reflectance value, I computed the statistical difference with the ANOVA and post hoc Dunn's test among the radiative forcing of the respective groups. The ANOVA test and Dunn's test conducted on the radiative forcing values for the clean snow, and treated snow (ash) reveal no significant difference between the clean snow and the snow with ash ($\rho = 1.000$). The colonized and untreated snow radiative forcing (red snow), however, was significantly different than the clean snow ($\rho = 0.000094$) and the treated snow (clean snow + ash), $\rho = 0.004684$), with the red snow having a mean radiative

forcing statistically higher. Despite adding wood ash in amounts about a hundred-fold of what is observed in snowpacks in North America following forest fires, I did not detect an increase in radiative forcing pre- and post-treatment. The lack of difference can be attributed to black carbon lowering snow albedo by approximately 2-6% only (Wang et al., 2020). Additionally, the actual proportion of black carbon particulate matter contained in the wood ash from the bioenergy plant is likely less than 50% of the total wood ash added to the plot, as characterization of wood ash composition from small-scale residential wood combustion of mixed hard- and softwood determined that black carbon comprised approximately 40% of the total particulate emission (Meyer, 2012).

Radiative Forcing

I calculated instantaneous radiative forcing (IRF) using the field-measured reflectance values collected under blue sky conditions on 3 and 4 June 2023 and modelled clean snow albedo from SNICAR (Whicker et al., 2022). The average IRF for the 'clean snow' is 38 ± 2 W m^{-2}, 192 ± 12 W m^{-2} for the red snow algae and 54 ± 4 W m^{-2} for the snow with wood ash (Fig. 2.6). The maximum IRF is respectively 88.6 ± 5.4, 274.2 ± 16.7 and 111.8 ± 7.44 W m^{-2} for the clean snow, red snow and snow with wood ash. The average estimated melt from the red snow algae is 27.8 mm w.e d^{-1} as calculated for June 3rd, 2023. This melt assumed clear skies conditions for the entire day and is calculated for the area measured directly under the field spectrometer.
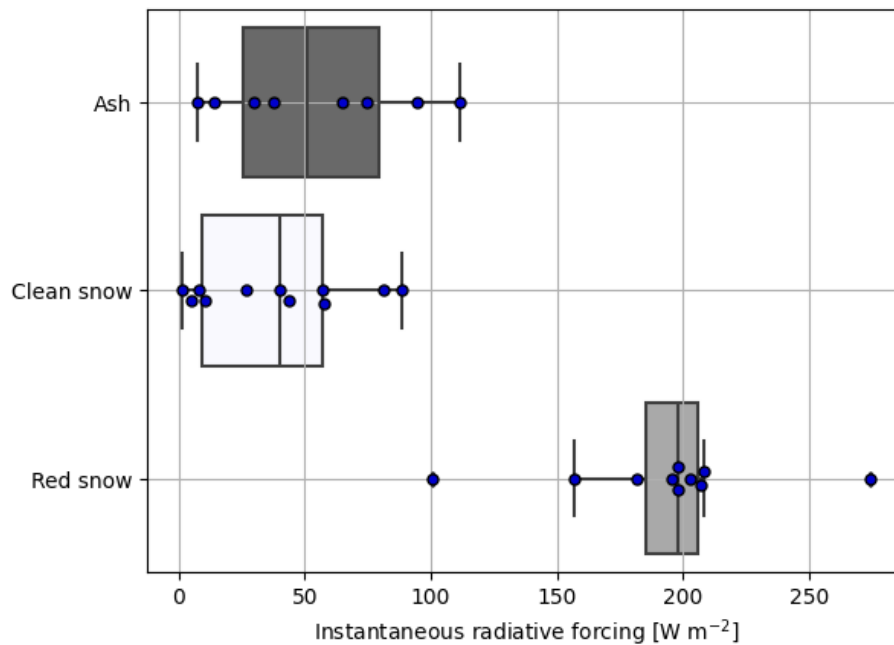
Figure 2-6: Instantaneous radiate,ve forcing or wood ash, clean snow and red snow as measured on June 4 and July 11 from the field spectrometer reflectance data.

In previous studies of snow algae, calculated radiative forcing varied from an average IRF of 21.6 W m^{-2} in Alaska (Ganey et al., 2017) and 88.0 W m^{-2} in Antarctica (Khan et al., 2021) to a peak bloom IRF of 235.56 W m^{-2} in the North Cascades, US (Healy & Khan, 2023) and 295 W m-2 in the southern Coast Mountains, BC (Engstrom et al., 2022). The average calculated IRF of snow algae in this study is comparable to the IRF calculated from peak algae blooms, even though the spectra used in this study were obtained during the early bloom. The IRF translate to a melt estimate of up to 27.8 mm w.e. d^{-1}. While this value represents the maximum potential red snow algae can melt under clear skies conditions, it shows that the snow-darkening effect from snow algae bloom, even during early blooms, can have great implications on snowmelt. As explained above, no difference in melt was measured between the colonized and non-colonized plots, which is in part attributed to the method. Nonetheless, those results

39

demonstrate that the potential melt contribution from snow algae on glaciers is non-negligible and should be considered when modelling glacier melt.

The wood IRF was on average 54 ± 4 W m^{-2} compared to 38 ± 2 W m^{-2} for the clean snow, but was not statistically different according to the ANOVA and Dunn's test. Field observations of black carbon in snow in the United States suggest radiative forcing can vary from 1 W m^{-2} for low black carbon concentration to above 100 W m^{-2} (Kang et al., 2020). Measured black carbon from surface snow samples in the Olympic Peninsula, US, post forest fire, totalled 3120 µg/L, corresponding to a radiative forcing of $37 - 53$ W m^{-2} (S. Kaspari et al., 2015). On the Juneau Icefield, they estimated a median radiative forcing of 40 W m^{-2} in July from black carbon only. Those values are comparable to the calculated IRF values of 54 ± 4 W m^{-2} for the wood ash. However, compared to the calculated IRF for the 'clean snow' plot, the increased IRF from the wood ash is lower than those observed in the previous study. Additionally, a visual inspection of airborne imaging spectroscopy of Place Glacier from before and after the wood ash was added failed to identify an increase in radiative forcing when integrated over a 2m pixel size (Chris Donahue, personal conversation). Such a small response was likely too weak to induce an increased melt or darkening effect and may explain why no significant difference was observed in the measured snowmelt.

2.4 Conclusion

The field experiment is inconclusive regarding wood ash treatment effects on snow algae growth. The nutrient analysis suggests, however, that iron may increase red snow algae growth while heavy metals such as chromium and lead may inhibit their growth. Iron and chromium were both found to be significantly more elevated on snow treated with wood ash. Due to limited data from

the last field visit, further studies are needed to assess the relationship between snow algae and forest fire ash. As forest fires in Western North America are predicted to increase in frequency and intensity, it is imperative to understand the feedback between snow algae and black carbon. Here, I showed that snow algae have the potential to increase radiative forcing to up to 274 ± 16 W m^{-2} and 192 ± 12 W m^{-2} on average during the early bloom stage, translating to a melt potential of 27.8 mm w.e. d^{-1}. Those results support the need to include bio-albedo reduction in predictive models of glacier change. In addition, this study suggests that higher-than-normal spring temperatures can shift snow algae bloom timing, which can have an exacerbating impact on seasonal snow cover on glaciated terrain and lead to early exposure of bare ice.

3   Chapter 3: Satellite and airborne remote sensing of snow algae in relation to black carbon deposition from forest fires in Western Canada

3.1   Introduction

Glaciers represent important sources of freshwater in western North America (Bonsal et al., 2020b). Yet, rates of glacier mass loss accelerated in the last decades (Bevington & Menounos, 2022; Hugonnet et al., 2021), leading to important impacts on stream flow and aquatic ecosystems due to changes in runoff (Huss & Hock, 2018). Seasonal and long-term decreases in albedo, or glacier darkening, represent one factor that could explain the accelerated mass loss from Western North America's glaciers in the last two decades, as surface albedo is an important factor controlling energy balance processes and melting at the surface of glaciers (Box et al., 2012). The formation of snow algae blooms and black carbon deposition from wildfire activity during the snowmelt season represent two processes that diminish glacier albedo. However, the interaction between snow algae and black carbon from forest fires remains uncertain.

Systematical mapping of snow algae blooms in North America from 2019 to 2022 shows that blooms occur on 5% of the total glaciated area (Engstrom & Quarmby, 2023) and can cover up to 60% of a glacier surface. Blooms of red snow algae appear on glaciers at the onset of snowmelt and remain on the surface until the end of the melt season (e.g. Engstrom et al., 2022). The algae produce carotenoid pigments to cope with the harsh glacial environment (Laybourn-Parry et al., 2012). The photoprotective carotenoid pigment, primarily astaxanthin, colours the snow red, reducing the albedo by up to 20% (Chevrollier et al., 2022; Ganey et al., 2017; Lutz et al., 2014). The excess energy absorbed by the pigment increases snowmelt on glaciers, which

can lead to earlier exposure of bare ice, thus further decreasing glacier albedo as ice is darker than snow. Previous studies used satellite imagery to study snow algae on snow and ice. Satellite imagery from Sentinel-2, SPOT and Landsat OLI combined with band ratios, as explained in section 2.1, have been widely used to map and quantify red snow algae bloom over glaciated terrain (e.g. Takeuchi et al., 2006. Engstrom et al., 2022; Ganey et al., 2017; Khan et al., 2021). Others have used Uncrewed Aerial Vehicles (UAV) surveys to analyze the impact of red snow algae blooms (Healy & Khan, 2023) on snow radiative properties. These studies provide evidence of the powerful potential of remote sensing techniques to study the distribution and impacts of red snow algae blooms on glaciated terrains.

Black carbon deposition on glacier surfaces from forest fires decreases glacier albedo and increases the absorption of shortwave radiation, accelerating melt. The excess energy absorbed by black carbon further decreases the albedo due to increased snow grain size (Hadley & Kirchstetter, 2012c). In the last two decades, forest fires in Western Canada increased in size, severity, duration and frequency (Hanes et al., 2018), leading to the deposition of black carbon over many glaciated areas downwind of the forest fires. In regions adjacent to frequent forest fire activities in British Columbia and Alberta, decadal decreasing trends in the glacier surface albedo were linked to changes in aerosol optical depth attributed to forest fire aerosols (Williamson & Menounos, 2021). Likewise, the albedo at Haig Glaciers, located in the Canadian Rocky Mountains, decreased to around 0.12 during years of heightened regional wildfire activity, like those observed in 2003 and 2017 (Marshall & Miller, 2020). The analysis of an ice core extracted from the South Cascade Glacier in Washington State, US, also indicated a high deposition of black carbon during wildfire events (S. D. Kaspari et al., 2020). As the severity and frequency of wildfires are expected to increase in western Canada (Coogan et al., 2019), the deposition of

black carbon over glaciers will also increase. While the distribution of light-absorbing particles like mineral dust on glaciers has been studied from space, identifying black carbon deposition over glaciers from multispectral satellites was deemed unlikely (Warren, 2013). The average amount of black carbon found in remote areas of the Northern Hemisphere reduce the visible albedo by approximately 1 to 6%, depending on the snow type (Warren & Wiscombe, 1980). Satellite measurements typically have errors of a few percent making the reduced albedo signal from black carbon challenging to detect from satellites (Warren, 2013). Moreover, black carbon has the same spectral signature as thin snow, making it difficult to detect in patchy areas. Therefore, atmospheric aerosol products such as the MERRA-2 black carbon flux provide a useful alternative method to track black carbon over glaciated areas, assuming part of the suspended black carbon gets deposited.

Recent studies combined available data from satellite imagery and data-driven models such as machine learning algorithms to automate the mapping of light-absorbing particles and snow and ice algae. Cook et al. (2020), for example, used a random forest classifier trained on spectra collected in the field to classify ice surfaces and map the albedo from UAV and Sentinel-2 images over the Greenland Ice sheet. Similarly, Engstrom & Quarmby (2024) developed a random forest classifier to systematically map red snow algae using Sentinel-2 satellite images over Western North America. Remote sensing observations and machine learning algorithms helped to improve our understanding of the distribution of mineral dust and algae on snow and ice and their impact on radiative forcing and albedo. However, despite the increasing interest in surface darkening processes on glaciers, to date, I am aware of no studies that examined the interaction between black carbon and snow algae using remote sensing data and machine learning methods.

The objective of this paper is to investigate the interaction between snow algae and black carbon from forest fires using remote sensing and machine learning. Since black carbon is not only emitted from forest fires, an assumption is being made in this chapter that it dominates the aerosol load, given the frequency and intensity of fires in the studied area. Here, I model the occurrence of snow algae blooms on glaciers in the Canadian Cordillera below 60ºN using satellite imagery from the Harmonized Landsat Sentinel 2.0 from 2015 to 2023 in conjunction with black carbon flux and dust flux from MERRA-2, and meteorological data from ERA-5 Land. Modelling red snow algae using machine learning helped to understand how the different variables affected the blooms and provided insight into interactive surface darkening processes.

3.2 Study area

The study area focused on glaciers in the Canadian Cordillera south of 60ºN and north of 49ºN, comprising all of Alberta and British Columbia glaciers, excluding the Insular mountains from Vancouver Island (Fig. 3-1). This mountainous region covers roughly 1,000,000 km^2 and can be subdivided into three main systems: the Western, Interior, and Eastern (Bolch et al., 2010). The Western System comprises the Insular, Coast and St. Elias Mountains. The Interior systems encompass the Purcell, Selkirk, Cariboo and Monashee in the south of the region and the Hazelton, Skeena, Cassiar and Omineca mountains in the north. The Canadian Rocky Mountains define the Eastern System. For this study, I excluded the Insular mountains due to the limited number and size of glaciated areas and subdivided the other mountain ranges into nine regions, as suggested by Schiefer et al. (2007). Each of these regions defined in figure 3-1 has a similar climate and glacier characteristics.
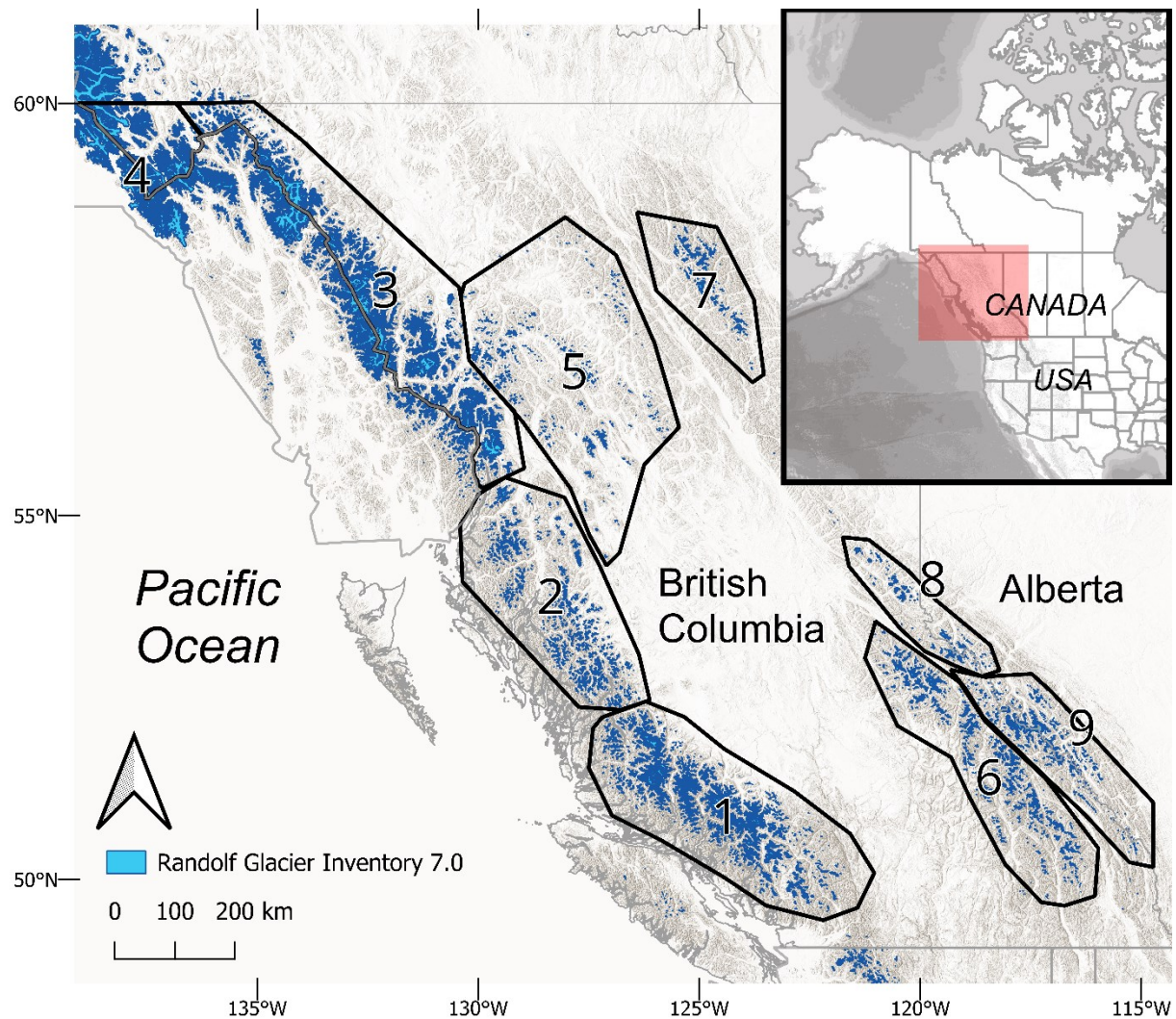
Figure 3-1: The glaciated region of the Canadian Cordillera below 60ºN is divided into nine regions. The small glaciers of the Insular Mountains on Vancouver Island are omitted in this study. Details about the regions are found in Table *3*.1.

Table 3-1: Glaciated area, and elevation of the nine regions

Region Number	Region Name	Glaciated Area (km2)	Mean Elevation (m)	Max Elevation (m)	Min Elevation (m)
1	Southern Coast Mountains	6535.35	2065	3444	521
2	Central Coast Mountains	1698.27	1620	2550	411
3	Northern Coast Mountains	8619.02	1650	2940	200
4	St. Elias	3199.29	1373	4297	136
5	Interior North	535.58	1884	2411	1167
6	Interior South	1929.01	2468	3239	1353
7	Northern Rockies	352.19	2249	2819	1604
8	Central Rockies	422.32	2362	3279	1532
9	Southern Rockies	1350.75	2629	3438	1630

3.3 Data

3.3.1 Harmonized Landsat Sentinel

For this study, I use surface reflectance data from NASA's Harmonized Landsat Sentinel (HLS) version 2.0. The HLS dataset combines and harmonizes Landsat8/9 Operational Land Imager (OLI) and Sentinel-2A/B Multi-Spectral Instrument (MSI) through a set of algorithms, including atmospheric correction, cloud and cloud shadow masking, geographic co-registration and common gridding, bidirectional reflectance distribution function (BRDF) normalization, and bandpass adjustment (Claverie et al., 2018). The HLS produces a seamless surface reflectance record with near-global coverage and revisits intervals every three days at the equator, increasing in frequency with increasing latitude. HLS data consists of two products, S30 (30m spatial resolution) derived from Sentinel-2 imagery and L30 (30m spatial resolution) derived from

Landsat 8-9/OLI, acquired since April 2013 (Landsat-8), November 2015 (Sentinal-2A), July 2017 (Sentinel-2B) and October 2021 (Landsat-9). In this study, I utilized L30 and S30 products from June 1st to September 30th from 2015 to 2023 inclusive.

3.3.2   Aerosol Optical Depth

The black carbon and mineral dust used in this chapter originates from NASA's Global Modeling and Assimilation Office (GMAO) Modern-Era Retrospective analysis for Research and Applications, Version 2 – MERRA-2 – reanalysis data (Gelaro et al., 2017). MERRA-2 is a reanalysis dataset that assimilates aerosol optical depth (AOD) from ground- and space-borne remote sensing platforms and meteorological observations from radiosondes and aircraft (Randles et al., 2017). The model is based on the Goddard Earth Observing System Model Version 5 (GEOS-5) and includes bias-corrected AOD datasets of Moderate Resolution Imaging Spectrometer (MODIS), Advanced Very High-Resolution Radiometer (AVHRR) instrument, AOD from Multi-Imaging Spectroradiometer (MSR) and direct measurements of the ground-based Aerosol Robotic Network (AERONET).

MERRA-2 models the spatial distribution of black carbon and mineral dust concentration since 1980 at a spatial resolution of 0.5º×0.625º and time scales of 1-hourly, 3-hourly and monthly. The data is available online through NASA's Goddard Earth Sciences (GES) Data and Information Services Center (DISC). I acquired all hourly black carbon and mineral dust grid cells that covered the glaciated regions from 2015 to 2023. Based on the hourly dataset, I obtained monthly mean and max from June 1st to September 30th of each year.

3.3.3 ERA5-Land – Climatic parameters

Weather and long-term monitoring stations are sporadic in mountainous landscapes and at high elevations where glaciers exist in Western Canada, preventing the use of climatic variables collected at discrete locations. Instead, I used the global climate reanalysis dataset of ERA5 Land (Muñoz-Sabater et al., 2021) to obtain climatic parameters over the study area from 2015 to 2023. I used the 2 m air temperature, snow density, snowfall, snowmelt, temperature of snow layer, and surface net solar radiation from ERA-5 Land hourly data produced at 9 km resolution (https://cds.climate.copernicus.eu/cdsapp#!/dataset/reanalysis-era5-land?tab=overview) resampled to a monthly average and monthly maximum. Previous studies suggest that climatic parameters and snow's physical conditions, such as snowmelt, snowfall and surface solar radiation and liquid water, impact snow algae abundance (Ganey et al., 2017; Onuma et al., 2016, 2022). Snow algae first appear on the snow surface when temperatures are above freezing (≥ 0 ºC) (Jones et al., 2001). The ERA5 Lands grids that covered the tile areas as per the HLS images from my glaciated region were aggregated into averages for each tile of the nine glacier regions.

3.4 Data Acquisition and Methods

In this study, I developed a framework to assess the interaction between red snow algae and black carbon. This framework consists of developing a dataset of red snow algae occurrence over the study area, referred to as the algae ratio, along with the predictor variables. Once the dataset was established, I assessed and preprocessed the data (section 3.3.4), then hypertuned and trained the machine learning models consistent with top machine learning practices (section 3.3.6). Next, I evaluated the model outputs and finally identified the key variables controlling the prediction of red snow algae (section 3.3.7). I explained the steps involved in acquiring and

preparing the red snow algae occurrence dataset in sections 3.3.1 to 3.3.3. The flow chart (Fig. 3-2) illustrates the process utilized to generate the red snow algae ratio dataset.
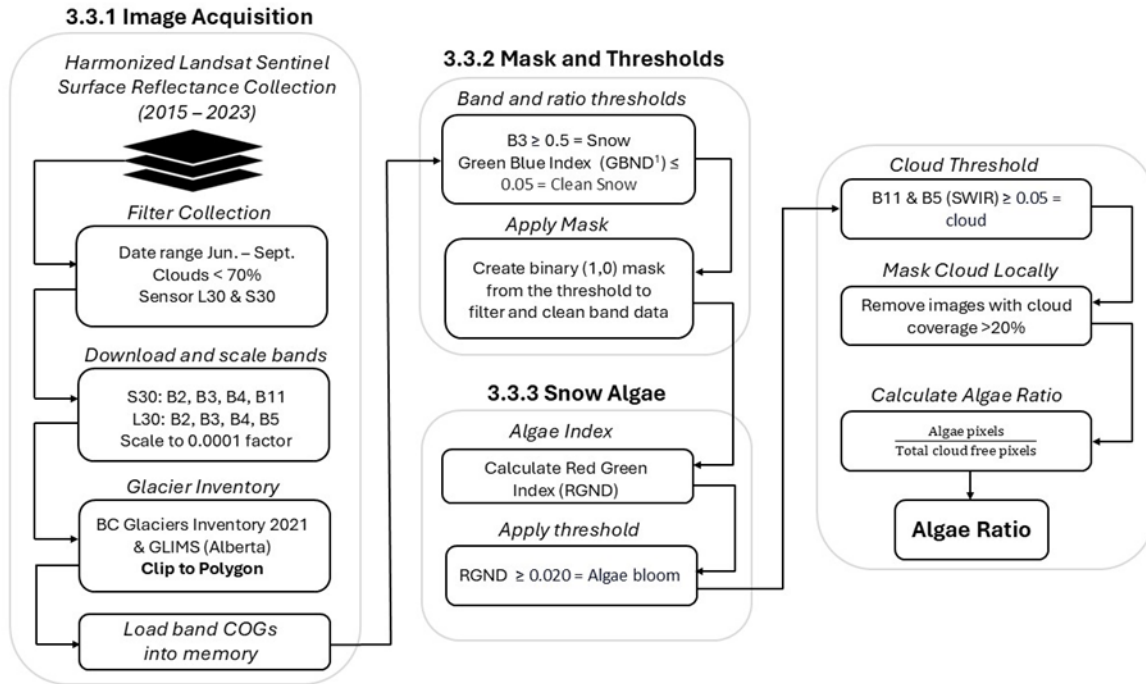
Figure 3-2: Flow chart of the workflow used to acquire the algae ratio from the HLS image collection. The section mentioned in the workflow corresponds to the next three sections.

3.4.1 Image acquisition

I used the HLS surface reflectance data to create eight melt-season (June- September) time series of algae blooms over the glaciated regions of British Columbia and Alberta from 2015 to 2023. I obtained all available HLS images filtered at 70% cloud coverage over the glaciated regions from June 1st to September 30th, which I assume to be the snow algae blooming season based on observations of blooms in Western North America (Engstrom & Quarmby, 2024). I used a high cloud cover filter in this first step to include as many images as possible that covered the glaciated regions. I processed entire HLS scenes, which can contain

less than 10% coverage of glaciers, and therefore, keeping a high cloud filter allowed me to include more images that may contain partial cloud coverage over glaciated areas, which otherwise would not have been included. From the HLS images collection, I loaded S30 B2, B3, B4 and B11 bands and L30 B2, B3, B4 and B5 bands in memory corresponding to the blue, green, red and SWIR bands. I used the glacier polygons from the BC Glacier Inventory 2021 (available here: https://catalogue.data.gov.bc.ca/dataset/glaciers) and Randolph Glacier Inventory 7.0 (RGI Consortium, 2023) Western Canada inventory (available here: https://nsidc.org/data/nsidc-0770/versions/7) to constrain the workflow to glacier polygons of British Columbia and Alberta only. The HLS bands were clipped to the glacier polygons, excluding all the data outside of the polygons. I then scaled the bands to a 0.0001 factor to bring the band values to a 0 to 1 scale as the HLS band data is provided in a 0 to 10000 scale.

3.4.2 Mask and threshold

Once the bands were loaded in memory, I applied a series of masks and thresholds to clean and prepare the data for the algae time series. I masked pixels with B3 < 0.5 to exclude bare ice. I used the green band to differentiate snow from ice rather than the Normalized Difference Snow Index (NDSI), as the NDSI overestimated snow coverage by including bare-ice pixels (A. Bevington, personal conversation). Since the images were already clipped to the glacier polygon, the need to apply an index to eliminate non-snow and ice surfaces was not necessary. I then applied the Green Blue Normalized Difference index (GBND) > 0.05 to mask rock fall and mineral debris on snow. The GBND ($\frac{B3-B2}{B3+B2}$) is a newly developed index by Di Mauro et al., (2024). The index is useful to differentiate mineral dust from algae blooms, as at low cell concentrations, the RGND index used to map snow algae can confound mineral dust to algal bloom (T. Painter et al., 2001).

3.4.3 Snow Algae Index

Finally, using the clean glacier image, I calculated the snow algae index for each pixel. I used the Red Green Normalized Difference (RGND), as explained in section 1.4, as it considers varying light intensity between the different images rather than the ratio between the red and green bands, as proposed by Takeuchi et al. (2006). RGND values above 0.02 were assigned as algal snow, and values below as algal-free snow. I chose to set a threshold of 0.02 as per my observations from hyperspectral data for Place Glacier. The snow samples with RGND values below 0.02 either had a very low concentration of cells or no cells. From the RGND pixel values, I quantify the occurrence of the algae blooms using the ratio of algal snow pixels over the total cloud-free pixels for a given glacier. Before calculating the ratio, I performed a second cloud mask utilizing the SWIR band, as clouds, compared to snow and ice surfaces, have high reflectance values in the SWIR band (A. Bevington, personal conversation). I applied a threshold of 0.05 on the SWIR band to mask clouds. I kept images with cloud coverage below 20% only for the analysis. The pixel ratio was determined for each tile based on the naming convention from the HLS image collection.

3.4.4 Data aggregation

The data used in this study comes from three spatially gridded products, the HLS, MERRA-2 and ERA5-Land, which all have different resolutions. To account for the difference in grid size, I spatially aggregated the data based on the HLS tile naming convention, where one tile is approximate 109 Km by 109 Km. Each glacier region contains from 6 (St.-Elias) to 18 tiles (Southern Coast Mountains), and on average, 9 tiles depending on the size of the region (Appendix C, Table C1). I averaged the ERA5-Land and MERRA-2 values that covered each tile when multiple grids covered the area of the HLS tile. Due to the MERRA-2 large grid size,

multiple HLS tiles were assigned to be the same value. Likewise, an HLS tile may be present in multiple regions, depending on where the boundary of the region versus the tile fell. In that case, the algae index contains a different value, but the ERA-5 Land and MERRA-2 values are the same. To account for the difference in spatial resolution, I extracted monthly values. I created two datasets for each HLS tile: the monthly mean and the monthly maximum values.

3.4.5   Trend analysis

I used 'linregress' from the Scipy stats library in Python to calculate the linear relationship between the algae ratio (dependent variable Y) and black carbon flux (independent variable X) for each mountain region. I calculated the Pearson correlation coefficients to assess the variation in the linear relationship amongst the different regions of the study area. I performed the linear regression calculation on the monthly max and monthly mean values. A correlation score of > 0.5 indicates a moderately positive linear relationship, and < 0.3 indicates a weak relationship. Furthermore, I obtained the ρ-value using a <0.05 confidence level for each correlation to determine the significance of the trend.

Additionally, I obtained the correlation matrices of the monthly mean and max of the nine predictors and one target variable to be used in the models. The correlation matrices provided insight into the data structure and collinearity of the predictor variables and the algae ratio. I utilized correlation matrices to identify multicollinearity within the predictor variables and guide which of the nine predictors provided redundancy in the model.

3.4.6   Data Preprocessing

Before performing the models, I preprocessed the data to address inconsistency and missing values in the datasets. The first preprocessing step involved cleaning the missing data

(NaNs) associated with the algae ratio. The data conversion to obtain the algae index from the HLS bands created NaNs values when the band values were infinite, or both the red and green band values were equal to zero. Additionally, the algae ratio calculation introduced NaNs if the cloud coverage over the glacier was above 20% (step 3.4.3). In that case the values were dropped due to the heterogenous distribution of algae bloom, making it difficult to use interpolation to infill values where clouds masked most of the glacier. The regions near the coast contained the most NaN values due to increased cloud coverage. Next, upon assessing the variable's distribution, I applied the log-scaling method to normalize variables with a skewed distribution. The algae ratio, the black carbon flux and snowmelt were transformed to the logarithmic scale. Finally, I conducted data normalization for the dependent and independent variables. Data normalization is a technique that transforms values on a similar scale, improving the model's performance and training stability. I used the min-max normalization method on all of the independent variables as follows:

$$x' = \frac{x - \min(x)}{\max(x) - \min(x)} \tag{2.1}$$

This method is preferred over the z-score for data that does not follow a Gaussian or normal distribution. The data was then ready for the machine learning models.

3.4.7   Models

To assess how red snow occurrence responds to every variable, I applied a Random Forest and XGBoost model. The predictor variables are black carbon flux, dust flux, longitude, latitude, surface air temperature, surface net solar radiation, snowmelt, temperature of the snow layer and snowfall. I then used permutation feature importance and Shapley Additive exPlanations (SHAP) to explain the output of the models and assess the relationship between

54

each variable and red snow algae. I applied the model to the entire datasets, years separately and using the previous year data for the black carbon to assess lag effect.

Random Forest Regressor

A Random Forest Regressor is an ensemble-based algorithm that combines the performance of multiple decision trees to predict the outcome value (Breiman, 2001). Random Forest Regressor is a non-parametric model, meaning it can deal with data that do not follow a normal distribution and can detect higher-order relationships between the predictors and the target data. The algorithm splits the data into multiple subsets of training data using the bootstrap aggregating or bagging technique, in which multiple subsets of the original training data are created. Decision trees have three main parts: root, internal and leaf nodes. The algorithm starts at the root node (the training dataset), followed by the internal node, where decision-making occurs. The leaf node is at the end and holds the final decision. At each node, a subset of the dataset is drawn at random. When the decision tree is finalized, a simple regression is performed on each leaf node to obtain the predicted dependent value. The Random Forest algorithm uses the bagging approach to aggregate multiple decision trees, in which each tree runs in parallel, meaning there are no interactions between individual trees. I utilized the random forest regressor from the Scikit-Learn Python library (Pedregosa et al., 2011) to determine the influence of the environmental and climatic variables on the monthly ratio of red snow algae from 2015 to 2023. I tuned the hyperparameters with the GridSearchCV from scikit-learn (Table 3.2). GridSearchCV uses all specified hyperparameter combinations to calculate and maximize the model performance.

Table 3-2: Parameters description and best value used for the Random Forest Regressor models

Parameter	Description	Monthly Mean	Monthly Max
n_estimators	The number of decision trees in the forest	100	2500
max_depth	The maximum depth of the tree	20	50
min_samples_split	The minimum number of samples needed to split an internal node.	2	3
min_samples_leaf	The minimum number of samples needed to create new leaves.	1	1
max_feature	The number of features to consider when seeking the best split.	sqrt'	sqrt'
bootstrap	Define if bootstrap samples are used when creating the decision trees	FALSE	FALSE

Extreme Gradient Boosting

Extreme Gradient Boosting (XGBoost) is a powerful machine learning algorithm based on decision trees introduced by Chen & Guestrin (2016). It is similar to the Random Forest model as it is based on decision trees, although the XGBoost algorithm learns by boosting, whereas the Random Forest learns by bagging. Boosting is an ensemble learning technique that combines multiple weak learners in sequence, where each subsequent model tries to correct the errors of its predecessor to improve the overall prediction accuracy. XGBoost utilizes the gradient boosting ensemble technique (Friedman, 2001) in which each new model reduces the residual error by optimizing a loss function using gradient descent, learning incrementally from previous iterations. This technique results in a model with low variance and low bias. The gradient boosting algorithm generated decision trees sequentially, learning from the last model until no more improvements occur or a threshold is reached. The algorithm utilizes a learning rate to scale the contribution of each tree. The learning rate leads to each tree having a more minor impact, increasing the total number of trees to reach the same level of accuracy. Using empirical evidence, Friedman (2002) showed that using multiple trees that point in the right

direction yields better prediction and lower variance than using a few decision trees with low bias and high variance. XGBoost builds on the gradient boosting model, improving its performance and speed. To improve computational efficiency, XGBoost enables parallel processing. The algorithm utilizes regularization techniques to improve the overall performance, constraining the model's complexity by penalizing overfitted models. Common regularization techniques include the Least Absolute Shrinkage and Selection Operator (Lasso/L1) and the Ridge (L2).

XGboost also uses a more sophisticated pruning strategy based on a maximum depth of tree and minimum loss reduction (gamma). The minimum loss reduction calculates the gain at each split as follows:

$$Gain = \frac{1}{2}\left[\frac{G_L^2}{H_L+\lambda} + \frac{G_R^2}{H_R+\lambda} - \frac{(G_L+G_R)^2}{H_L+H_R+\lambda}\right] - \gamma \qquad (2.2)$$

Where G and H are the gradients and second-order gradients, L and R define the left and right child nodes, λ is the regularization term, and γ is the minimum loss reduction. If the gain (reduction in the loss) is less than gamma, then the split is pruned (discarded). Using this method, XGboost prunes the trees while in the building process rather than after the trees are fully grown. The final prediction from the algorithm is a weighted sum of all the weak predictive models.

I implemented XGBoost using the xgboost library in Python (Chen & Guestrin, 2016) and used GridSearchVC from Skikit-learn to tune the parameters described above. The parameters used in this study are outlined in Table 3.3. Once the model was tuned and trained, I evaluated the feature importance and SHAP values (Lundberg & Lee, 2017), as explained in

section 3.4.3, to gain insight into which input variables yield the best estimate of the predicted

values.

Table 3-3: Parameters description and best value used for the XGBoost models

Parameter	Description	Monthly Mean	Monthly Max
max_depth	The maximum depth of the tree	9	8
min_child_weight	The minimum weight needed to create a new node in the decision tree. A large min_child_weigth leads to a more conservation algorithm.	1	5
gamma	The minimum loss reduction required for a node to make a split.	0	0
subsample	Specifies the ratio of observation to subsample for each iteration.	0.6	0.6
colsample_bytree	The ratio of variables to be used.	0.8	0.8
reg_alpha	L1 regularization term on weights. Can reduce the number of features to create a more interpretable model.	0.01	0.1
learning_rate	Specifies the step size used to scale the contribution of each new tree. A small learning rate reduces the impact of each tree.	0.01	0.01
n_estimators	The number of decision trees in the forest	1000	1000

I ran the Random Forest and XGBoost models on the monthly mean and monthly max

datasets. To assess whether years of high forest fire activity influenced the models' performance,

I ran the models on the monthly mean datasets for each year. Due to a lack of data from the

monthly mean dataset in 2016, I ran 2016 with the monthly max dataset. Lastly, I applied the

model to the monthly mean dataset, using the black carbon flux from the previous year, such as

the 2016 dataset used the 2015 black carbon flux, to evaluate the lag-year effect from the black

carbon. All the models' variable importance was assessed with the permutation feature

importance and the Shapley Additive Explanation as described below.

3.4.8   Evaluating Variables Importance

Once the models were tuned and trained, I evaluated the feature importance of each variable using the permutation feature importance and SHapley Additive explanation (SHAP) values (Lundberg & Lee, 2017) to gain insight into which input variables yield the best estimate of the predicted values.

Permutation Feature Importance

The permutation feature importance uses a model inspection technique to measure how much each feature contributes to the model's statistical score. The model inspection is done by randomly shuffling the values of a feature and measuring how much it decreases the resulting model's score. The advantage of the permutation feature importance technique is that it is model-agnostic and is particularly helpful when using non-linear predictors (Breiman, 2001). The one downside of the permutation technique is when two features are strongly correlated. If one of the correlated features is permuted, the model can still access the latter from its correlated feature, resulting in a lower reported importance value for the two features than it might be. One way to counter this issue is to cluster highly correlated features and retain only one feature from the cluster (Scikit Learn, 2024). The permutation feature importance provides insight into which features have the most impact on the model's score.

Shapeley Additive Explanation

The SHAP (Shapley Additive exPlanation) is a method introduced by Lundberg and Lee (2017) to interpret predictions from complex models, such as ensemble models like the one used in this study. SHAP values are based on cooperative game theory in that they measure a player's individual contribution (or variable) to the model's output for each set of observations. The

SHAP values are computed by evaluating the impact on the model's prediction when including or excluding each feature across all possible variable combinations. The larger the SHAP value, the higher the contribution of a variable to the model's outcome. The SHAP technique indicates whether a predictor has a positive, negative or neutral relationship with the target value, as visualized through the SHAP beeswarm plots.

3.5   Results

3.5.1   Correlation

Region Correlation

The correlation between black carbon and red snow algae occurrence is generally weak to moderate, with interior and southern regions exhibiting stronger relationships than coastal and northern regions. Overall, the correlation coefficient between black carbon and snow algae indicates weak [0.1 to 0.3] to moderate [0.3 to 0.5] positive linear relationships, except for the St. Elias subregion, which indicates a weak negative linear relationship (Fig. 3-3). The Central Rockies subregion has the strongest relationship with R scores of 0.55 and 0.47 for the monthly mean and monthly max values, followed by the Interior South with R scores of 0.37 and 0.43, respectively. The correlation coefficient is generally higher for the interior regions than the coastal regions, and stronger for the southern regions than the northern regions. The Northern Coast Mountains, Northern Interior and St. Elias subregion depict the weakest relationship with R-score varying from -0.12 to 0.17.
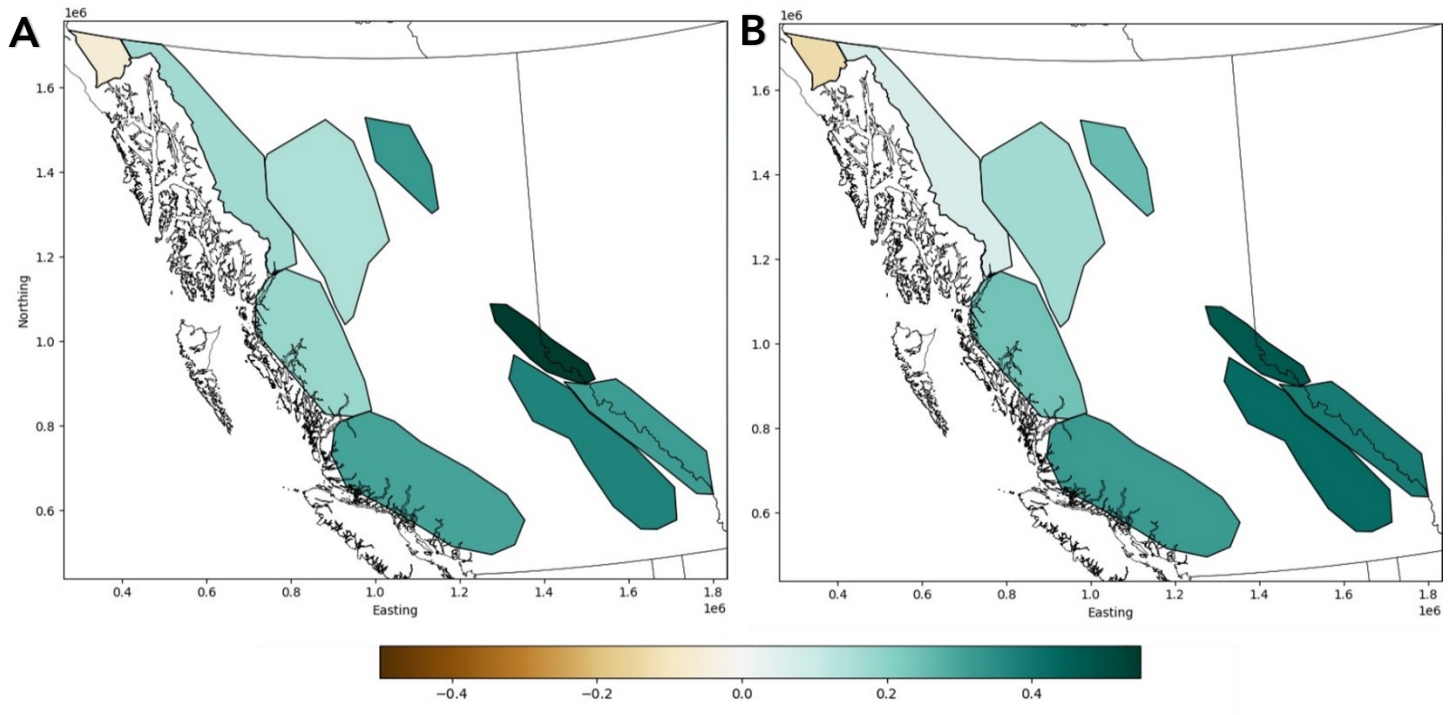
Figure 3-3: Pearson correlation coefficient between black carbon flux and red snow algae ratio for the nine subregions A. Monthly mean correlation and B. Monthly max correlation

Variables Covariance

The correlation between red snow algae ratio and environmental variables varies in strength and direction, with temperature, black carbon flux, and solar radiation showing moderate positive relationships. The monthly mean temperature at 2 m (t2m), black carbon flux, mean longitude, and monthly mean surface solar radiation (ssr) have the highest positive correlation with the monthly mean algae ratio with R-scores of 0.361, 0.348, 0.336 and 0.305, respectively, indicating a moderate positive correlation (Fig. 3-4). Both the monthly mean latitude and dust flux have a weak negative correlation with the monthly mean algae ratio with r-score values of -0.214 and -0.131, respectively. Similarly, the max longitudes and monthly max temperature at 2 m (t2m), black carbon flux and surface solar radiation (ssr) have the strongest correlation coefficient with the monthly-max algae ratio, albeit at lower scores than the monthly

mean values. The r-scores are respectively 0.281, 0.259, 0.188 and 0.138. Likewise, the max latitude [-0.172] and monthly max dust flux [-0.207] show a weak negative correlation with the monthly max algae ratio. I calculate the p-value to assess the significance of the correlation ($\rho \leq$ 0.05). The mean dataset has 2 non-significant correlations (sf – snow algae and rsn – tsn), and the max dataset has four non-significant correlations (tp – lat, tp – algae ratio, tp, rsn and ssr – dust flux) (Appendix E, Table E1 & E2). Based on the correlation matrix, I selected which predictors to be used in the model.

Figure 3-4: Correlation matrices of the A. Monthly mean and B. Monthly max predictors and target (algae ratio) values.

Correlation among the predictor variables ranges from weak to high. Predictors with high correlation coefficients indicate collinearity and can lead to re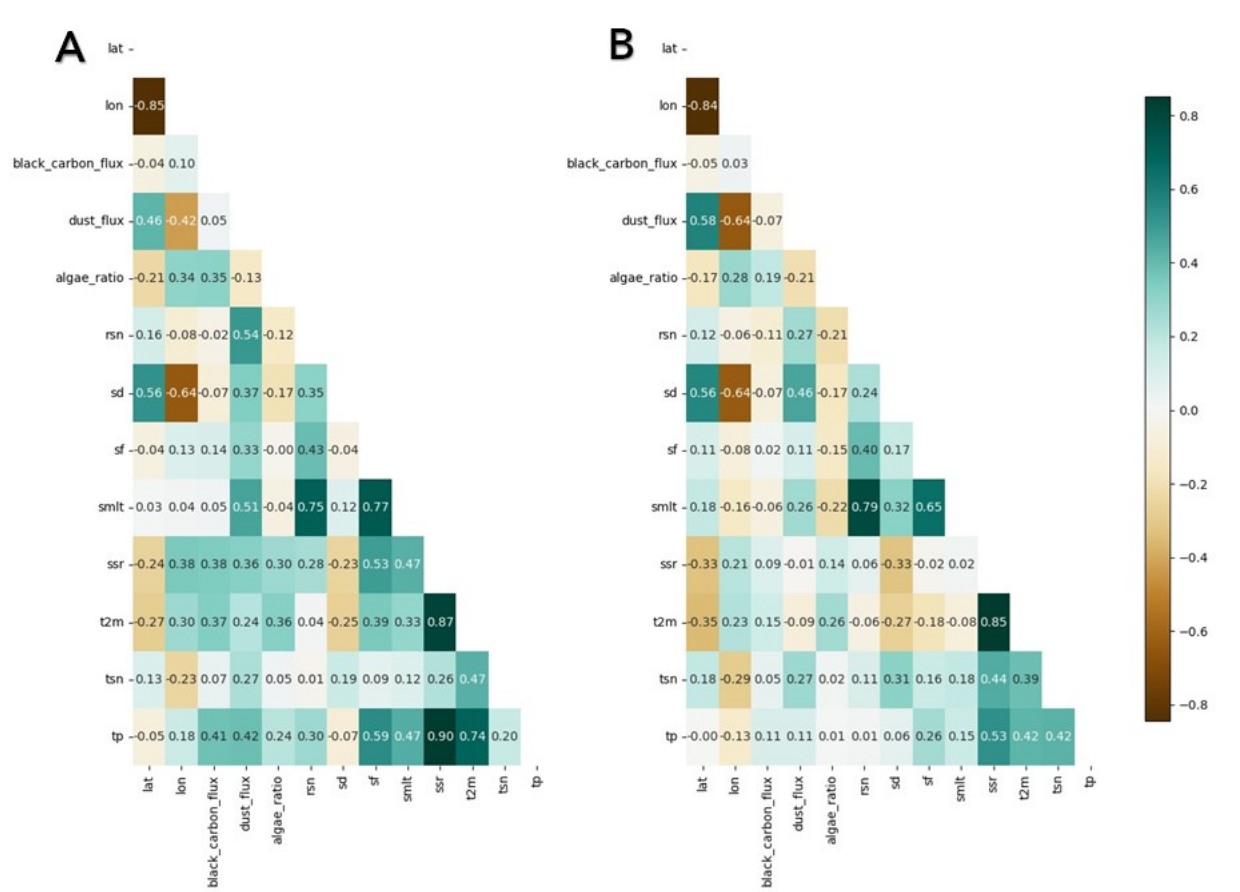dundancy in the random forest and XGboost model despite their robustness against multicollinearity. The surface solar radiation (ssr) and temperature at 2 m (t2m) have a very high correlation for both the monthly mean (0.866) and monthly max (0.851), as expected, indicating that areas with high surface solar radiation tend to have high temperatures. Snow density (rsn) and snowmelt (smlt) show high correlations with each other for the monthly mean (0.752) and monthly max (0.790), suggesting that they capture related snow dynamic processes. Dense snow has reduced air content and increased liquid water content, bringing it closer to the "ripe" state and making it more susceptible to melting, as it requires less energy for melting to occur. Based on manual iterations of the model with different combinations of the highly correlated pairs and their resulting importance, I removed snow density (rsn) from the predictor list as it decreased the models' performance. Removing surface solar radiation and/or temperature at 2m did not improve the model's robustness; therefore, both predictors were kept in the final models. The latitudes and longitudes had a strong negative correlation, likely because they were geographic coordinates, and a shift in one typically correlated to a specific shift in the other. The final retained variables for the model based on the correlation matrices were longitude, latitude, black carbon flux, dust flux, surface air temperature, net surface solar radiation, snowmelt, the temperature of the snow layer and snowfall.

3.5.2 The relation between Algae Ratio and the Environmental, Climatic and Geographic Variables

I calculated the feature importance from the Random Forest and XGBoost model using SHAP feature importance techniques and the permutation feature (Fig. 3-5 & 3-6). The different

models reveal similar patterns of feature importance. The most important variables for all model iterations are the longitude, then black carbon flux, followed by the two-metre air temperature, and the least important variable is snowfall.

SHAP features importance

The SHAP values range approximately from -0.2 to 0.3, implying that the variables moderately impact the final predictions. Furthermore, the relatively small SHAP values indicate that the prediction of the model outcome, the algae ratio, is not dominated by a single variable but is rather influenced by all variables, with increased contribution from higher-rated variables. The beeswarm plots (Fig. 3-5) order the variables by their importance, suggesting that longitudes, black carbon flux and 2-metre air temperatures have the most impact on predicting the algae ratio, as they are the top three variables in all four model iterations. The x-axis of the beeswarm plots indicates the impact of a variable on the model output, and the colour map is associated with the value of the variable, where blue indicates a high value and brown is a low value. Dust flux, latitude and snowmelt typically follow in the middle of the order, and surface solar radiation, the temperature of the snow layer and snowfall are generally the least impactful variables in the models, sitting at the bottom of the list.

When assessing the relationship between the predictors and target variable, the SHAP values for the Random Forest and XGBoost, using the monthly mean datasets, show that four predictors depict a clear linear relationship between the predictor values and their impact on the algae ratio (Fig. 3.5). Those are the longitude, 2 metres air temperature, black carbon flux, and the snowmelt. The other predictors do not have a clear impact on the model outcome. High air temperature values and black carbon flux are linked to a positive impact on the algae ratio value

and vice versa. Low longitude values indicate an eastward location or a large distance from the coast and are associated with a high predicted algae ratio. Similarly, low surface melt values result in a high model output. The model results from the monthly max datasets depict a slightly different outcome. While the longitudes and 2-metre air temperature still show a relatively clear linear relationship to the algae ratio, the monthly maximum black carbon flux does not indicate a clear linear relationship with the predicted algae ratio. The latitude, on the other end, has a positive linear impact on the algae ratio when using the maximum values.
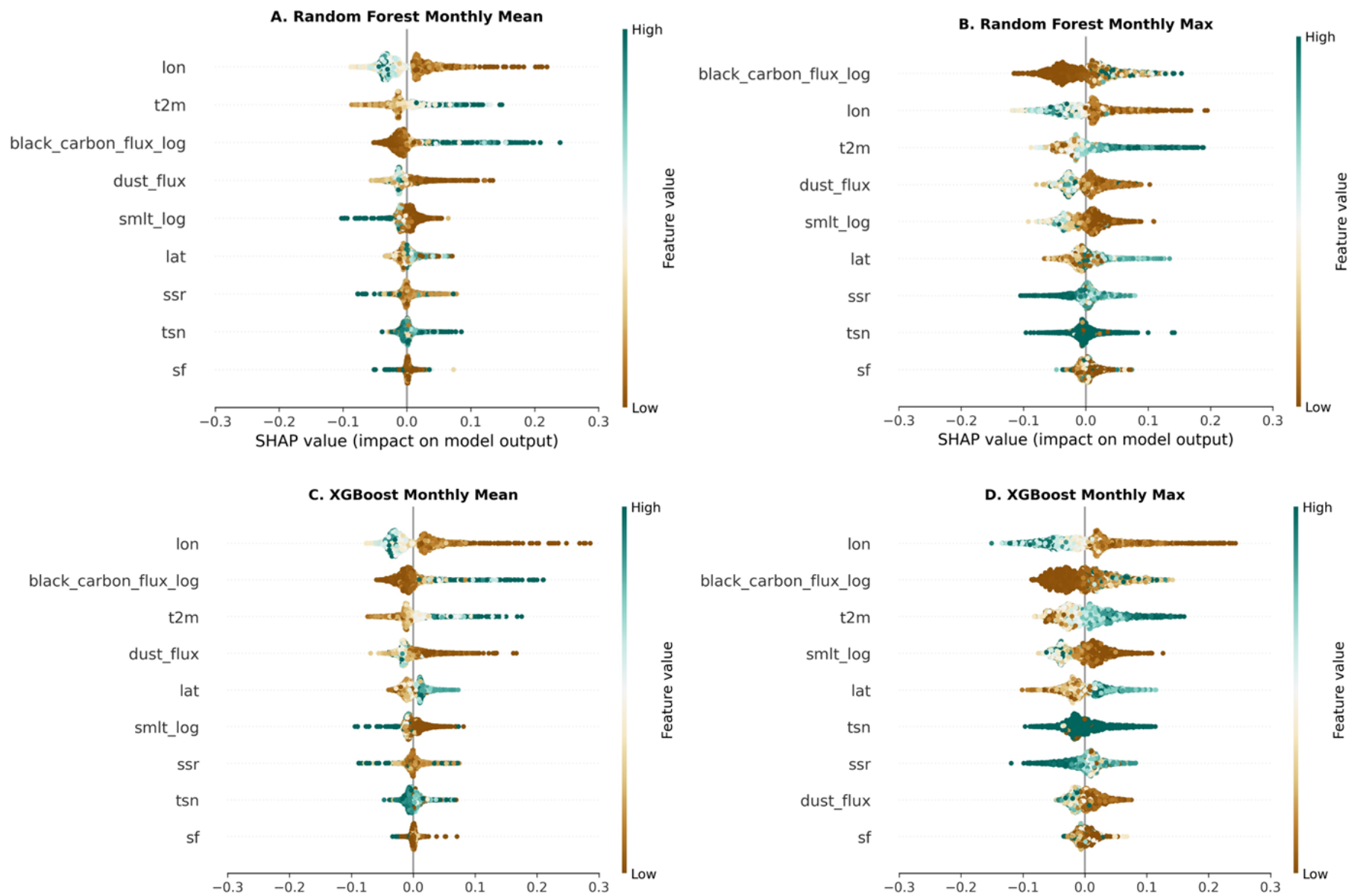
Figure 3-5: Beeswarm plots for the SHAP variable importance for the algae predictors with the Random Forest and XGBoost models.

Permutation feature importance

        The permutation feature importance calculates on the model predictors indicate their contribution to the model outcome (Fig. 3-6). According to the permutation technique, the longitude is the strongest predictor of red snow algae occurrence. The R^2 for the Random Forest and XGBoost models will decrease by respectively 45.6% and 37.0% for the monthly mean values and 38.9% and 41.3% for the monthly max values when the longitude is not included in the model. The second most important predictor is the black carbon flux. The Random Forest scores will decrease by 38.4% and 35.2% for the monthly mean and monthly max and the XGBoost, respectively, by 31.1% and 23.6%. The 2-metre air temperature has the third highest permutation scores for the two models, contributing on average to 23.4% of the model outcome values. The other predictors, the dust flux, surface solar radiation, the latitudes, the snow and the temperature of the snow layer, contribute to less than 20% of the model and are not consistently rated among the Random Forest and XGBoost iterations. The snowfall has the least impact on the model, with a permutation score of 4.9% and 8.9% for the Random Forest monthly mean and monthly max and a score of 2.4 and 5.7% for the XGBoost monthly mean and monthly max.
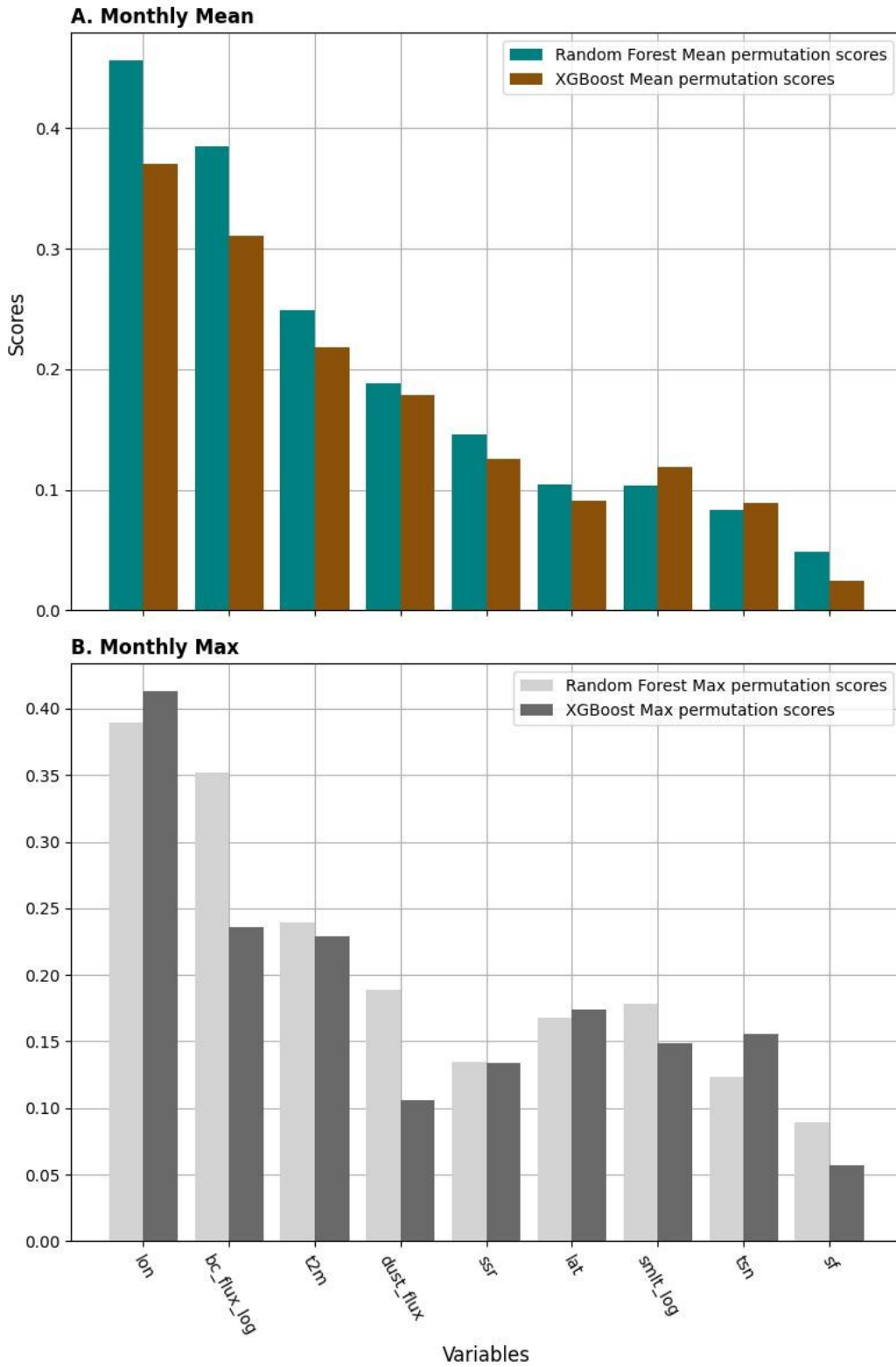
Figure 3-6: Permutation feature importance scores for the Random Forest and XGBoost for the A. Monthly mean dataset and B. Monthly max dataset

3.5.3   Main Model Performances Evaluation

The Random Forest and XGBoost performed moderately well, with R-score values ranging from 0.546±0.028 to 0.613±0.027 (Fig. 3-7). The Random Forest models have a mean R-scores of 0.600, RMSE of 0.0453 and MAE of 0.0795 for the monthly mean and an R-scores of 0.533, RMSE of 0.0861 and MAE of 0.131 for the monthly max. For the XGBoost model, the average R^2 are 0.604 and 0.564, the RMSE are 0.0455 and 0.0827, and the MAE are 0.0793 and 0.127 for the monthly mean and max. The Random Forest regressor and the XGBoost models performed similarly, and they both performed slightly better when executed on the monthly mean versus the monthly max values. All models have a slightly higher MAE than RMSE, indicating that most of the model's errors are small, with a few large errors.
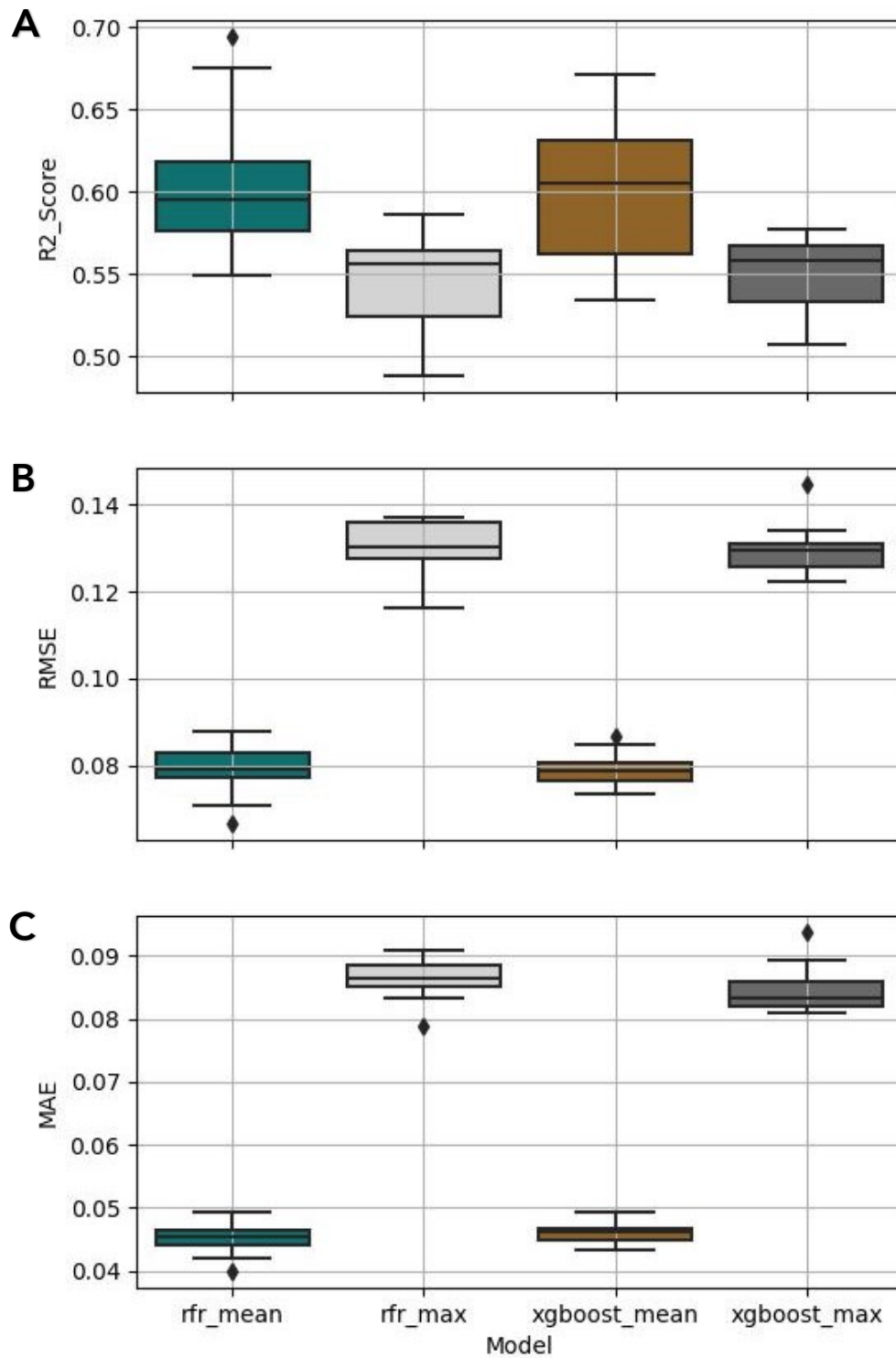
Figure 3-7: Boxplot representing the A. Coefficient of determination (R2) B. Root Mean Squared Error (RMSE), and C. Mean Absolute Error (MAE) for each of the models using the mean and max dataset. The scores *were calculated for 50 training and testing dataset* iterations.

Comparing the predicted value to the test datasets provide information on the fitting of the models. The plots for the Random Forest and XGBoost for the monthly mean dataset (Fig. 3-8 A & C) depict a similar trend in that the main cluster of points follows the x = y line moderately well. The monthly mean models show outliers on both sides of the x = y line, with a minor trend towards underfitting the actual algae ratio for values above 0.2. The monthly max plots (Fig. 3-8 B & D) show a slightly worse fit than the monthly mean plot, with larger residual errors as implied by the larger RMSE. The cluster of points for the monthly max plots trend lightly steeper than the x = y line, suggesting a light overfitting model. All four models indicate that the bulk of the monthly algae ratio values are within 0.0 to 0.1 for the monthly mean and 0.0 to 0.2 for the monthly max.
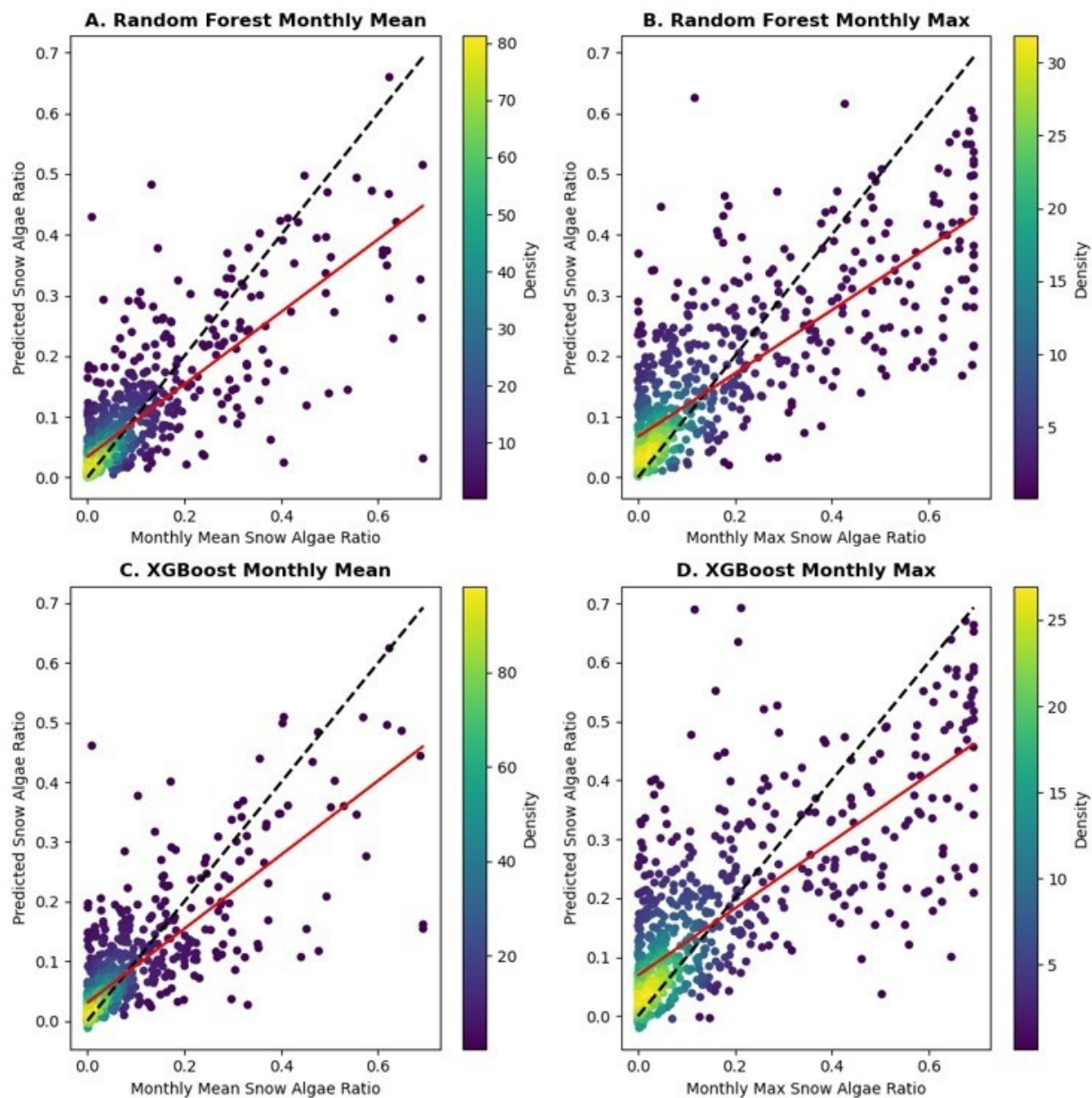
Figure 3-8: Plots of actual vs predicted algae ratio value for A. Random Forest Monthly Mean, B. Random Forest Monthly Max, C. XGBoost Monthly Mean and D. XGBoost Monthly Max. The dash line is a 1:1 line and the red lines are linear regression model.

3.5.4 Annual Models Performance and Feature Importance

The annual models' R2 score range from 0.043±0.239 to 0.703±0.094 for the random

forest and 0.064±0.160 to 0.706±0.118 for the XGBoost (Fig. 3-9). The random forest performed

slightly better than the XGBoost on the annual datasets. The 2019 model yield the lowest

performance in the models and 2018 the best performance. The 2015 XGBoost model has the

largest variation in model performance, with a standard deviation of 0.63. In general, the annual

model's R2 score is lower than the one obtained for the models run on the entire dataset, and

there are no differences in the model performance between the low fire seasons (2016, 2019,

2020 and 2022) and high fire seasons (2015, 2017, 2018, 2021 and 2023).
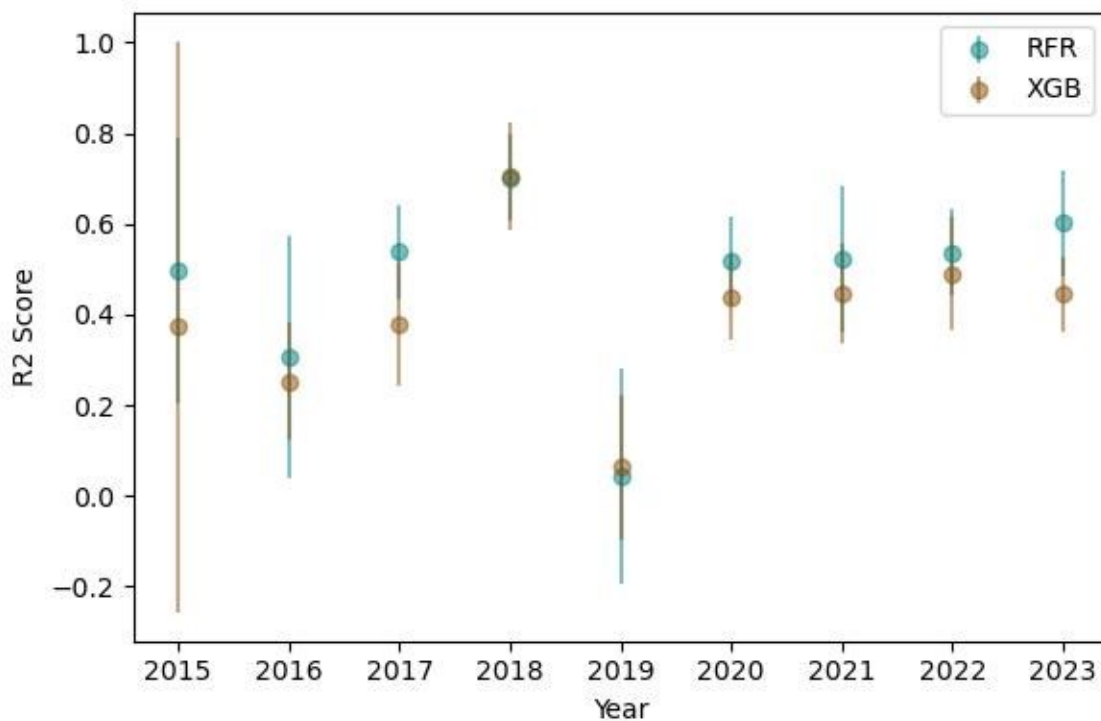
Figure 3-9: Random Forest (teal) and XGBoost (brown) R2 Score when applied to the model run
on a singular year. All models were run on the mean dataset except for 2016, which was run on
the max dataset.

Regarding the variable importance, the permutation feature value ranges from 0.007 to 0.370 for the random forest and 0.011 to 0.487 for the XGBoost. The SHAP values range from 0.0009 to 0.0424 and 0.0008 to 0.0389 for the random forest and XGBoost, respectively. When averaged across the annual models, the dust flux is the most important variable, followed by the longitude (Fig. 3-10). While the dust flux is ranked first in the XGBoost, it has the largest value range among the nine predictor variables. Although the black carbon flux and 2-metre air temperature ranked in the top three variables in the overall model, they have a much lower impact on the model output when assessed with the annual model. The permutation feature importance value is less than 0.1 for the surface air temperature and black carbon and less than 0.01 for the SHAP values. The variable importance amongst the nine annual models is inconsistent, as shown in the permutation feature and SHAP plots (Appendix F & G, Fig F 1-18 & Fig G 1-18).
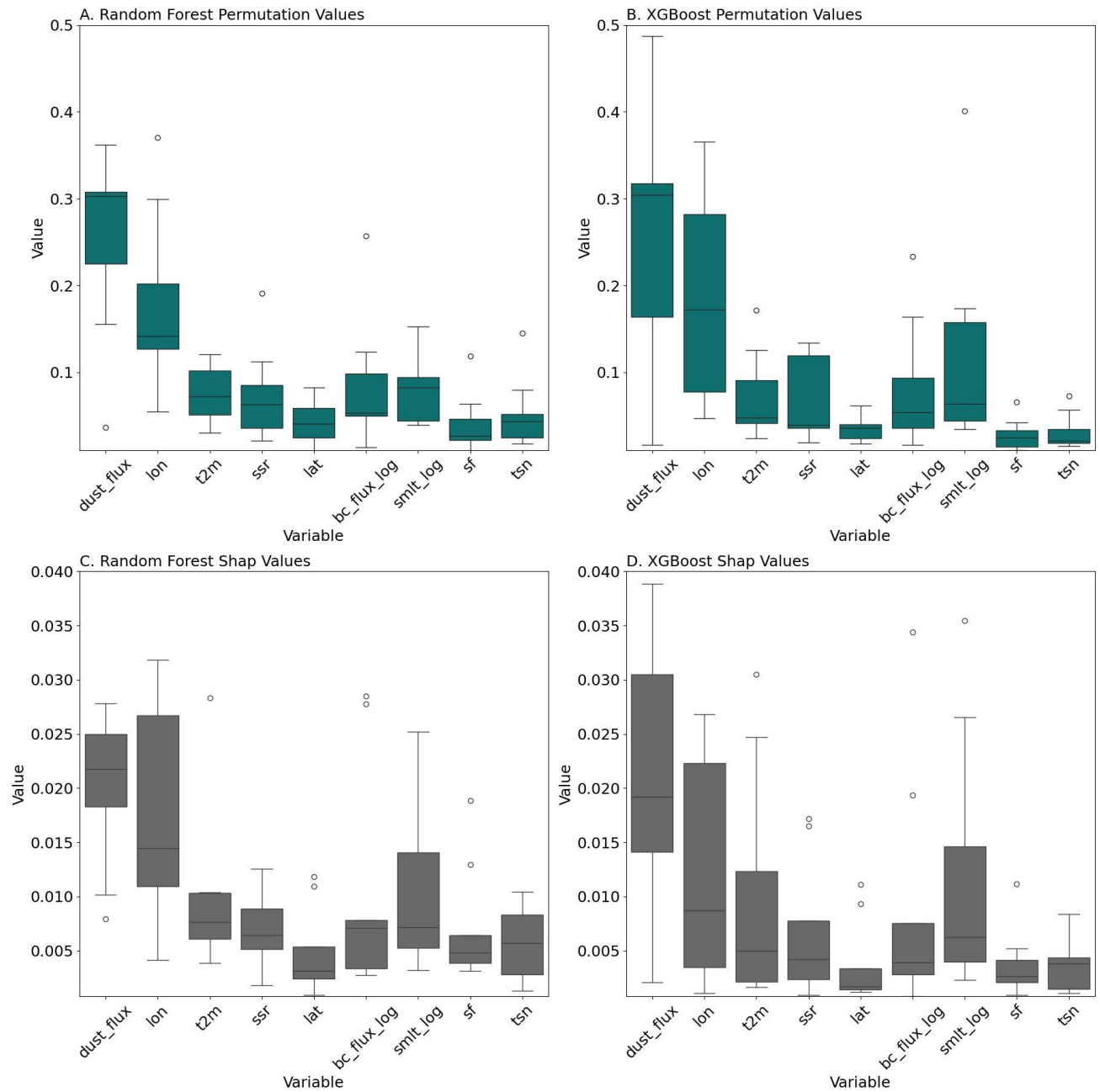
Figure 3-10: Feature importance for the model run annually. A. Random Forest Permutation Values, B. XGBoost Permutaiton values, C. Random Forest Shap values and D. XGBoost Shap values.

3.5.5 Lag-year model performance and feature importance

The model R2-score performed with the lag-year black carbon flux dataset is 0.606 ± 0.043 for the random forest and 0.603 ± 0.049 for the XGBoost. The RMSE and MAE are respectively 0.069 ± 0.006 and 0.039 ± 0.003 for the random forest and 0.070 ± 0.006 and 0.049 ± 0.003 for the XGBoost. The random forest XGBoost performed very similarly on the lag-year dataset. According to the permutation feature importance and SHAP value (Fig. 3-11 & 3-12), longitude and dust flux are the most important variables when using the lag-year dataset. The SHAP beeswarm plots (Fig. 3-12) indicate that low longitude value, thus eastward location, and low dust flux value positively influence the red snow algae. The temperature of the snow layer (tsn) is the third most important variable according to the permutation feature importance and the SHAP value for the XGBoost. It ranked fourth for the random forest SHAP beeswarm plot (Fig. 3-12.A.). The next most important variable is the surface air temperature (t2m). The black carbon flux has less impact on the red snow algae ratio for the model ran on the lag year dataset. The snowfall and latitude remain among the weakest variables for the lag-year models.

Figure 3-11: Permutation feature importance for the lag-year model for A. the random forest and B. the XGBoost.
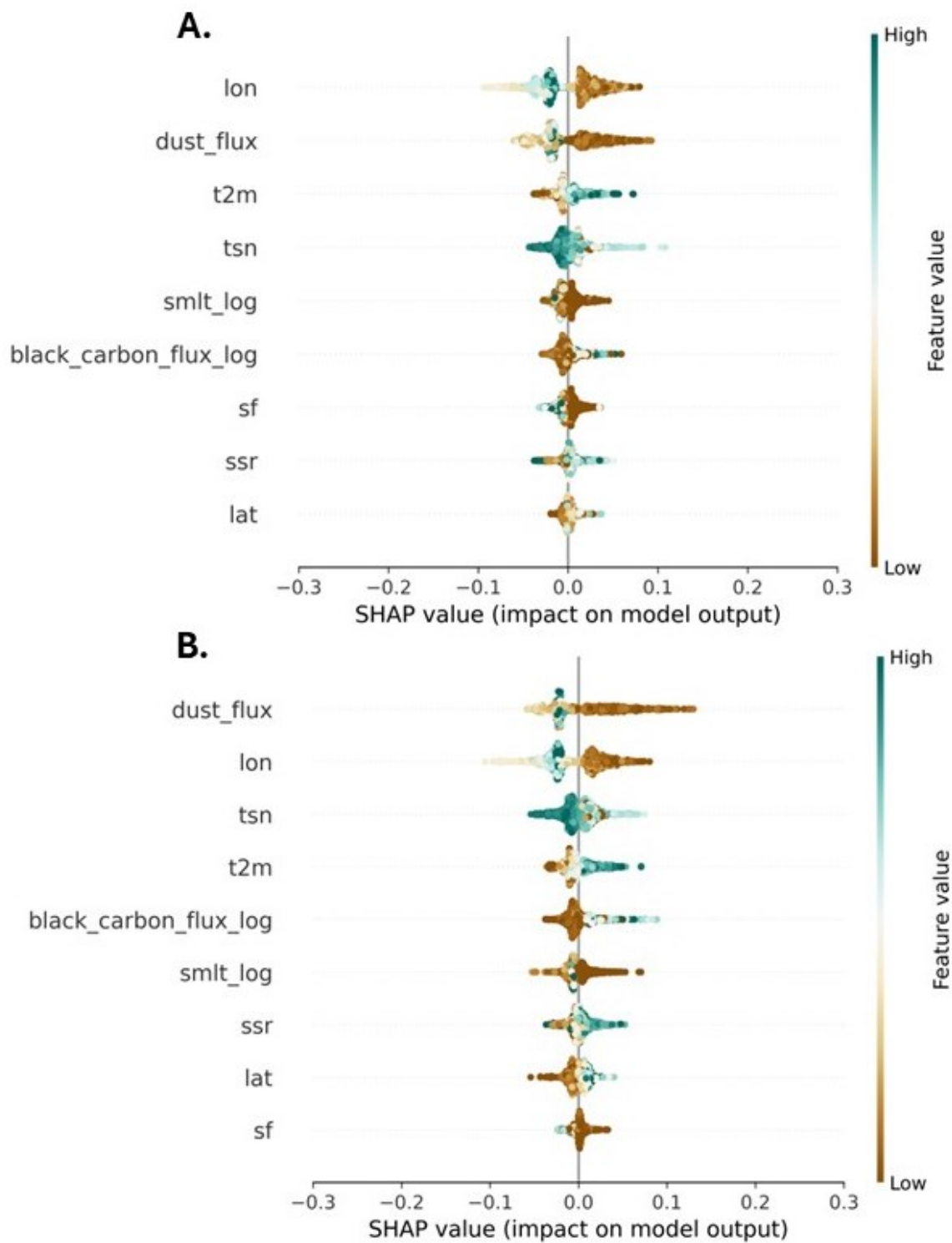
Figure 3-12: Beeswarm plots of SHAP values performed on the lag-year dataset for the A. random forest and B. XGBoost model.

3.6   Discussion

3.6.1   Variables Influence from the Main Models

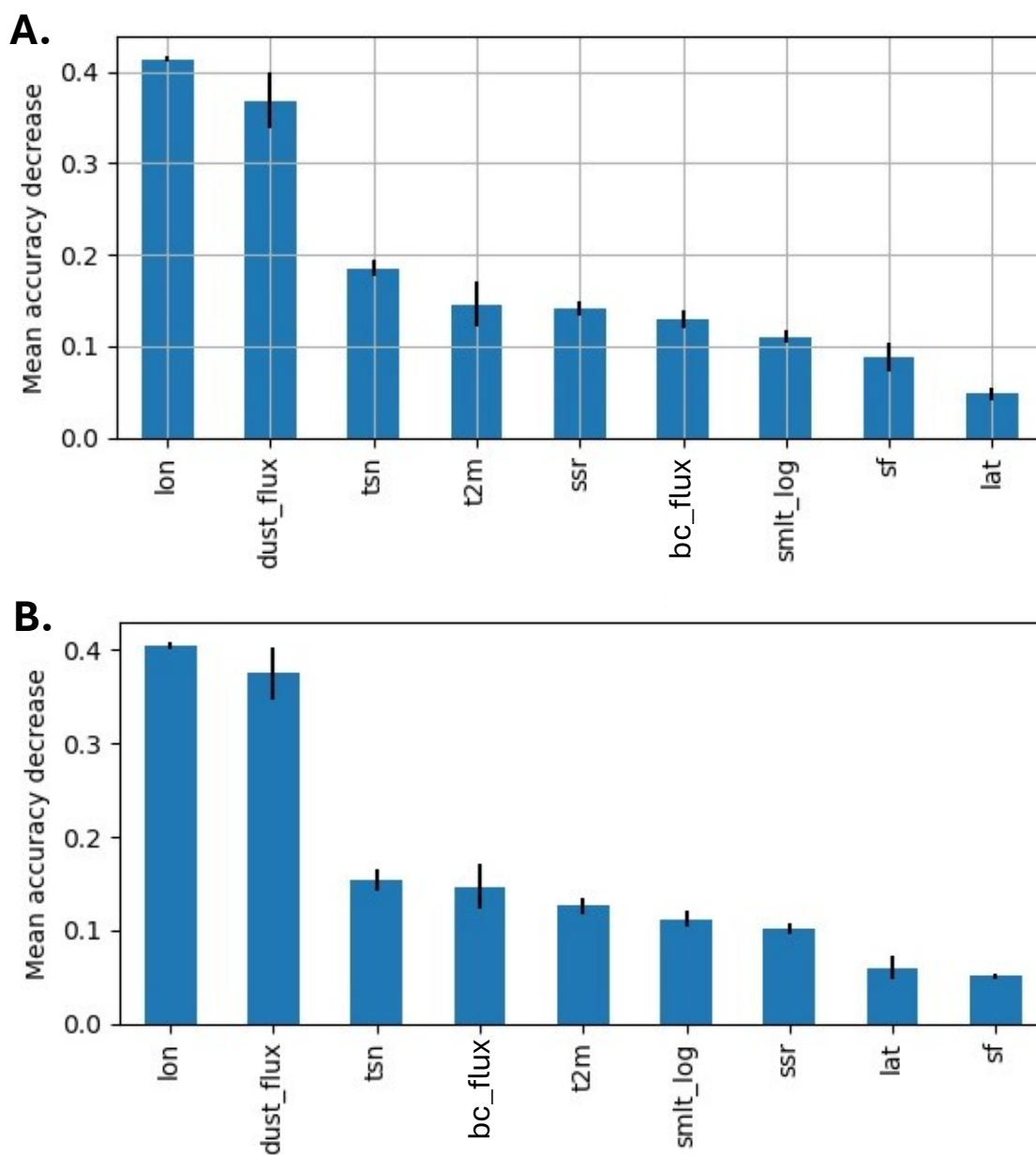The models' variable importance provides valuable knowledge on the influence of each variable on the occurrence of red snow algae. The combination and comparison of the two machine learning models consolidate the results. The section below explains the variables' influence and implication with previous studies.

Influence of Longitude

The models' feature importance indicates that the longitude is the most important predictor explaining the monthly red snow algae ratio, with low longitude values (eastern location) positively related to the bloom occurrence. In this study area, eastern longitudes indicate glaciers located further away from the coast, such as the Interior and Canadian Rocky Mountains. Previous studies observed a similar pattern in the distribution of red snow algae. Takeuchi et al. (2006) found that red snow algae were more predominant on the inland side of the Harding Icefield, Alaska than on the coastal side. They hypothesized that this spatial pattern was due to geographic effect on snow chemistry, such as higher sea salt content inhibiting snow algae propagation on the coastal side of the range and/or greater nutrient input from terrestrial aerosols on the continental side than the coastal side promoting algae growth. Similarly, Enstrom and Quarmy (2024) found that snow algae bloom preferentially grew on the lee side of the southern Coast Mountains. They associated the high concentration of algae blooms on the continental side with lower cloud cover and higher summer air temperatures than the coastal side of the range.

The SHAP value indicates that the red snow algae ratio increases along the eastern longitudes, suggesting that continental glaciers support a greater proportion of red snow algae in this study. The Interior and Rocky Mountains are the easternmost regions of the study area. Both regions depict a continental climate, with warm and dry summers and low cloud coverage. Additionally, because westerlies are the prevailing wind direction in Western Canada, the Interior and Rocky Mountains may receive greater amounts of terrestrial aerosols due to their inland and downwind location. The permutation feature importance indicates that the models' ability to predict red snow algae occurrence can decrease by up to 40% when longitude is removed as a predictor.

Influence of black carbon flux

The second most important variable in this study explaining red snow algae occurrence on glaciers is the black carbon flux, with increased black carbon flux contributing positively to the red snow algae ratio. Interestingly, the regions located directly downwind from the Interior Plateau, such as the southern Interior, central Rocky and southern Rocky Mountain, where most of the large forest fires occurred between 2015 and 2023, as depicted in Fig. 3-13, have the highest correlation coefficient between the red snow algae and black carbon flux. Due to their downwind location from frequent large forest fires, those three regions likely received high concentrations of black carbon during years of high fire activity, as observed by other studies (e.g. Marshall & Miller, 2020; Williamson & Menounos, 2021). Those three regions are also the most eastward locations from the study area, suggesting that the black carbon flux and longitude variables are co-related. In contrast, the eastern location may have the greatest influence on snow algae occurrence because they are the most impacted by black carbon.

It is not currently known if black carbon directly induces red algae growth. The results from this study indicate a positive relationship between the two. An explanation of the positive relationship between black carbon flux and the ratio of red snow algae is that the decrease in albedo from the black carbon increases liquid water content throughout the snowpack, which was found to be a limiting growth factor for red snow algae (Ganey et al., 2017). An alternative explanation is that black carbon provides a source of nutrients for the red snow algae, thus promoting growth.
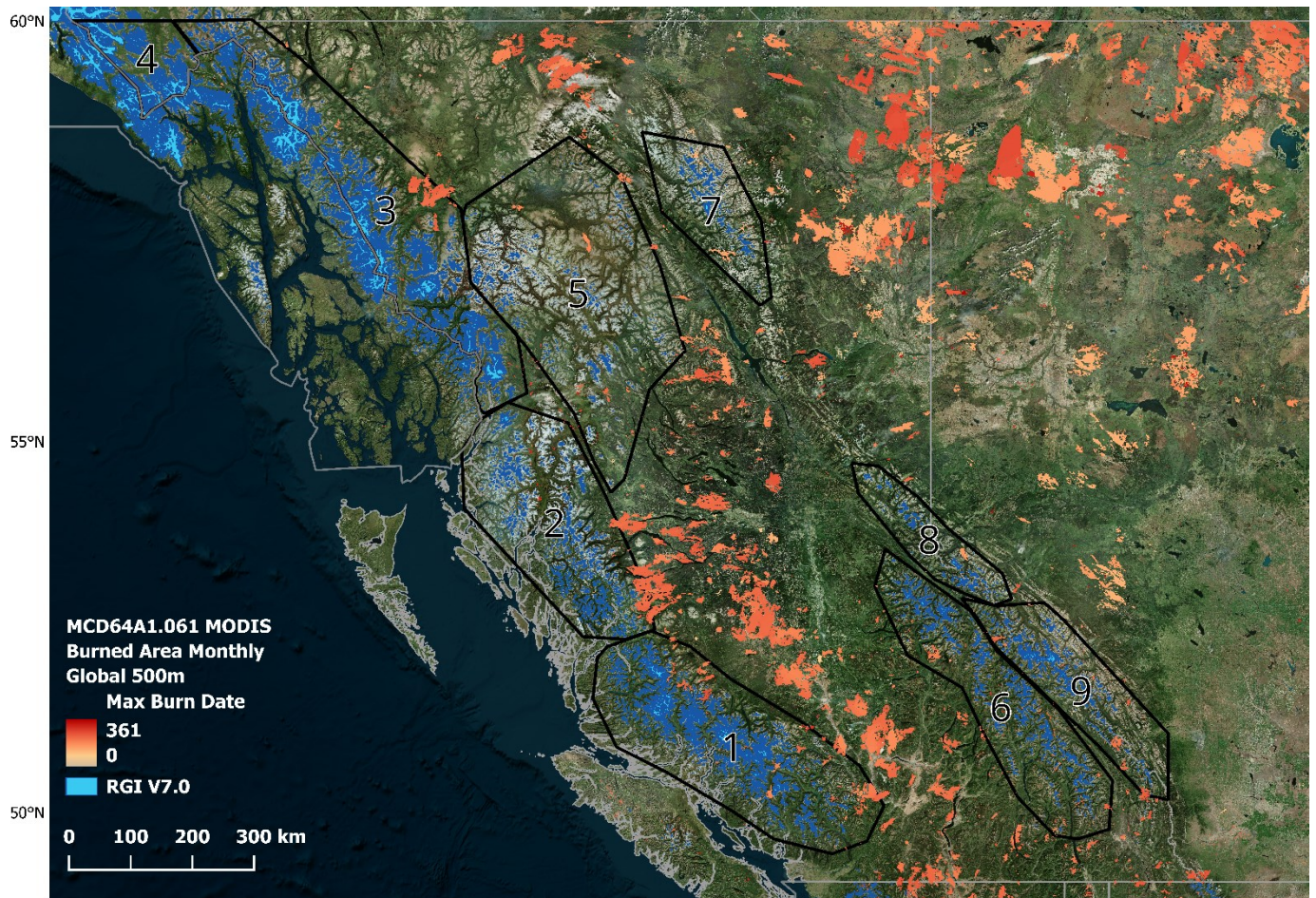

Figure 3-13: Burned area from 2015 to 2023 from MODIS Burned Area Monthly Global 500m.

Black carbon flux had a clear positive relationship with the red snow algae occurrence for the model performed on the monthly mean dataset only. The monthly max plots indicate that the lowest black carbon flux tends to have a negative impact on the red snow algae; however, the relationship for the rest of the black carbon flux is unclear. Likewise, the correlation between monthly max black carbon flux and red snow algae was generally lower than when calculated on the monthly mean dataset. This could be explained by the fact that the maximum value may introduce a bias in the dataset by representing a single event of rapid but intense duration releasing a high amount of black carbon over a short period into the atmosphere. Such events may not lead to significant black carbon deposition over glaciated terrain due to its brief duration, explaining the unclear relationship between large black carbon flux and red snow algae for the maximum dataset. In comparison, a large monthly mean black carbon flux likely represents a consistent input of black carbon in the atmosphere over a month, which is more likely to deposit black carbon on glaciers.

Influence of 2-metre air temperature

According to the Random Forest and XGBoost models, the 2-metre air temperature is an important variable explaining red snow algae occurrence on glaciers. This finding accords with previous studies that found red snow algae experience more growth or will expand under warm conditions (e.g. Onuma et al., 2022; Healy & Khan, 2023). One of the challenges, however, is the covariance between black carbon and surface air temperature, where years of high temperatures tend to be years with high forest fire activity. The SHAP beeswarm plots (Fig. 3-5) for the four models show that higher temperatures positively impact the red snow algae occurrence. This positive relationship can be explained by the fact that red snow algae require liquid water to bloom (Labourn Parry et al., 2000). Thus, warmer average air temperatures will

likely promote growth via increased meltwater and suitable areas for red snow algae. Cold temperatures, on the other side, can prevent snow algae bloom, such as in the St-Elias Mountains, where sparse algae blooms were linked to below-freezing average summer temperatures (Engstrom & Quarmy, 2024) or at high elevations where snow remains dry during the summer. Air temperature is also linked to other factors that may influence the occurrence of red snow algae bloom, such as the duration of the growth period and the precipitation type. Onuma et al. (2022) found that one of the main factors affecting snow algae growth was interruption from new snow covers, which is linked to cold air temperatures. Overall, the result suggests that warmer air temperature is positively related to the occurrence of red snow algae

Influence of dust flux

Dust flux contributes less than 20% of the model outcome. Its low explanation for the red snow algae ratio in the models from this study indicates that atmospheric dust flux is not a good predictor for red snow algae occurrence. These findings differ from previous studies that found snow algae growth is promoted by mineral dust from the local lithology. For example, in Greenland, phosphorous-rich mineral dust promotes ice algae growth (McCutcheon et al., 2021), and on stratovolcano in the Pacific Northwest, US, snow algae utilized Fe, Mn and P leached from local rocks (Hamilton & Havig, 2017). The dust flux used in the model was obtained from MERRA-2, which mainly captures dues aerosol from large barren and arid land regions such as the Sahara Desert and the North American desert, where strong winds transport soil particles into the atmosphere (Global Modeling and Assimilation Office (GMAO), 2015). Therefore, it is possible that global and regional dust flux patterns do not have a significant impact on snow algae. However, localized mineral dust, which may not be captured in MERRA-2, still provides the nutrients for snow algae. This process, however, was not captured in the model.

Predictors with low influence

The results show that surface net solar radiation, latitude, snowmelt, snow layer temperature, and snowfall have the lowest impact on snow algae occurrence with the lowest contribution to the model outcome. The model indicates that surface solar net radiation has minimal impact on the algae ratio. While red snow algae are photosynthetic microbes, net solar radiation does not negatively or positively impact growth in this study. Red snow algae blooms occur in Antarctica (e.g. Huovinen et al., 2018), in the Arctic (e.g. Lutz et al., 2017), and in alpine areas worldwide (e.g. Engstrom et al., 2020; Yoshimura et al.,1997). Yet, snow algae blooms do not differ between areas that receive additional solar radiation during the summer, such as the poles and at high elevations, versus lower latitudes and elevation areas where net solar radiation is lower. To adapt to the change in solar radiation and other environmental factors, studies observed a change in the red snow algae community structure with altitude (Takeuchi, 2013; Yoshimura et al., 1997) and locations (Engstrom et al., 2020; Lutz et al., 2016) instead.

Latitude was a variable of low importance overall. The model made no distinction between the north and south distribution of snow algae. Red snow algae blooms have been observed from the Sierra Nevada, California US (Painter et al., 2001) to the Eastern Alaska Mountains. While those two locations extend from 37.55 °N to 64°N along the North American Cordillera system, their maximum algae cell concentration in cells per meter square are both in the order of 10^7, supporting that latitude does not impact snow algae bloom.

The results show that snowmelt has a weak negative relation with red snow algae. In a previous study, the duration of snow cover throughout the summer season was noted to impact the bloom extent (Engstrom & Quarmby, 2024). Years with summer snowpack that persisted late into the season resulted in a large bloom extent. In contrast, in 2021, during the Pacific

Northwest heat wave, early snow loss over Western Canada and the Pacific Northwest US was linked to a weak snow algae bloom. The snowfall, which was moderately to highly correlated with snowmelt, is a variable with a low or no explanation for the red snow algae occurrence in the models. In Onuma et al. (2022) snow algae model, snowfall events impacted the timing of red snow algae appearance and could temporarily reduce snow algae growth. In this study, snowfall is not an important variable for red snow algae. An explanation for the lack of importance of snowfall can be related to the differences in the temporal resolution of the datasets. Daily snowfall may impact red snow algae growth; however, when averaged over the month, the snowfall effect is likely too small to be picked up by the model. The temperature of the snow layer is also of low importance for the algae occurrence in the models. Red snow algae blooms are restricted to periods when liquid water is available (Laybourn-Parry et al., 2012). Liquid water content in the snowpack decreases rapidly when the snow temperature drops below 0°C (Pomeroy & Brun, 2010). In this study, snow layer temperature was not a good proxy for liquid water availability.

3.6.2 Annual models and black carbon lag year models

Annual models

I ran the annual models to assess whether the years of high fire activity yield better predictions. The models' performance did not vary accordingly and explained about 40% of the results except for 2018 and 2019. The 2018 model performed relatively well, with an R^2 score of 0.7 and the 2019 performed poorly, with an average R^2 of 0.1. The 2019 dataset, compared to the other years, has more noise, outliers and extreme values, making it hard for the model to capture meaningful relationships and thus create an accurate prediction. This explains why the 2019 model performed poorly. As for 2018 performance, it may be due to a higher correlation between

variables, greater variation in the predictor variables or clean patterns in the 2018 data compared to the other datasets. The 2018 season was a high forest fire year in British Columbia, however, it is the only year with high forest fire activity with an elevated R2 score. Therefore, it does not provide an explanation for high forest fire season leading to better predictions.

The overall lower performance compared to the main model may be explained by the small dataset used to run the annual model. The size of the dataset can also influence the variables' importance. The annual models were run on datasets with approximately 150 data points. Such low data points can lead the model to rank irrelevant variables as important because those variables are the best at explaining noise in the dataset. Small datasets can also influence the ranking of variable importance due to the limited examples of certain relationships between the different predictors and the target variable, leading to incorrect attributes of variable importance. While most variables varied in importance among the nine annual models, the dust flux and longitude consistently ranked as the top two variables with the most influence on the algae ratio. The SHAP beeswarm plots (Appendix G, Fig G.1-18) indicate that low dust flux and eastward longitude are linked to high algae ratio, agreeing with the findings from the main models.

Lag year model

I perform the lag year model to assess whether a lag year relationship exists between black carbon and algae, in which red snow algae are more predominant in years following high forest fire season. The lag year model performed similarly to the main model. However, the variable importance differs slightly compared to the main model. In the lag year model, black carbon is not among the top predictors, and the dust flux and temperature of the snow layer became more important. The black carbon is likely not an important predictor in the lag year

model as it refers to the monthly black carbon from the previous year. In the main model, black carbon is one of the strongest predictors and is positively related to the red snow algae ratio. Thus, using the monthly black carbon from the previous year likely leads to irrelevant patterns or correlations with the current red snow algae, explaining why it is not rated as an important predictor for that model. The dust flux, then, likely becomes more important to fill the gap introduced by the lag year black carbon data points. The lag year model does not provide evidence that years following high fire season lead to strong red snow algae bloom. The lag year model likely performs similarly to the main model as both random forest and XGBoost rely on aggregating multiple weak trees, making those models less sensitive to removing individual variables. The model may also find some level of relationship between the lag year black carbon and red snow algae, thus resulting in an unchanged performance score.

3.6.3   Models Performance and Associate Limitations

The performance of the random forest and XGBoost models was evaluated using independent test datasets. The main models performed moderately well, with the best performance attained on the monthly mean datasets in both models. This is likely because the maximum datasets capture the monthly extreme, which may not provide a good proxy for modelling the red snow algae occurrence, as the extremes are not representative of the general trend over the month and can bias the model. While both models provide similar performance, utilizing multiple machine-learning algorithms improves the robustness of the performance and interpretability of the models' results. While the models did not fully capture all the variables that contribute toward the occurrence of red snow algae blooms, they contributed to improving our understanding of the relevant drivers to model red snow algae bloom and suggest that black carbon may positively influence red snow algae.

The annual models' performed on average moderately weak. Those models were run on a much smaller dataset, as explained above; therefore, it is not surprising to observe a lower performance. Since small datasets contain fewer data points, the diversity and variability in the data are generally lower than for large datasets. Moreover, since random forest and XGBoost rely on the data to capture patterns and relationships, the small dataset may not provide enough information to the model to result in accurate predictions or trends among the data may be too weak for the model to detect. Small datasets can also lead to higher model bias because there is less data to approximate the true relationship. This would explain why the main and lag-year models performed better, as they were run on much larger datasets.

The uncertainties and biases associated with the predictor variables and target value ultimately affect the models' performance. In terms of target value, although the RGND has been widely used in previous studies to map and quantify snow algae (e.g. Ganey et al., 2017; Huovinen et al., 2018), it can overestimate the extent of red snow algae bloom. For example, Healy & Khan (2023) found that their optimized red/green band index applied to the MicaSense bands tends to overestimate the extent of the algae bloom in the late season when debris-covered snow is more common. However, they found that the red/green index had the most success at mapping snow algae in their study compared to a machine learning method. To minimize the uncertainty related to the index, I followed the approach suggested by (Di Mauro et al., 2024) to mask rockfall and debris prior to applying the RGND index.

The use of meteorological reanalysis data such as ERA5-Land can result in bias, especially in mountainous locations where ground stations are sporadic. Zhao & He (2022) report through correlation and RMSE analysis that while ERA5-Land properly captured the temperature trends over the Chinese Qilian Mountains, the value scale is not adequately

represented. Similarly, in a study evaluating ERA5-Land reanalysis as an input dataset for surface energy balance modelling over mountain glaciers in Western Canada, Draeger et al. (2024) found that ERA5-Land simulated the mean melt energy well if the temperature is corrected through a lapse rate. While accurate magnitudes in temperature value are needed to simulate daily melt energy, the monthly trend likely provides sufficient information for modelling the occurrence of red snow algae as it is not based on energy balance calculation. As for the snow variables, a study evaluating the snow cover properties of ERA5-Land found that the snow cover extent is accurately represented compared to satellite-based datasets (Kouki et al., 2023). Due to ERA5-Land being a relatively new product, evaluation of the net surface solar radiation, snowmelt, and temperature of the snow layer has yet to be conducted.

The coarse resolution of the ERA5-Land dataset introduces some limitations as meteorological values vary widely spatially and vertically. In terms of snow data in the model, snowmelt and snow temperature vary with elevation, which is not captured in the current model. The current grid size generally covers the entire glacier surface for the small-scale glaciers, or a small aggregate of grid points covers the large icefields. Resolving this lack of resolution in the dataset could help increase the accuracy of the model overall.

Another limitation of the models is related to the MERRA-2 black carbon aerosol datasets and the assumption that most black carbon aerosols are emitted by forest fires rather than anthropogenic sources. No studies have characterized the provenance of aerosols deposited over glacier surfaces in western Canada. A study from the Pacific Northwest, US, however, found that radiative forcing from black carbon over snow and ice was generally low except for regions that are being impacted by forest fires (Skiles et al., 2018), suggesting that forest fire aerosols likely dominate black carbon deposition in mountainous areas in Western Canada.

Moreover, previous studies investigating black carbon concentration produced during forest fires in 2019 in Indonesia (Julian Sari et al., 2022) and from forest fires in Siberia between 2000 and 2016 (Sitnov et al., 2020) found a good positive correlation between BC aerosols from MERRA-2 and forest fire hot spot.

3.7   Conclusions

Here, I assessed the interaction between black carbon, red snow algae and multiple other environmental, climatic and geographical variables using decision-tree-based random forest regressor and XGBoost machine learning models. The two main algorithms performed moderately well at predicting the occurrence of red snow algae when compared to the testing dataset. The models' performance suggests that the predictor variables explained part of the red snow algae distribution but that other variables likely played a role in this complex phenomenon. Due to the limited availability of widespread datasets of snow wetness covering all Western Canada, the models did not include a predictor for snow liquid water content. Previous studies identified snow wetness as a limiting factor controlling snow algae growth and appearance; thus, integrating a value to quantify snow-liquid water would likely increase the model accuracy. In this study, the data was constrained to the coarse spatial resolution from freely available satellite imagery, meteorological reanalysis, and aerosol datasets, as well as the intermittent temporal availability of multispectral satellite imagery. Applying the model to a finer spatial and temporal resolution would capture subtle localized and seasonal effects that were missed in this model.

The most important variables that explained red snow algae occurrence in the models are longitudes, black carbon and surface air temperatures. The positive relationship between snow algae and air temperatures aligns with previous studies that suggest that the red snow algae range is likely to expand with warming temperatures. Based on the geographical location of the study

area, the easternmost location had the strongest impact on the red snow algae. Those eastern regions also have the strongest correlation between snow algae and black carbon, likely due to their location downwind from the major forest fires that happened between 2015 and 2023. Therefore, those results suggest that black carbon may induce snow algae growth, although further studies observing the direct relationship are needed to confirm the interaction.

This study shows that leveraging machine learning can further our understanding of the factors controlling the distribution of red snow algae blooms. It also shows that machine learning is a powerful tool for investigating the interactions between glacier-darkening processes such as snow algae and black carbon. Understanding the different factors influencing the distribution and occurrence of red snow algae bloom enhances our ability to simulate glacier albedo and predict glacier melt.

4 Chapter 4: Thesis Conclusions

This thesis investigated the relationship between red snow algae and black carbon via two methodologies. First, I described and presented the findings from the field experiment I conducted on Place Glacier during the summer of 2023, where I fertilized snow with wood ash and compared snow algae growth and snow melt from a control and treated group. Second, I applied random forest and XGBoost models using data from the Harmonized Landsat Sentinel dataset, Merra-2 aerosol product and ERA5-Land climate reanalysis dataset to assess the importance of various variables, including black carbon in modelling red snow algae occurrence. Understanding interactions between glacier surface darkening agents such as red snow algae and black carbon from forest fires provides insight into glacier albedo processes. Since, surface glacier ablation is controlled mainly by surface air temperature and albedo, understanding the interaction between surface darkening processes helps to improve our ability to predict glacier albedo and surface melt. The significant findings of this study are as follows:

- The field experiment presents no statistical evidence that wood ash enhances red snow algae growth.

- During the early bloom stage, the instantaneous radiative forcing of red snow algae in the southern Coast Mountains of British Columbia I calculated was, on average, 192 ± 12 W m^{-2} with a maximum of 274 ± 16 W m^{-2}. This increase in radiative forcing translates to a melt potential of 27.8 mm w.e. d^{-1}. Those results support previous studies that found that snowmelt induced by red snow algae is sufficient to increase glacier melt rates.

- The random forest and XGBoost models suggest that black carbon flux from forest fire positively influences red snow algae blooms. The models also imply that the occurrence

of red snow algae bloom is a complex phenomenon and that other factors likely influence the distribution and occurrence of the blooms.

- Red snow algae bloom in British Columbia and Alberta preferentially grows on continental glaciers. Those regions are adjacent to the main area affected by large forest fires in British Columbia supporting the idea that black carbon may promote red snow algae growth.

A few main limitations inherently constrain the findings from this study. First, the temporal resolution of the data from the field experiment and the remote sensing analysis limits the quality of the results as the two analyses relied on temporally fixed data points. The field experiment relied on three field visits, making a small dataset despite having multiple replicates, limiting the statistical power of the analysis and the ability to capture the natural variability in the trends. Moreover, with only three field visits, the dataset is more sensitive to human errors and incidents. For instance, on the third field visit, the snow had melted in most of the plots, significantly reducing the representativeness of the data and complicating trend analysis. To mitigate these challenges, using automated instruments such as automated ablation stakes, temperature sensors, and time-lapse cameras would help to supplement the in-person data collection. On the other end, the remote sensing analysis was limited by the availability of satellite imagery. Satellite imagery from the Harmonized Landsat Sentinel dataset is constrained by the re-visit time and obstruction from clouds. Consequently, cloud-free images are not available at regular time intervals, especially when acquired over a large study area as used in this study, making it difficult to create time series. The use of monthly datasets instead of a continuous time series limits the ability of the analysis to capture short-term environmental variations or trends that could be significant for red snow algae growth. Moreover, identifying

precise timing and sequence of ephemeral factors driving algae bloom growth, such as summer snowfall, becomes challenging when using monthly data.

Second, red snow algae are an intricate phenomenon, and while machine learning models such as random forest and XGBoost are great tools for capturing complex patterns, the performance and accuracy of the models are limited by the data inputs. Utilizing remote sensing and reanalysis datasets allowed me to apply the model to a large study area; however, it limited the variable inputs to readily available datasets. For example, the black carbon and dust flux datasets refer to aerosol rather than deposited aerosols over glaciers, leading to the assumption that high concentrations of atmospheric black carbon and dust lead to large deposition rates over glaciers. Previous studies found that red snow algae are limited by the availability of liquid water (eg. Ganey et al., 2017); however, identifying snow wetness over glaciers is challenging. Therefore, the model did not include snow wetness even though it has been found to influence snow algae distribution and growth.

To conclude, here are a few suggestions that can be undertaken from this thesis for future research. First, the interaction between black carbon and red snow algae could be further analyzed via a nutrient addition incubation experiment as conducted by McCutcheon et al. (2021). While snow algae cultivation generally targets one species, such an experiment would allow complete control of exterior factors and directly investigate the interaction between the algae and the black carbon. This experiment, however, would only assess whether the algae utilized the black carbon as a source of nutrients and would not evaluate if the increased liquid water from the black carbon radiative forcing led to increased algae growth. A second recommendation is to increase the temporal and spatial resolution of the dataset used in the machine learning models by applying the model to multiple small regions, or target regions

adjacent to frequent forest fire activity. By doing so, the model could capture fine-scale variations in environmental factors such as snowpack characteristics, microclimate or terrain conditions that may influence snow algae blooms. Increasing the temporal resolution would help to capture short-term changes in the weather and extremes such as snowfall and heatwave events or rapidly changing snowpack conditions. Finally, glacier melt models should quantify albedo change with respect to biological LAPs and inorganic LAPs. As Chapter two findings indicate, red snow algae snowmelt contribution is substantial and needs to be considered in the glacier melt rates. Considerations should also be taken for the interactions between red snow algae and inorganic LAPs.

5 References

Anesio, A. M., & Laybourn-Parry, J. (2012). Glaciers and ice sheets as a biome. *Trends in Ecology & Evolution*, *27*(4), 219–225. https://doi.org/https://doi.org/10.1016/j.tree.2011.09.012

Ardyna, M., Hamilton, D. S., Harmel, T., Lacour, L., Bernstein, D. N., Laliberté, J., Horvat, C., Laxenaire, R., Mills, M. M., van Dijken, G., Polyakov, I., Claustre, H., Mahowald, N., & Arrigo, K. R. (2022). Wildfire aerosol deposition likely amplified a summertime Arctic phytoplankton bloom. *Communications Earth & Environment*, *3*(1), 201. https://doi.org/10.1038/s43247-022-00511-9

Aubry-Wake, C., Bertoncini, A., & Pomeroy, J. W. (2022). Fire and Ice: The Impact of Wildfire-Affected Albedo and Irradiance on Glacier Melt. *Earth's Future*, *10*(4), e2022EF002685. https://doi.org/10.1029/2022EF002685

Barnaba, F., Angelini, F., Curci, G., & Gobbi, G. P. (2011). An important fingerprint of wildfires on the European aerosol load. *Atmospheric Chemistry and Physics*, *11*(20), 10487–10501. https://doi.org/10.5194/acp-11-10487-2011

Bevington, A. R., & Menounos, B. (2022). Accelerated change in the glaciated environments of western Canada revealed through trend analysis of optical satellite imagery. *Remote Sensing of Environment*, *270*, 112862. https://doi.org/https://doi.org/10.1016/j.rse.2021.112862

Bolch, T., Menounos, B., & Wheate, R. (2010). Landsat-based inventory of glaciers in western Canada, 1985-2005. *Remote Sensing of Environment*, *114*(1), 127–137. https://doi.org/10.1016/j.rse.2009.08.015

Bonsal, B., Shrestha, R. R., Dibike, Y., Peters, D. L., Spence, C., Mudryk, L., & Yang, D. (2020a). Western Canadian freshwater availability: current and future vulnerabilities. *Environmental Reviews*, *28*(4), 528–545. https://doi.org/10.1139/er-2020-0040

Bonsal, B., Shrestha, R. R., Dibike, Y., Peters, D. L., Spence, C., Mudryk, L., & Yang, D. (2020b). Western Canadian freshwater availability: current and future vulnerabilities. *Environmental Reviews*, *28*(4), 528–545. https://doi.org/10.1139/er-2020-0040

Box, J. E., Fettweis, X., Stroeve, J. C., Tedesco, M., Hall, D. K., & Steffen, K. (2012). Greenland ice sheet albedo feedback: thermodynamics and atmospheric drivers. *The Cryosphere*, *6*(4), 821–839. https://doi.org/10.5194/tc-6-821-2012

Breiman, L. (2001). *Random Forests* (Vol. 45).

Chen, T., & Guestrin, C. (2016). XGBoost: A scalable tree boosting system. *Proceedings of the ACM SIGKDD International Conference on Knowledge Discovery and Data Mining*, *13-17-August-2016*, 785–794. https://doi.org/10.1145/2939672.2939785

Chen, X., Kang, S., Yang, J., & Hu, Y. (2023). Contributions of biomass burning in 2019 and 2020 to Arctic black carbon and its transport pathways. *Atmospheric Research*, *296*, 107069. https://doi.org/https://doi.org/10.1016/j.atmosres.2023.107069

Chevrollier, L.-A., Cook, J. M., Halbach, L., Jakobsen, H., Benning, L. G., Anesio, A. M., & Tranter, M. (2022). Light absorption and albedo reduction by pigmented microalgae on snow and ice. *Journal of Glaciology*, 1–9. https://doi.org/10.1017/JOG.2022.64

Clarke, G. K. C., Jarosch, A. H., Anslow, F. S., Radić, V., & Menounos, B. (2015). Projected deglaciation of western Canada in the twenty-first century. *Nature Geoscience 2014 8:5*, *8*(5), 372–377. https://doi.org/10.1038/ngeo2407

Claverie, M., Ju, J., Masek, J. G., Dungan, J. L., Vermote, E. F., Roger, J.-C., Skakun, S. V, & Justice, C. (2018). The Harmonized Landsat and Sentinel-2 surface reflectance data set. *Remote Sensing of Environment*, *219*, 145–161. https://doi.org/https://doi.org/10.1016/j.rse.2018.09.002

Coogan, S. C. P., Robinne, F.-N., Jain, P., & Flannigan, M. D. (2019). Scientists' warning on wildfire — a Canadian perspective. *Canadian Journal of Forest Research*, *49*(9), 1015–1023. https://doi.org/10.1139/cjfr-2019-0094

Cook, J. M., Hodson, A. J., Taggart, A. J., Mernild, S. H., & Tranter, M. (2017). A predictive model for the spectral "bioalbedo" of snow. *Journal of Geophysical Research: Earth Surface*, *122*(1), 434–454. https://doi.org/https://doi.org/10.1002/2016JF003932

Cook, J. M., Tedstone, A. J., Williamson, C., McCutcheon, J., Hodson, A. J., Dayal, A., Skiles, M., Hofer, S., Bryant, R., McAree, O., McGonigle, A., Ryan, J., Anesio, A. M., Irvine-Fynn, T. D. L., Hubbard, A., Hanna, E., Flanner, M., Mayanna, S., Benning, L. G., … Tranter, M. (2020). Glacier algae accelerate melt rates on the south-western Greenland Ice Sheet. *The Cryosphere*, *14*(1), 309–330. https://doi.org/10.5194/tc-14-309-2020

Di Mauro, B. (2020). A darker cryosphere in a warming world. *Nature Climate Change*, *10*(11), 979–980. https://doi.org/10.1038/s41558-020-00911-9

Di Mauro, B., Fava, F., Ferrero, L., Garzonio, R., Baccolo, G., Delmonte, B., & Colombo, R. (2015). Mineral dust impact on snow radiative properties in the European Alps combining

ground, UAV, and satellite observations. *Journal of Geophysical Research: Atmospheres*, *120*(12), 6080–6097. https://doi.org/https://doi.org/10.1002/2015JD023287

Di Mauro, B., Garzonio, R., Ravasio, C., Orlandi, V., Baccolo, G., Gilardoni, S., Remias, D., Leoni, B., Rossini, M., & Colombo, R. (2024). Combined effect of algae and dust on snow spectral and broadband albedo. *Journal of Quantitative Spectroscopy and Radiative Transfer*, *316*, 108906. https://doi.org/https://doi.org/10.1016/j.jqsrt.2024.108906

Donahue, C. P., Menounos, B., Viner, N., Skiles, S. M., Beffort, S., Denouden, T., Arriola, S. G., White, R., & Heathfield, D. (2023). Bridging the gap between airborne and spaceborne imaging spectroscopy for mountain glacier surface property retrievals. *Remote Sensing of Environment*, *299*, 113849. https://doi.org/https://doi.org/10.1016/j.rse.2023.113849

Dumont, M., Gardelle, J., Sirguey, P., Guillot, A., Six, D., Rabatel, A., & Arnaud, Y. (2012). Linking glacier annual mass balance and glacier albedo retrieved from MODIS data. *The Cryosphere*, *6*(6), 1527–1539. https://doi.org/10.5194/tc-6-1527-2012

Engstrom, C. B., & Quarmby, L. M. (2024). Satellite mapping of red snow on North American glaciers. *Science Advances*, *9*(47), eadi3268. https://doi.org/10.1126/sciadv.adi3268

Engstrom, C. B., Williamson, S. N., Gamon, J. A., & Quarmby, L. M. (2022). Seasonal development and radiative forcing of red snow algal blooms on two glaciers in British Columbia, Canada, summer 2020. *Remote Sensing of Environment*, *280*, 113164. https://doi.org/https://doi.org/10.1016/j.rse.2022.113164

Flanner, M. G., Arnheim, J. B., Cook, J. M., Dang, C., He, C., Huang, X., Singh, D., Skiles, S. M., Whicker, C. A., & Zender, C. S. (2021). SNICAR-ADv3: a community tool for

modeling spectral snow albedo. *Geoscientific Model Development*, *14*(12), 7673–7704.

https://doi.org/10.5194/gmd-14-7673-2021

Flanner, M. G., Zender, C. S., Randerson, J. T., & Rasch, P. J. (2007). Present-day climate

forcing and response from black carbon in snow. *Journal of Geophysical Research:*

Atmospheres, *112*(D11). https://doi.org/https://doi.org/10.1029/2006JD008003

Friedman, J. H. (2001). Greedy function approximation: A gradient boosting machine. *The*

Annals of Statistics, *29*(5), 1189–1232. https://doi.org/10.1214/aos/1013203451

Ganey, G. Q., Loso, M. G., Burgess, A. B., & Dial, R. J. (2017). The role of microbes in

snowmelt and radiative forcing on an Alaskan icefield. *Nature Geoscience 2017 10:10*,

10(10), 754–759. https://doi.org/10.1038/ngeo3027

Gelaro, R., McCarty, W., Suárez, M. J., Todling, R., Molod, A., Takacs, L., Randles, C. A.,

Darmenov, A., Bosilovich, M. G., Reichle, R., Wargan, K., Coy, L., Cullather, R., Draper,

C., Akella, S., Buchard, V., Conaty, A., da Silva, A. M., Gu, W., … Zhao, B. (2017). The

modern-era retrospective analysis for research and applications, version 2 (MERRA-2).

Journal of Climate, *30*(14), 5419–5454. https://doi.org/10.1175/JCLI-D-16-0758.1

Government of British Columbia. (2024, April 26). *Wildfire Averages*.

Gray, A., Krolikowski, M., Fretwell, P., Convey, P., Peck, L. S., Mendelova, M., Smith, A. G., &

Davey, M. P. (2020). Remote sensing reveals Antarctic green snow algae as important

terrestrial carbon sink. *Nature Communications*, *11*(1), 2527.

https://doi.org/10.1038/s41467-020-16018-w

Hadley, O. L., & Kirchstetter, T. W. (2012a). Black-carbon reduction of snow albedo. *Nature Climate Change*, *2*(6), 437–440. https://doi.org/10.1038/nclimate1433

Hadley, O. L., & Kirchstetter, T. W. (2012b). Black-carbon reduction of snow albedo. *Nature Climate Change*, *2*(6), 437–440. https://doi.org/10.1038/nclimate1433

Hadley, O. L., & Kirchstetter, T. W. (2012c). Black-carbon reduction of snow albedo. *Nature Climate Change*, *2*(6), 437–440. https://doi.org/10.1038/nclimate1433

Hamilton, T. L., & Havig, J. (2017). Primary productivity of snow algae communities on stratovolcanoes of the Pacific Northwest. *Geobiology*, *15*(2), 280–295. https://doi.org/10.1111/GBI.12219

Hamilton, T. L., & Havig, J. R. (2020). Inorganic carbon addition stimulates snow algae primary productivity. *The ISME Journal*, *14*(3), 857–860. https://doi.org/10.1038/s41396-018-0048-6

Hanes, C. C., Wang, X., Jain, P., Parisien, M.-A., Little, J. M., & Flannigan, M. D. (2018). Fire-regime changes in Canada over the last half century. *Canadian Journal of Forest Research*, *49*(3), 256–269. https://doi.org/10.1139/cjfr-2018-0293

Healy, S. M., & Khan, A. L. (2023). Albedo change from snow algae blooms can contribute substantially to snow melt in the North Cascades, USA. *Communications Earth & Environment*, *4*(1), 142. https://doi.org/10.1038/s43247-023-00768-8

Hock, R., Bliss, A., Marzeion, B. E. N., Giesen, R. H., Hirabayashi, Y., Huss, M., Radić, V., & Slangen, A. B. A. (2019a). GlacierMIP – A model intercomparison of global-scale glacier

mass-balance models and projections. *Journal of Glaciology*, *65*(251), 453–467.
https://doi.org/DOI: 10.1017/jog.2019.22

Hock, R., Bliss, A., Marzeion, B. E. N., Giesen, R. H., Hirabayashi, Y., Huss, M., Radić, V., &
Slangen, A. B. A. (2019b). GlacierMIP – A model intercomparison of global-scale glacier
mass-balance models and projections. *Journal of Glaciology*, *65*(251), 453–467.
https://doi.org/DOI: 10.1017/jog.2019.22

Hodson, A. J., Sabacka, M., Dayal, A., Edwards, A., Cook, J., Convey, P., Redeker, K., & Pearce,
D. A. (2021). Marked Seasonal Changes in the Microbial Production, Community
Composition, and Biogeochemistry of Glacial Snowpack Ecosystems in the Maritime
Antarctic. *Journal of Geophysical Research Biogeosciences*, *126*(7).
https://doi.org/10.1029/2020jg005706

Hugonnet, R., McNabb, R., Berthier, E., Menounos, B., Nuth, C., Girod, L., Farinotti, D., Huss,
M., Dussaillant, I., Brun, F., & Kääb, A. (2021). Accelerated global glacier mass loss in the
early twenty-first century. *Nature*, *592*(7856), 726–731. https://doi.org/10.1038/s41586-021-
03436-z

Huovinen, P., Ramírez, J., & Gómez, I. (2018). Remote sensing of albedo-reducing snow algae
and impurities in the Maritime Antarctica. *ISPRS Journal of Photogrammetry and Remote
Sensing*, *146*, 507–517. https://doi.org/https://doi.org/10.1016/j.isprsjprs.2018.10.015

Huss, M. (2011). Present and future contribution of glacier storage change to runoff from
macroscale drainage basins in Europe. *Water Resources Research*, *47*(7).
https://doi.org/https://doi.org/10.1029/2010WR010299

Huss, M., & Hock, R. (2018). Global-scale hydrological response to future glacier mass loss. *Nature Climate Change*, *8*(2), 135–140. https://doi.org/10.1038/s41558-017-0049-x

Jensen, A. R., Anderson, K. S., Holmgren, W. F., Mikofski, M. A., Hansen, C. W., Boeman, L. J., & Loonen, R. (2023). pvlib iotools—Open-source Python functions for seamless access to solar irradiance data. *Solar Energy*, *266*, 112092. https://doi.org/10.1016/j.solener.2023.112092

Jones, H. G., Pomeroy, J. W., Walker, D. A., & Hoham, R. W. (2001). *Snow Ecology: An Interdisciplinary Examination of Snow-Covered Ecosystems* (1st ed.). Cambridge University Press.

Jost, G., Moore, R. D., Menounos, B., & Wheate, R. (2012). Quantifying the contribution of glacier runoff to streamflow in the upper Columbia River Basin, Canada. *Hydrology and Earth System Sciences*, *16*(3), 849–860. https://doi.org/10.5194/hess-16-849-2012

Kang, S., Zhang, Y., Qian, Y., & Wang, H. (2020). A review of black carbon in snow and ice and its impact on the cryosphere. *Earth-Science Reviews*, *210*, 103346. https://doi.org/https://doi.org/10.1016/j.earscirev.2020.103346

Kaspari, S. D., Pittenger, D., Jenk, T. M., Morgenstern, U., Schwikowski, M., Buenning, N., & Stott, L. (2020). Twentieth Century Black Carbon and Dust Deposition on South Cascade Glacier, Washington State, USA, as Reconstructed From a 158-m-Long Ice Core. *Journal of Geophysical Research: Atmospheres*, *125*(11), e2019JD031126. https://doi.org/https://doi.org/10.1029/2019JD031126

Kaspari, S., McKenzie Skiles, S., Delaney, I., Dixon, D., & Painter, T. H. (2015). Accelerated glacier melt on Snow Dome, Mount Olympus, Washington, USA, due to deposition of black

carbon and mineral dust from wildfire. *Journal of Geophysical Research: Atmospheres*, *120*(7), 2793–2807. https://doi.org/https://doi.org/10.1002/2014JD022676

Keegan, K. M., Albert, M. R., McConnell, J. R., & Baker, I. (2014). Climate change and forest fires synergistically drive widespread melt events of the Greenland Ice Sheet. *Proceedings of the National Academy of Sciences*, *111*(22), 7964–7967. https://doi.org/10.1073/pnas.1405397111

Khan, A. L., Dierssen, H. M., Scambos, T. A., Höfer, J., & Cordero, R. R. (2021). Spectral characterization, radiative forcing and pigment content of coastal Antarctic snow algae: approaches to spectrally discriminate red and green communities and their impact on snowmelt. *The Cryosphere*, *15*(1), 133–148. https://doi.org/10.5194/tc-15-133-2021

Kim, Y., Hatsushika, H., Muskett, R., & Yamazaki, K. (2005). Possible Effect of Black Carbon Wildfire Soot on Arctic Sea Ice and Alaska Glaciers. *AGU Fall Meeting Abstracts*, *39*.

Kondo, Y., Matsui, H., Moteki, N., Sahu, L., Takegawa, N., Kajino, M., Zhao, Y., Cubison, M. J., Jimenez, J. L., Vay, S., Diskin, G. S., Anderson, B., Wisthaler, A., Mikoviny, T., Fuelberg, H. E., Blake, D. R., Huey, G., Weinheimer, A. J., Knapp, D. J., & Brune, W. H. (2011). Emissions of black carbon, organic, and inorganic aerosols from biomass burning in North America and Asia in 2008. *Journal of Geophysical Research: Atmospheres*, *116*(D8). https://doi.org/https://doi.org/10.1029/2010JD015152

L., W. A., G., H. H., R., C. D., & W., S. T. (2006). Warming and Earlier Spring Increase Western U.S. Forest Wildfire Activity. *Science*, *313*(5789), 940–943. https://doi.org/10.1126/science.1128834

Laybourn-Parry, J., Tranter, M., & Hodson, A. J. (2012). *The Ecology of Snow and Ice Environments*. Oxford University Press.

Lundberg, S. M., & Lee, S.-I. (2017). A Unified Approach to Interpreting Model Predictions. In I. Guyon, U. Von Luxburg, S. Bengio, H. Wallach, R. Fergus, S. Vishwanathan, & R. Garnett (Eds.), *Advances in Neural Information Processing Systems* (Vol. 30). Curran Associates, Inc. https://proceedings.neurips.cc/paper_files/paper/2017/file/8a20a8621978632d76c43dfd28b67767-Paper.pdf

Lutz, S., Anesio, A. M., Edwards, A., & Benning, L. G. (2015). Microbial diversity on Icelandic glaciers and ice caps. *Frontiers in Microbiology*, *6*. https://www.frontiersin.org/articles/10.3389/fmicb.2015.00307

Lutz, S., Anesio, A. M., Jorge Villar, S. E., & Benning, L. G. (2014). Variations of algal communities cause darkening of a Greenland glacier. *FEMS Microbiology Ecology*, *89*(2), 402–414. https://doi.org/10.1111/1574-6941.12351

Marshall, S. J., & Miller, K. (2020). Seasonal and interannual variability of melt-season albedo at Haig Glacier, Canadian Rocky Mountains. *The Cryosphere*, *14*(10), 3249–3267. https://doi.org/10.5194/tc-14-3249-2020

Matsumoto, M., Hanneman, C., Camara, A. G., Krueger-Hadfield, S. A., Hamilton, T. L., & Kodner, R. B. (2024). Hypothesized life cycle of the snow algae Chlainomonas sp. (Chlamydomonadales, Chlorophyta) from the Cascade Mountains, USA. *Journal of Phycology*, *n/a*(n/a). https://doi.org/https://doi.org/10.1111/jpy.13454

McCutcheon, J., Lutz, S., Williamson, C., Cook, J. M., Tedstone, A. J., Vanderstraeten, A., Wilson, S. A., Stockdale, A., Bonneville, S., Anesio, A. M., Yallop, M. L., McQuaid, J. B., Tranter, M., & Benning, L. G. (2021). Mineral phosphorus drives glacier algal blooms on the Greenland Ice Sheet. *Nature Communications 2021 12:1*, *12*(1), 1–11. https://doi.org/10.1038/s41467-020-20627-w

Meyer, N. K. (2012). Particulate, black carbon and organic emissions from small-scale residential wood combustion appliances in Switzerland. *Biomass and Bioenergy*, *36*, 31–42. https://doi.org/https://doi.org/10.1016/j.biombioe.2011.09.023

Moore, R. D., Fleming, S. W., Menounos, B., Wheate, R., Fountain, A., Stahl, K., Holm, K., & Jakob, M. (2009a). Glacier change in western North America: influences on hydrology, geomorphic hazards and water quality. *Hydrological Processes*, *23*(1), 42–61. https://doi.org/https://doi.org/10.1002/hyp.7162

Moore, R. D., Fleming, S. W., Menounos, B., Wheate, R., Fountain, A., Stahl, K., Holm, K., & Jakob, M. (2009b). Glacier change in western North America: influences on hydrology, geomorphic hazards and water quality. *Hydrological Processes*, *23*(1), 42–61. https://doi.org/https://doi.org/10.1002/hyp.7162

Moore, R. D., Pelto, B., Menounos, B., & Hutchinson, D. (2020). Detecting the Effects of Sustained Glacier Wastage on Streamflow in Variably Glacierized Catchments. *Frontiers in Earth Science*, *8*. https://doi.org/10.3389/feart.2020.00136

Mukherjee, K., Menounos, B., Shea, J., Mortezapour, M., Ednie, M., & Demuth, M. N. (2022). Evaluation of surface mass-balance records using geodetic data and physically-based

modelling, Place and Peyto glaciers, western Canada. *Journal of Glaciology*, 1–18.
https://doi.org/DOI: 10.1017/jog.2022.83

Müller, T., Bleiß, W., Martin, C.-D., Rogaschewski, S., & Fuhr, G. (1998). Snow algae from
northwest Svalbard: their identification, distribution, pigment and nutrient content. *Polar Biology*, *20*(1), 14–32. https://doi.org/10.1007/s003000050272

Muñoz-Sabater, J., Dutra, E., Agust\'\i-Panareda, A., Albergel, C., Arduini, G., Balsamo, G., Boussetta, S., Choulga, M., Harrigan, S., Hersbach, H., Martens, B., Miralles, D. G., Piles, M., Rodr\'\iguez-Fernández, N. J., Zsoter, E., Buontempo, C., & Thépaut, J.-N. (2021). ERA5-Land: a state-of-the-art global reanalysis dataset for land applications. *Earth System Science Data*, *13*(9), 4349–4383. https://doi.org/10.5194/essd-13-4349-2021

Nagorski, S. A., Kaspari, S. D., Hood, E., Fellman, J. B., & Skiles, S. M. (2019). Radiative Forcing by Dust and Black Carbon on the Juneau Icefield, Alaska. *Journal of Geophysical Research: Atmospheres*, *124*(7), 3943–3959. https://doi.org/10.1029/2018JD029411

Onuma, Y., Takeuchi, N., & Takeuchi, Y. (2016). Temporal changes in snow algal abundance on surface snow in Tohkamachi, Japan. *Bulletin of Glaciological Research*, *34*, 21–31. https://api.semanticscholar.org/CorpusID:132841299

Onuma, Y., Yoshimura, K., & Takeuchi, N. (2022). Global Simulation of Snow Algal Blooming by Coupling a Land Surface and Newly Developed Snow Algae Models. *Journal of Geophysical Research: Biogeosciences*, *127*(2). https://doi.org/10.1029/2021JG006339

Painter, T., Duval, B., William, T. H., Mendez, M., Hentzelman, S., & Dozier, J. (2001). Detection and Quantification of Snow Algae with an Airborne Imaging Spectrometer.

Applied and Environmental Microbiology, *67*(11), 5267–5272.

https://doi.org/10.1128/AEM.67.11.5267-5272.2001

Painter, T. H., Seidel, F. C., Bryant, A. C., McKenzie Skiles, S., & Rittger, K. (2013). Imaging

spectroscopy of albedo and radiative forcing by light-absorbing impurities in mountain

snow. *Journal of Geophysical Research: Atmospheres*, *118*(17), 9511–9523.

https://doi.org/https://doi.org/10.1002/jgrd.50520

Pedregosa, F., Varoquaux, G., Gramfort, A., Michel, V., Thirion, B., Grisel, O., Blondel, M.,

Prettenhofer, P., Weiss, R., Dubourg, V., Vanderpla, J., Passos, A., D., C., Brucher, M.,

Perrot, M., & Duchesnay, E. (2011). Scikit-learn: Machine Learning in Python. *Journal of

Machine Learning Research*, *12*, 2825–2830.

Phillips-Lander, C. M., Harrold, Z., Hausrath, E. M., Lanzirotti, A., Newville, M., Adcock, C. T.,

Raymond, J. A., Huang, S., Tschauner, O., & Sanchez, A. (2020). Snow Algae Preferentially

Grow on Fe-containing Minerals and Contribute to the Formation of Fe Phases.

Geomicrobiology Journal, *37*(6), 572–581. https://doi.org/10.1080/01490451.2020.1739176

Pu, W., Cui, J., Wu, D., Shi, T., Chen, Y., Xing, Y., Zhou, Y., & Wang, X. (2021). Unprecedented

snow darkening and melting in New Zealand due to 2019–2020 Australian wildfires.

Fundamental Research, *1*(3), 224–231.

https://doi.org/https://doi.org/10.1016/j.fmre.2021.04.001

Qin, W., Zhang, Y., Chen, J., Yu, Q., Cheng, S., Li, W., Liu, X., & Tian, H. (2019). Variation,

sources and historical trend of black carbon in Beijing, China based on ground observation

and MERRA-2 reanalysis data. *Environmental Pollution*, *245*, 853–863.

https://doi.org/https://doi.org/10.1016/j.envpol.2018.11.063

Randles, C. A., Da Silva, A. M., Buchard, V., Colarco, P. R., Darmenov, A., Govindaraju, R., Smirnov, A., Holben, B., Ferrare, R., Hair, J., Shinozuka, Y., & Flynn, C. J. (n.d.). *The MERRA-2 Aerosol Reanalysis, 1980 Onward. Part I: System Description and Data Assimilation Evaluation*. https://doi.org/10.1175/JCLI-D-16-0609.s1

RGI Consortium. (2023). *Randolph Glacier Inventory - A Dataset of Global Glacier Outlines, Version 7 [Data Set]*. National Snow and Ice Data Center.

Schoen, E. R., Wipfli, M. S., Trammell, E. J., Rinella, D. J., Floyd, A. L., Grunblatt, J., McCarthy, M. D., Meyer, B. E., Morton, J. M., Powell, J. E., Prakash, A., Reimer, M. N., Stuefer, S. L., Toniolo, H., Wells, B. M., & Witmer, F. D. W. (2017). Future of Pacific Salmon in the Face of Environmental Change: Lessons from One of the World's Remaining Productive Salmon Regions. *Fisheries*, *42*(10), 538–553. https://doi.org/https://doi.org/10.1080/03632415.2017.1374251

Scikit learn. (2024). *Permutation feature importance*.

Shea, J. M., Dan Moore, R., & Stahl, K. (2009). Derivation of melt factors from glacier mass-balance records in western Canada. *Journal of Glaciology*, *55*(189), 123–130. https://doi.org/DOI: 10.3189/002214309788608886

Sitnov, S. A., Mokhov, I. I., & Likhosherstova, A. A. (2020). Exploring large-scale black-carbon air pollution over Northern Eurasia in summer 2016 using MERRA-2 reanalysis data. *Atmospheric Research*, *235*, 104763. https://doi.org/https://doi.org/10.1016/j.atmosres.2019.104763

Skiles, S. M., Flanner, M., Cook, J. M., Dumont, M., & Painter, T. H. (2018). Radiative forcing

    by light-absorbing particles in snow. *Nature Climate Change*, *8*(11), 964–971.

    https://doi.org/10.1038/s41558-018-0296-5

Stahl, K., & Moore, R. D. (2006). Influence of watershed glacier coverage on summer

    streamflow in British Columbia, Canada. *Water Resources Research*, *42*(6).

    https://doi.org/https://doi.org/10.1029/2006WR005022

Takeuchi, N. (2013). Seasonal and altitudinal variations in snow algal communities on an

    Alaskan glacier (Gulkana glacier in the Alaska range). *Environmental Research Letters*,

    8(3), 35002. https://doi.org/10.1088/1748-9326/8/3/035002

Takeuchi, N., Dial, R., Kohshima, S., Segawa, T., & Uetake, J. (2006). Spatial distribution and

    abundance of red snow algae on the Harding Icefield, Alaska derived from a satellite image.

    Geophysical Research Letters, *33*(21). https://doi.org/10.1029/2006GL027819

Thomas, J. L., Polashenski, C. M., Soja, A. J., Marelle, L., Casey, K. A., Choi, H. D., Raut, J.-C.,

    Wiedinmyer, C., Emmons, L. K., Fast, J. D., Pelon, J., Law, K. S., Flanner, M. G., & Dibb,

    J. E. (2017). Quantifying black carbon deposition over the Greenland ice sheet from forest

    fires in Canada. *Geophysical Research Letters*, *44*(15), 7965–7974.

    https://doi.org/https://doi.org/10.1002/2017GL073701

U.S. Environmental Protection Agency. (1994a). *Determination of metals and trace elements in*

    water and wastes by inductively coupled plasma-atomic emission spectrometry .

U.S. Environmental Protection Agency. (1994b). *Sample preparation procedure for*

    spectrochemical determination of total recoverable elements.

https://www.epa.gov/sites/default/files/2015-08/documents/method_200-2_rev_2-8_1994.pdf

Wang, X., Shi, T., Zhang, X., & Chen, Y. (2020). An Overview of Snow Albedo Sensitivity to Black Carbon Contamination and Snow Grain Properties Based on Experimental Datasets Across the Northern Hemisphere. *Current Pollution Reports*, *6*(4), 368–379. https://doi.org/10.1007/s40726-020-00157-1

Warren, S. G. (1982). Optical properties of snow. *Reviews of Geophysics*, *20*(1), 67–89. https://doi.org/https://doi.org/10.1029/RG020i001p00067

Warren, S. G. (2013). Can black carbon in snow be detected by remote sensing? *Journal of Geophysical Research: Atmospheres*, *118*(2), 779–786. https://doi.org/https://doi.org/10.1029/2012JD018476

Warren, S. G., & Wiscombe, W. J. (1980). A Model for the Spectral Albedo of Snow. II: Snow Containing Atmospheric Aerosols. *Journal of Atmospheric Sciences*, *37*(12), 2734–2745. https://doi.org/10.1175/1520-0469(1980)037<2734:AMFTSA>2.0.CO;2

Whicker, C. A., Flanner, M. G., Dang, C., Zender, C. S., Cook, J. M., & Gardner, A. S. (2022). SNICAR-ADv4: a physically based radiative transfer model to represent the spectral albedo of glacier ice. *The Cryosphere*, *16*(4), 1197–1220. https://doi.org/10.5194/tc-16-1197-2022

Williamson, S. N., & Menounos, B. (2021). The influence of forest fire aerosol and air temperature on glacier albedo, western North America. *Remote Sensing of Environment*, *267*, 112732. https://doi.org/10.1016/j.rse.2021.112732

Wiscombe, W. J., & Warren, S. G. (1980). A Model for the Spectral Albedo of Snow. I: Pure

  Snow. *Journal of Atmospheric Sciences*, *37*(12), 2712–2733. https://doi.org/10.1175/1520-

  0469(1980)037<2712:AMFTSA>2.0.CO;2

You, C., Yao, T., Xu, B., Xu, C., Zhao, H., & Song, L. (2016). Effects of sources, transport, and

  postdepositional processes on levoglucosan records in southeastern Tibetan glaciers.

  Journal of Geophysical Research: Atmospheres, *121*(14), 8701–8711.

  https://doi.org/https://doi.org/10.1002/2016JD024904

Zhang, H.-M., Huang, B., Lawrimore, J., Menne, M., & Smith, T. M. (n.d.). *NOAA Global*

  Surface Temperature Dataset (NOAAGlobalTemp), Version 5. NOAA National Centers for

  Environmental Information. https://doi.org/doi:10.25921/9qth-2p70

6 Appendices

6.1 Appendix A: Spring surface air temperature at Place Glacier
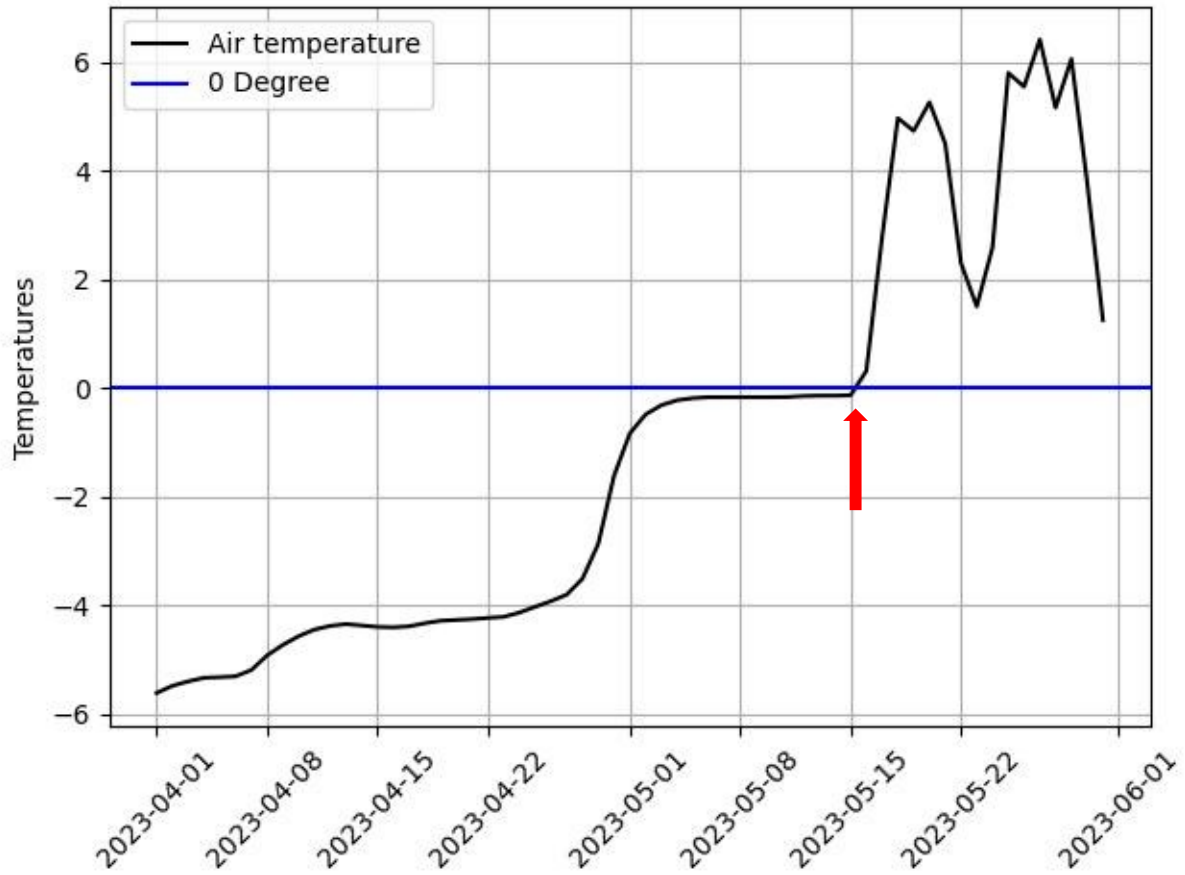
Figure A.1: Surface air temperature at Place Glacier in April and May 2023 from HOBO temperature sensor, elevation 1924 m. a.s.l. The red arrow indicates the approximate date when the air temperature sensor is uncovered and above the snowpack/ice surface.

6.2 Appendix B: Elemental metal concentration of the wood ash, control and treated samples.

Table B 1: Elemental metal concentration for the wood ash, control and treated samples. Rows in bold represent elements with significantly higher concentrations in the treated samples.

Metals	Wood Ash (mg Kg-1)	Control Sample (mg L-1)	Treated Sample (mg L-1)	P - Value
Aluminum	**10395**	**0.208**	**0.311**	**0.00579**
Arsenic	<20	<0.02	<0.02	NaN
Boron	321	<0.001	<0.001	0.329
Barium	**3054**	**0.002**	**0.033**	**0.0**
Calcium	**246384**	**0.072**	**2.064**	**0.0**
Cadmium	19	<0.0004	<0.0004	NaN
Cobalt	9	<0.001	<0.001	NaN
Chromium	**66**	**<0.001**	**0.001**	**0.0**
Copper	110	<0.002	<0.002	NaN
Iron	**12092**	**0.228**	**0.345**	**0.00328**
Potassium	**29355**	**0.132**	**0.271**	**0.00118**
Magnesium	**25205**	**0.093**	**0.374**	**0.0**
Manganese	**15000**	**0.004**	**0.140**	**0.0**
Molybdenum	8	<0.003	<0.003	NaN
Sodium	6184	0.078	0.098	0.391
Nickel	**59**	**<0.001**	**0.001**	**0.00455**
Phosphorus	**12298**	**0.009**	**0.108**	**0.0**
Lead	13	<0.004	0.001	0.155
Sulfur	10327	<0.08	<0.08	NaN
Antimony	42	<0.01	<0.01	NaN
Selenium	<20	<0.02	<0.02	NaN
Tin	79	<0.01	<0.01	NaN
Uranium	35	<0.01	<0.01	NaN
Vanadium	25	<0.001	<0.001	NaN
Zinc	3550	0.064	0.059	0.0106

6.3 Appendix C: HLS tile names per Mountain Regions

Table C 1: HLS tile names per Mountain Regions

Region Number	Region Name	HLS Tile Name
1	Southern Coast Mountains	T09UXS
		T09UXT
		T09UXU
		T09UYR
		T09UYS
		T09UYT
		T09UYT
		T09UYU
		T10UCA
		T10UCB
		T10UCC
		T10UCD
		T10UDA
		T10UDB
		T10UDC
		T10UEA
		T10UEB
		T10UEV
2	Central Coast Mountains	T09UVA
		T09UVB
		T09UVV
		T09UWA
		T09UWB
		T09UWU
		T09UWV
		T09UXU
		T09UXV
3	Northern Coast Mountains	T08VML
		T08VMM
		T08VNK
		T08VNL
		T08VNM
		T08VPH
		T09UVB
		T09VUC
		T09VVC
		T09VVD
4	St. Elias	T07VEG

		T07VFF
		T07VFG
		T08VLL
		T08VLM
		T08VMM
5	Interior North	T+C45:C6009UWA
		T09UWB
		T09UXA
		T09UXB
		T09VVC
		T09VVD
		T09VVE
		T09VWC
		T09VWD
		T09VWE
		T09VWF
		T09VXC
		T09VXD
		T09VXE
		T10VCH
		T10VCJ
6	Interior South	T10UFD
		T10UFE
		T10UGB
		T10UGC
		T10UGD
		T11ULS
		T11ULT
		T11ULU
		T11UMR
		T11UMS
		T11UMT
		T11UNR
		T11UNS
7	Northern Rockies	T09VXE
		T09VXF
		T10VCJ
		T10VCK
		T10VC
		T10VDJ
		T10VDK
8	Central Rockies	T10UEF
		T10UFE

		T10UFF
		T10UGD
		T10UGE
		T11ULU
		T11ULV
9	Southern Rockies	T10UGD
		T10UGE
		T11ULT
		T11ULU
		T11ULV
		T11UMT
		T11UMU
		T11UMV
		T11UNS
		T11UNT
		T11UNU
		T11UPR
		T11UPS

6.4 Appendix D: Parameters used for Random Forest and the XGBoost models for the Annual and lag year model

Table D 1: Random forest parameters used for the annual models and the lag model. The 'F' and "T" stands for True and False. Table 3.2 describes the parameters.

Parameters	2015	2016	2017	2018	2019	2020	2021	2022	2023	Lag Year
n_estimators	1000	200	100	100	2500	500	500	300	200	100
max_depth	60	40	40	100	40	60	40	100	200	80
min_samples_splits	3	2	3	3	5	3	2	3	3	5
min_samples_leaf	1	5	3	3	2	1	1	1	1	2
max_feature	sqrt'	log2'	sqrt'	sqrt'	sqrt'	log2'	log2'	log2'	log2'	log2'
Bootstrap	F	T	T	F	F	T	T	T	F	F

Table D 2: XGBoost parameters used for the annual models and the lag model. Table 3.3 describes the parameters.

Parameters	2015	2016	2017	2018	2019	2020	2021	2022	2023	Lag Year
learning_rate	0.2	0.01	0.01	0.2	0.01	0.01	0.1	0.01	0.01	0.01
n_estimator	300	100	100	300	100	100	100	300	100	1000
max_depth	4	6	9	7	6	5	5	3	7	7
min_child_weigth	5	1	1	2	3	4	1	1	1	4
gamma	0	0	0	0	0	0	0	0	0	0
subsamble	0.6	0.6	0.9	0.8	0.6	0.9	0.9	0.6	0.7	0.9
colsample_bytree	0.8	0.8	0.8	0.8	0.7	0.8	0.8	0.9	0.8	0.6
reg_alpha	0	0	1E-05	0	0	0	0.01	1	0	0.1

6.5 Appendix E: Correlation matrix significance values
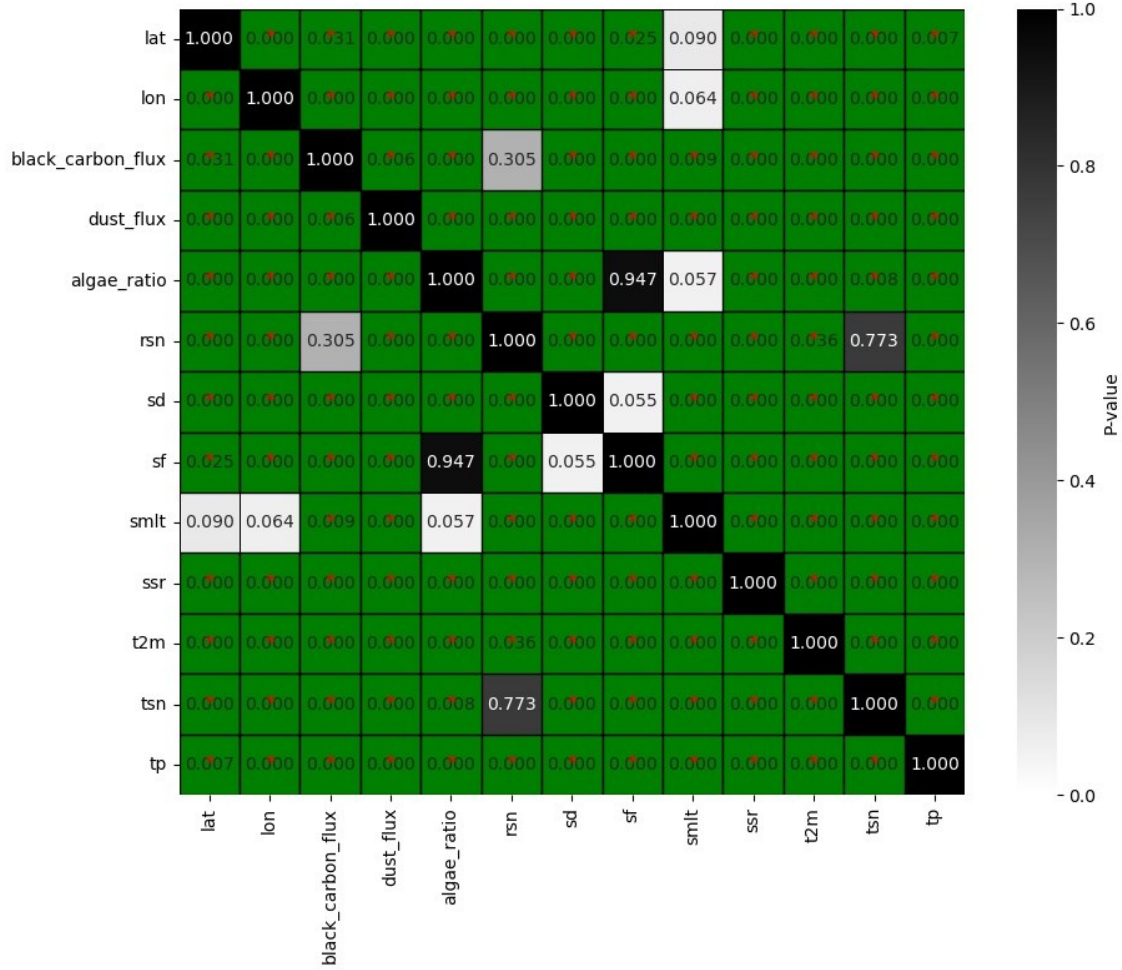
Figure E 1: Mean variables correlation's significance for the correlation matrix. The green indicates a correlation with ρ< 0.05, thus significant.
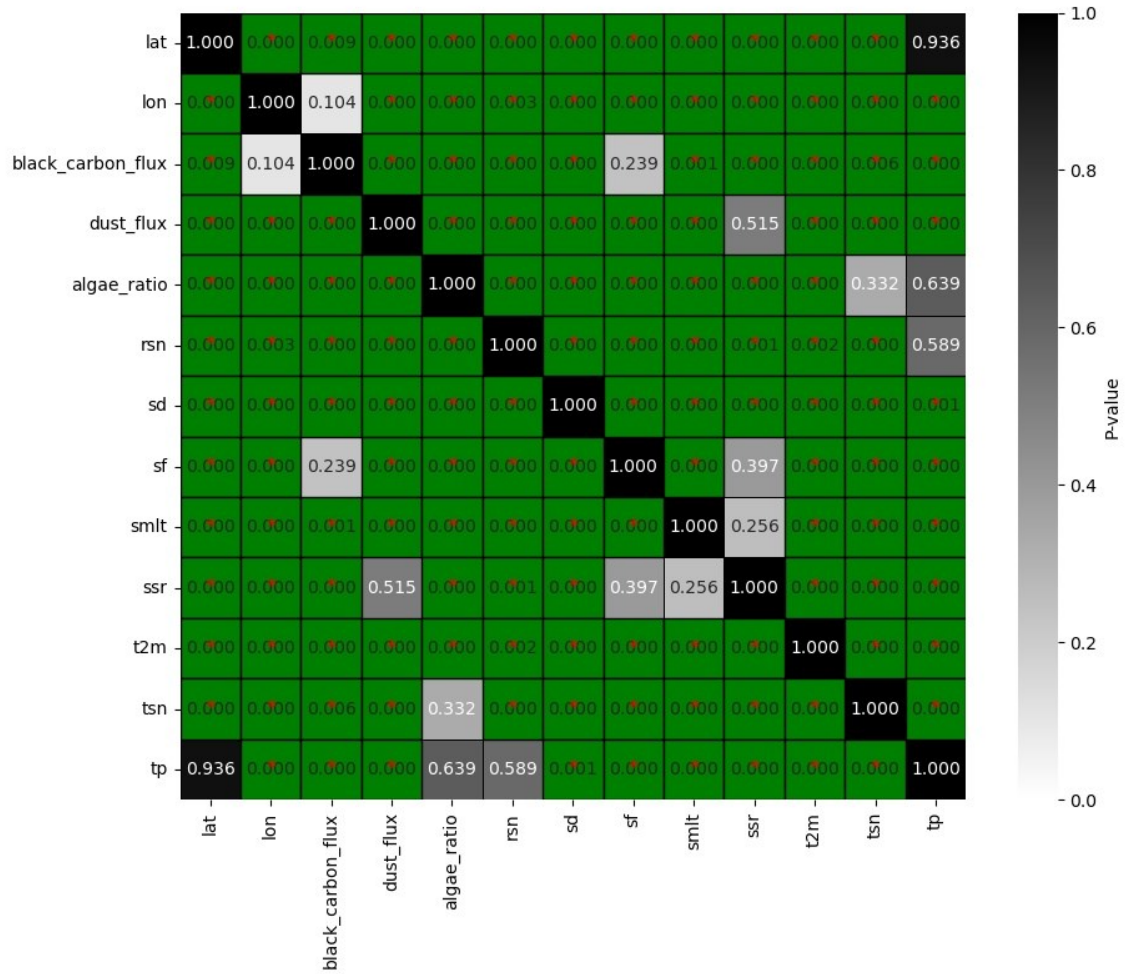
Figure E 2: Max variables correlation's significance for the correlation matrix. The green indicates a correlation with ρ< 0.05, thus significant.

6.6   Appendix F: Annual model permutation feature importance
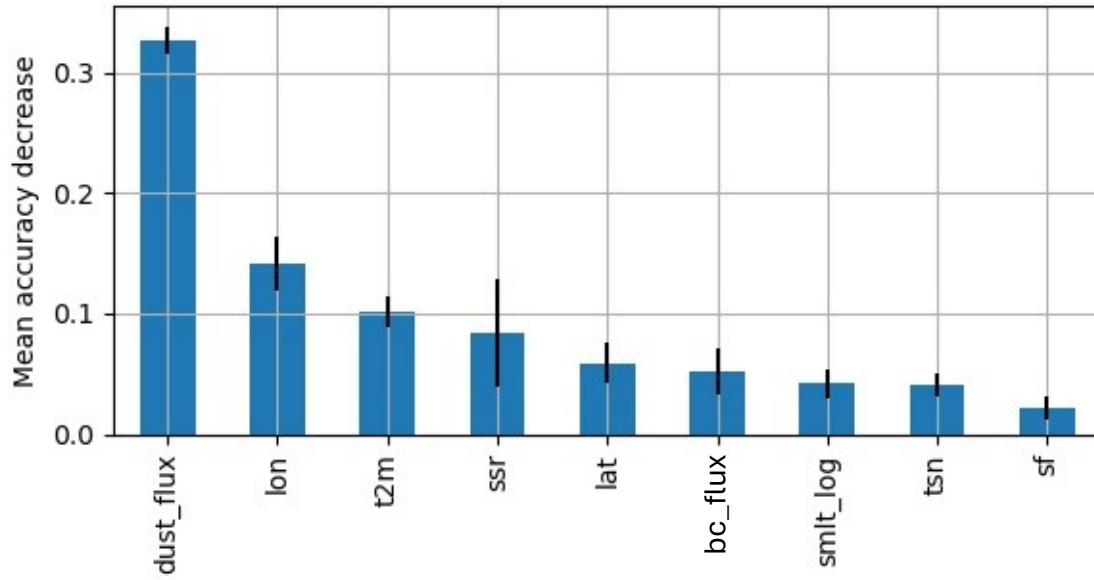
Figure F 1: Permutation feature importance for the random forest on the annual model 2015
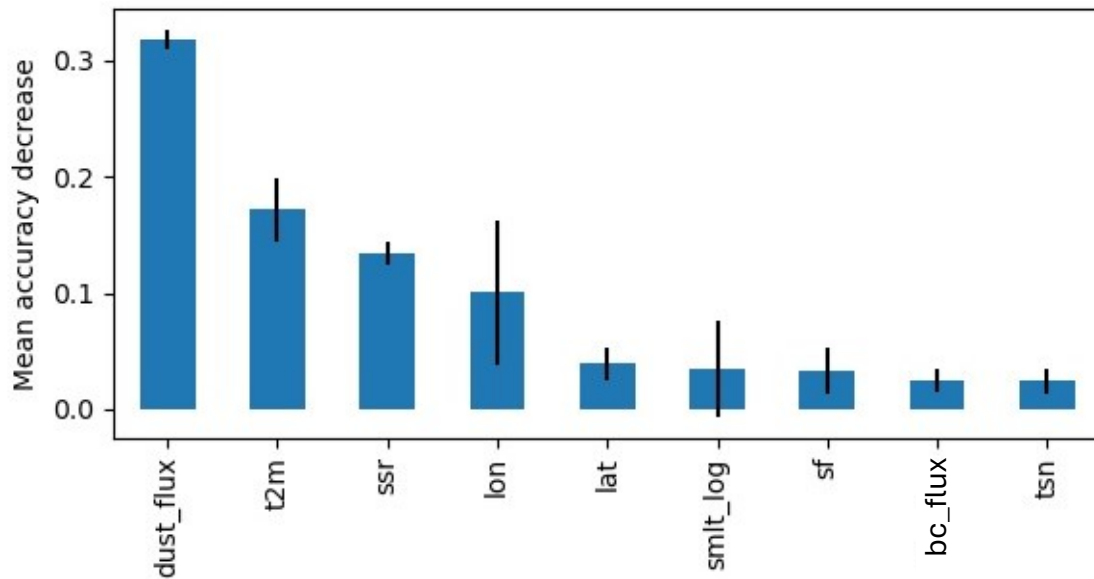
Figure F.2: Permutation feature importance for the XGBoost on the annual model 2015
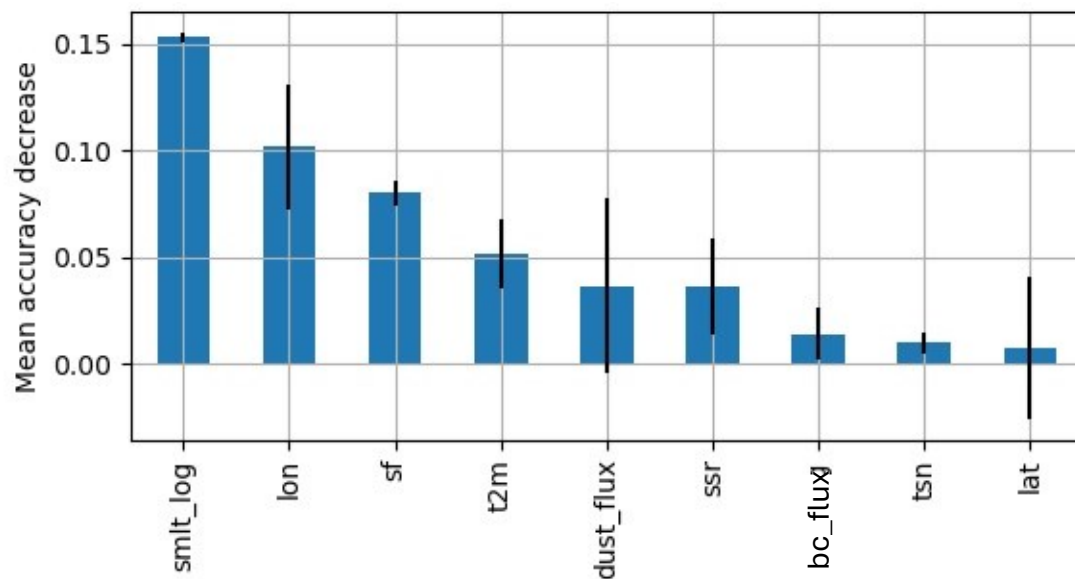
Figure F.3 : Permutation feature importance for the random forest on the annual model 2016
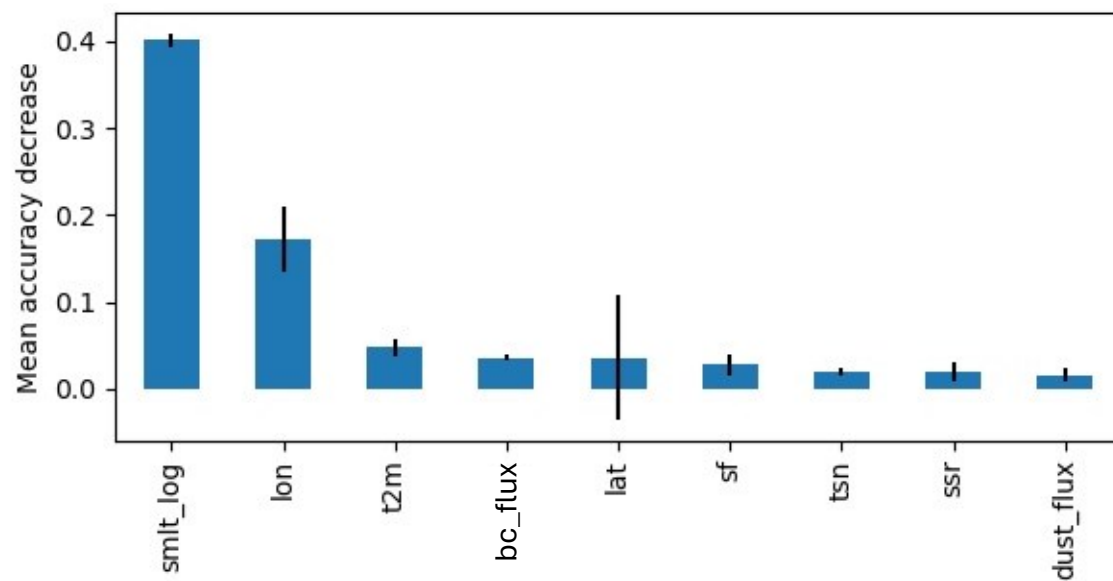
Figure F.4: Permutation feature importance for the XGBoost on the annual model 2016
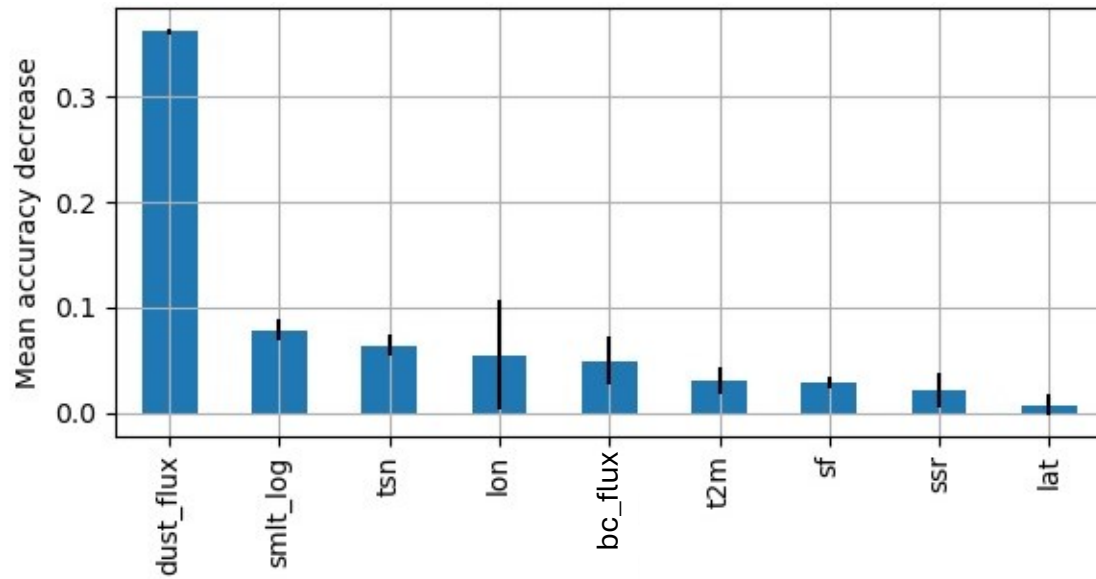
Figure F.5: Permutation feature importance for the random forest on the annual model 2017
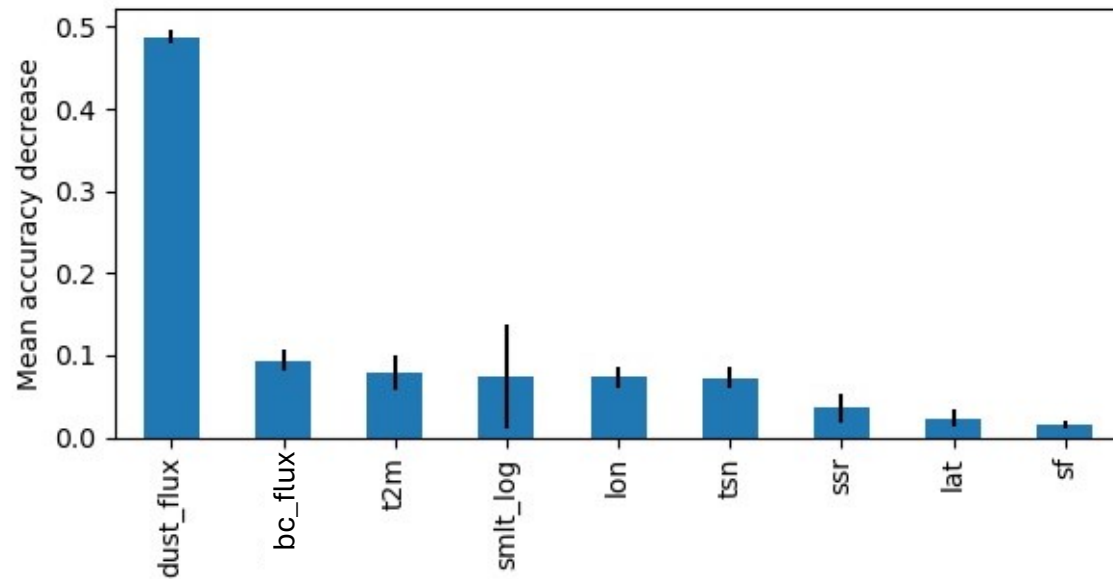
Figure F.6: Permutation feature importance for the XGBoost on the annual model 2017
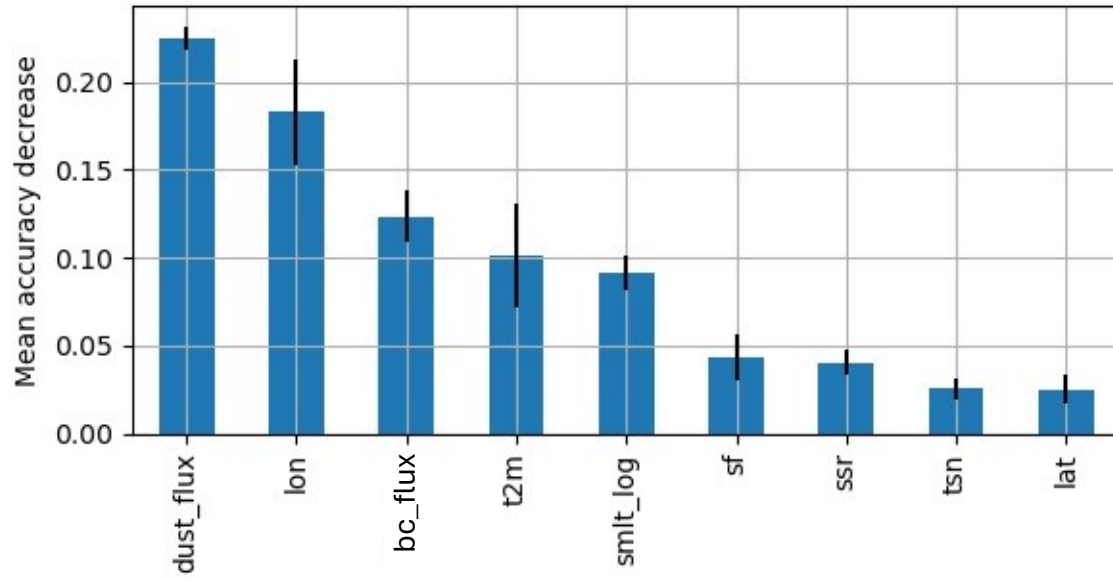
Figure F.7: Permutation feature importance for the random forest on the annual model 2018
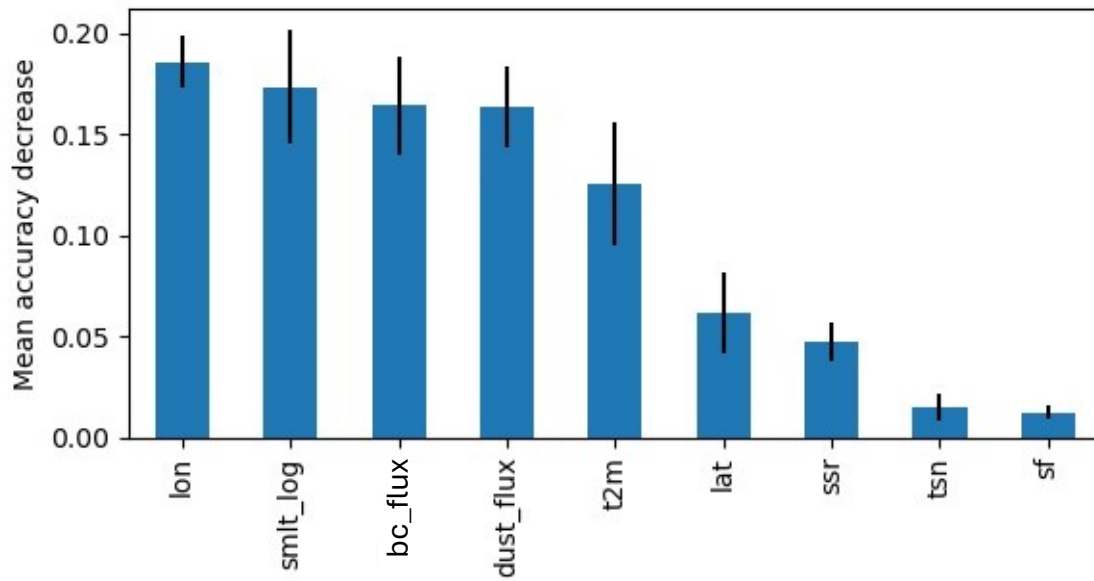
Figure F.8 : Permutation feature importance for the XGBoost on the annual model 2018
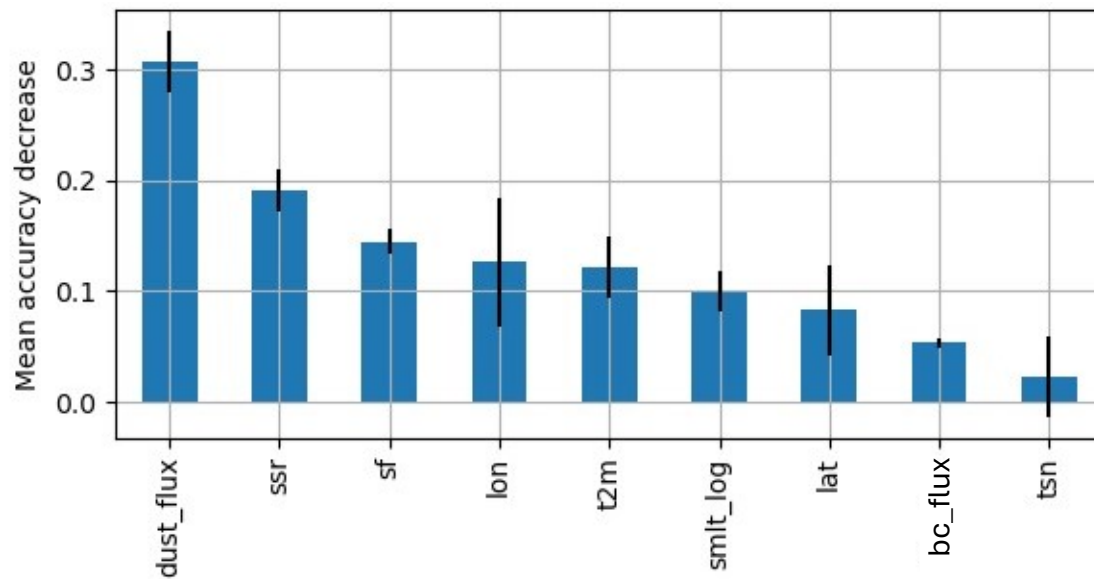
Figure F.9: Permutation feature importance for the random forest on the annual model 2019
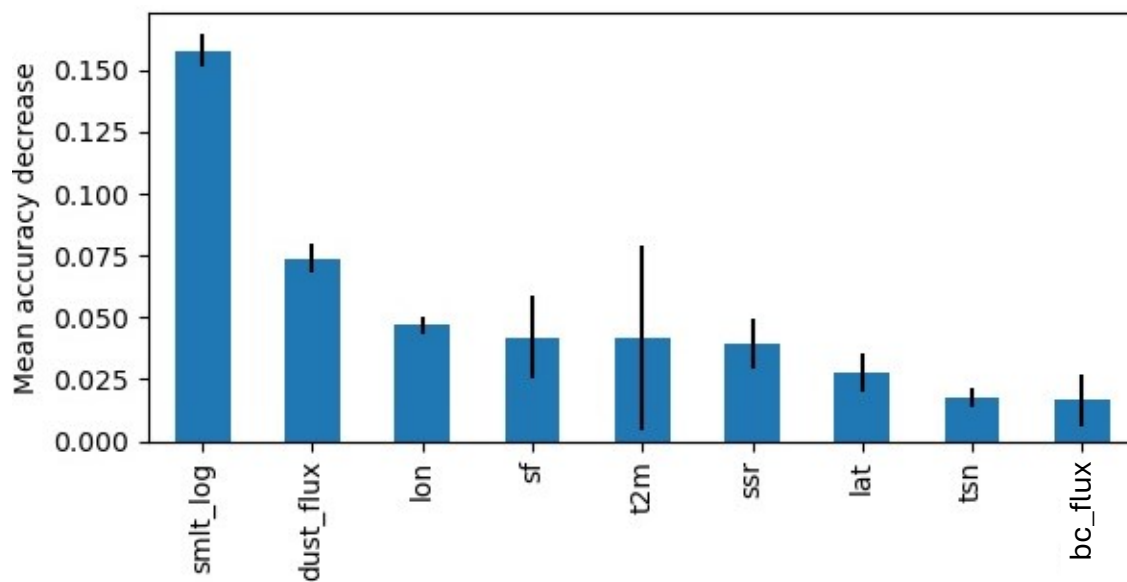
Figure F.10: Permutation feature importance for the XGBoost on the annual model 2019
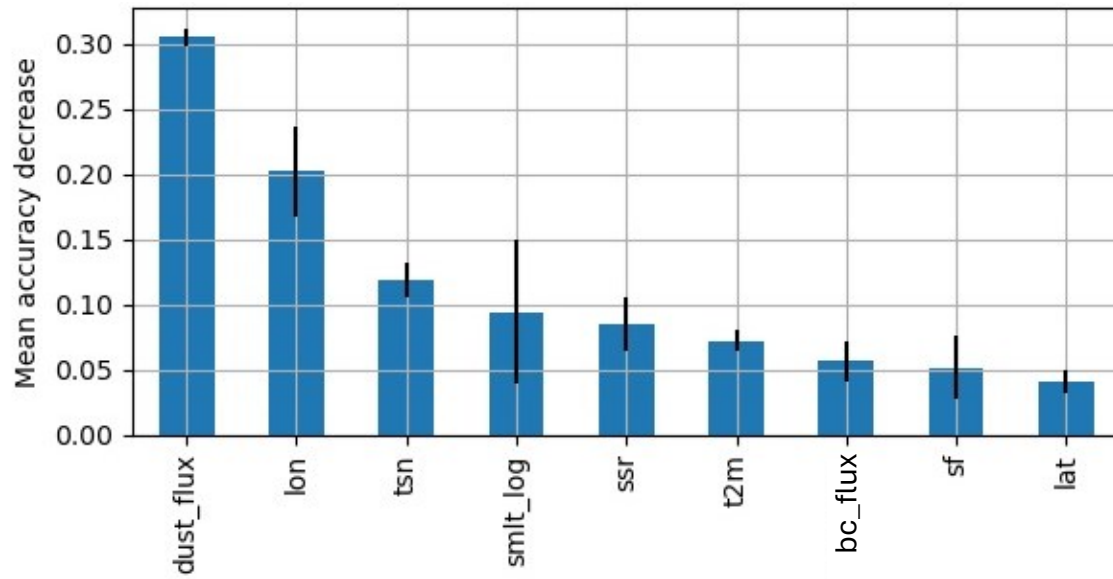
Figure F.11: Permutation feature importance for the random forest on the annual model 2020
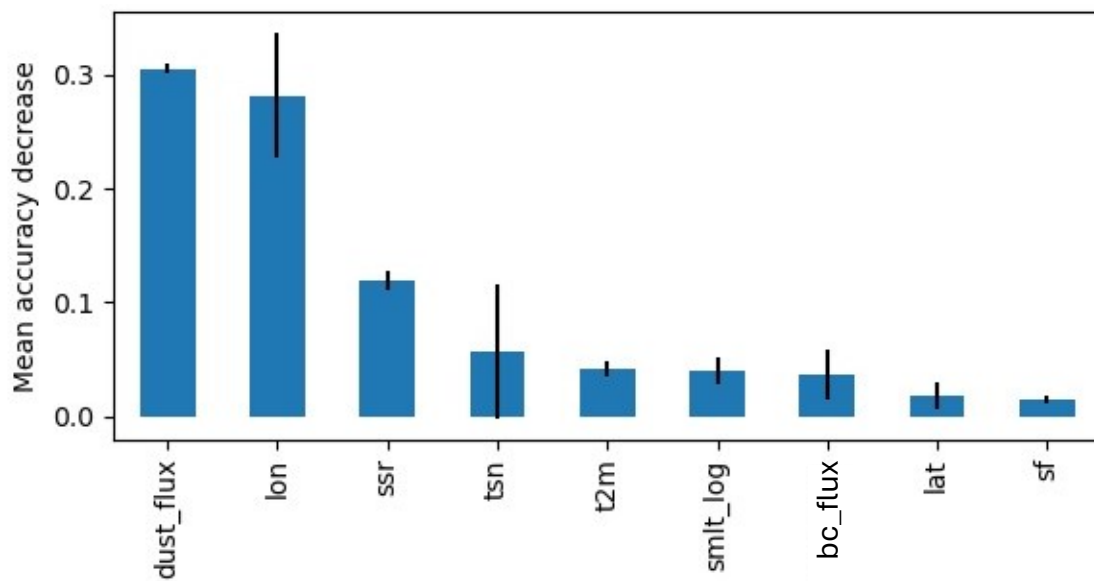
Figure F.12: Permutation feature importance for the XGBoost on the annual model 2020
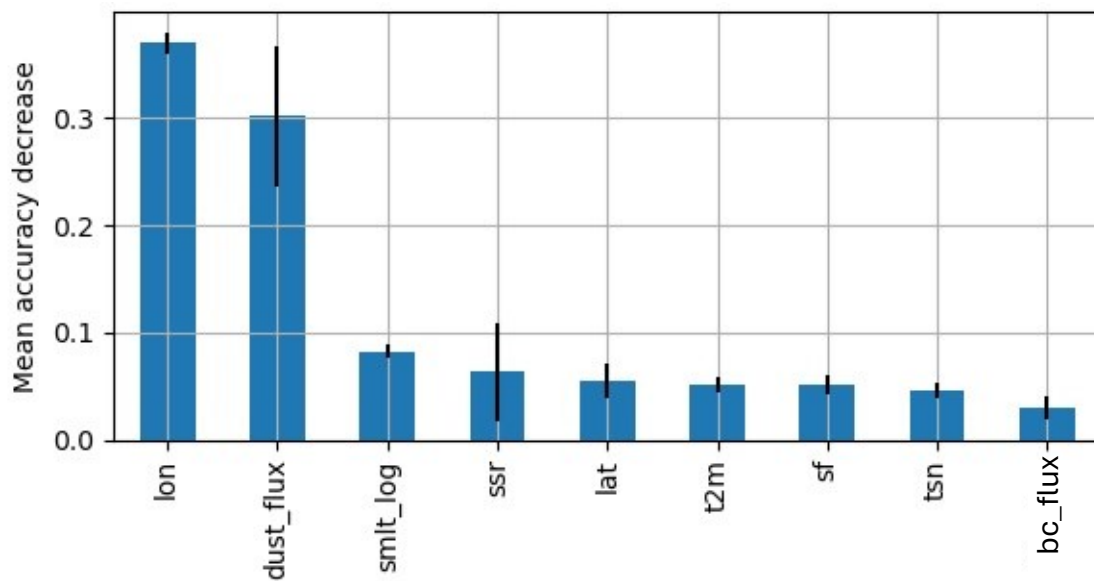
Figure F.13: Permutation feature importance for the random forest on the annual model 2021
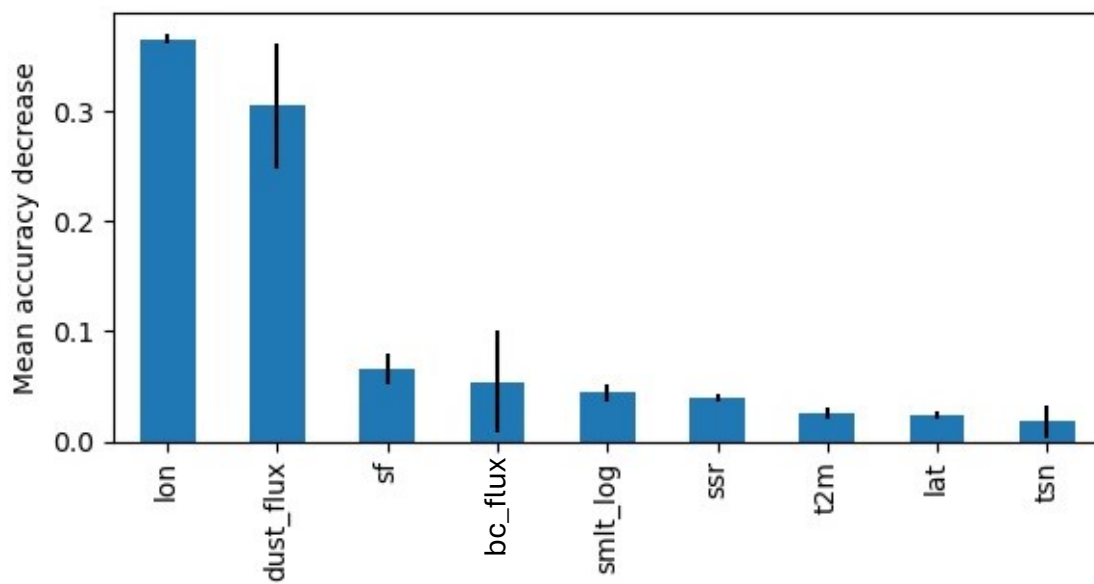
Figure F.14: Permutation feature importance for the XGBoost on the annual model 2021
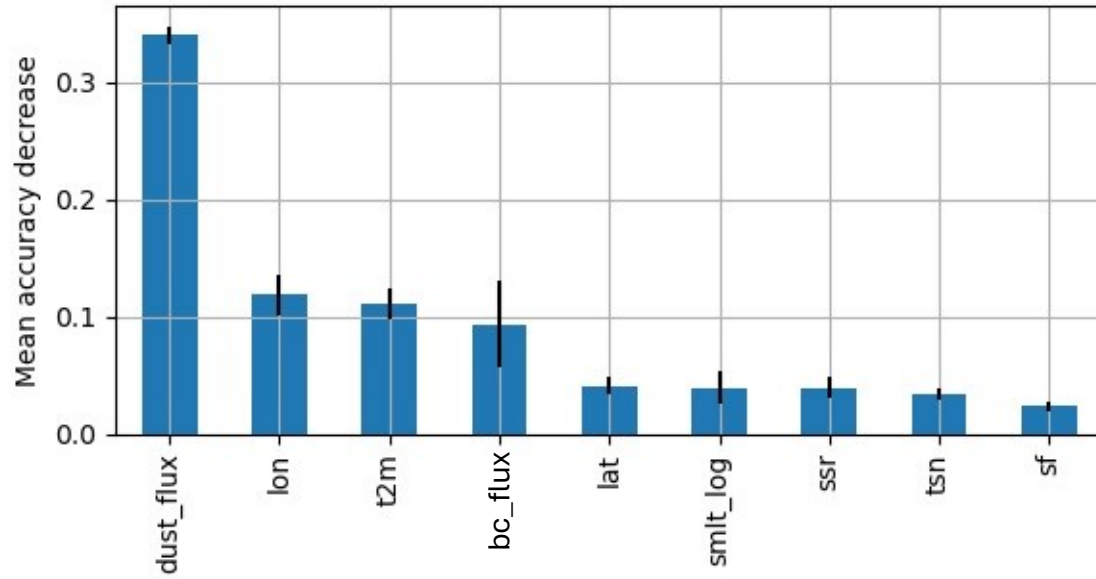
Figure F.15: Permutation feature importance for the random forest on the annual model 2022
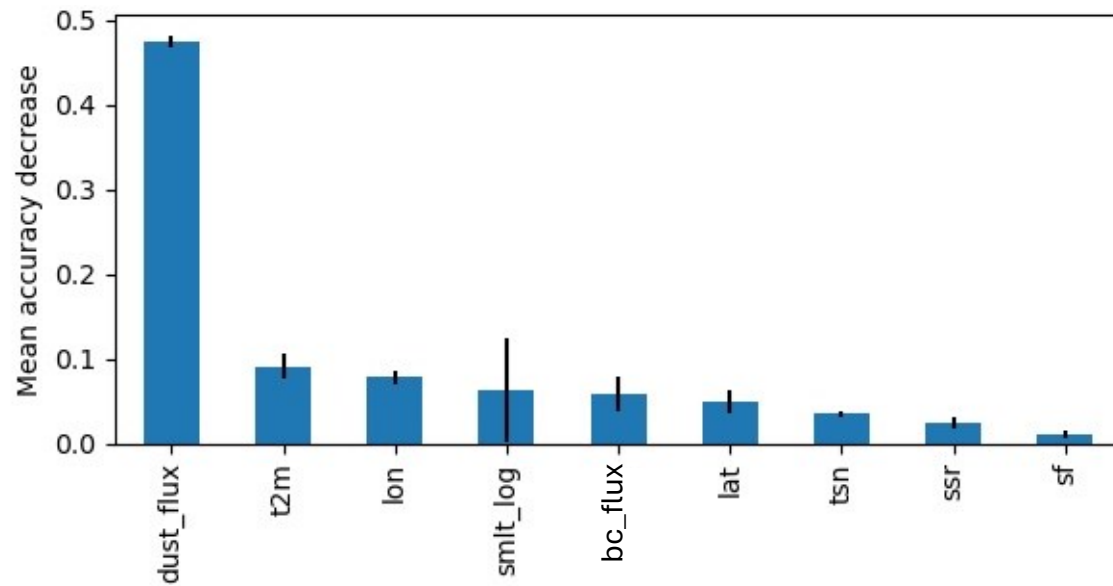
Figure F.16: Permutation feature importance for the XGBoost on the annual model 2022
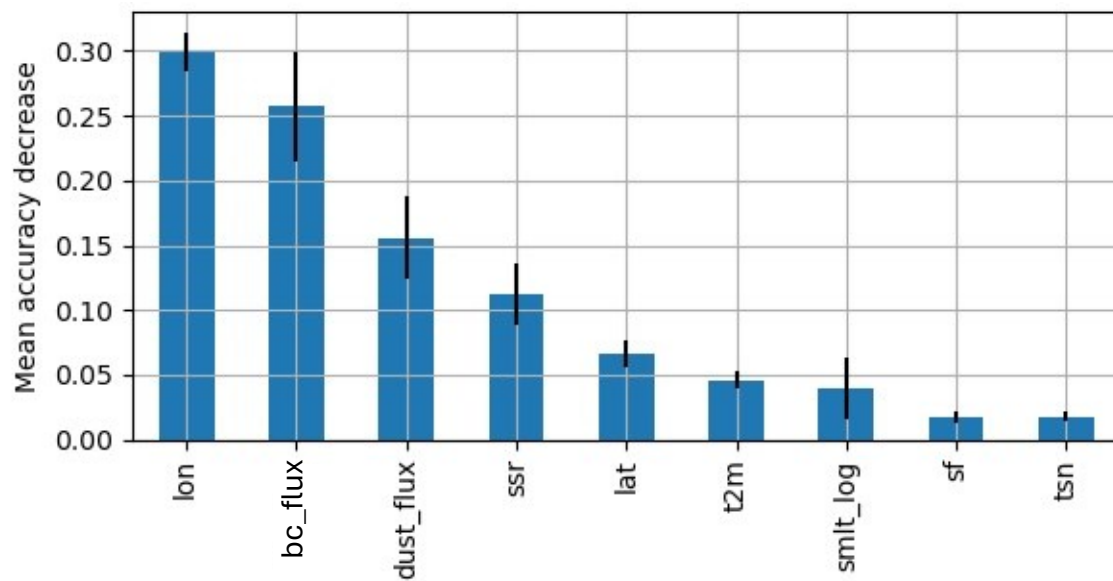
Figure F.17: Permutation feature importance for the random forest on the annual model 2023
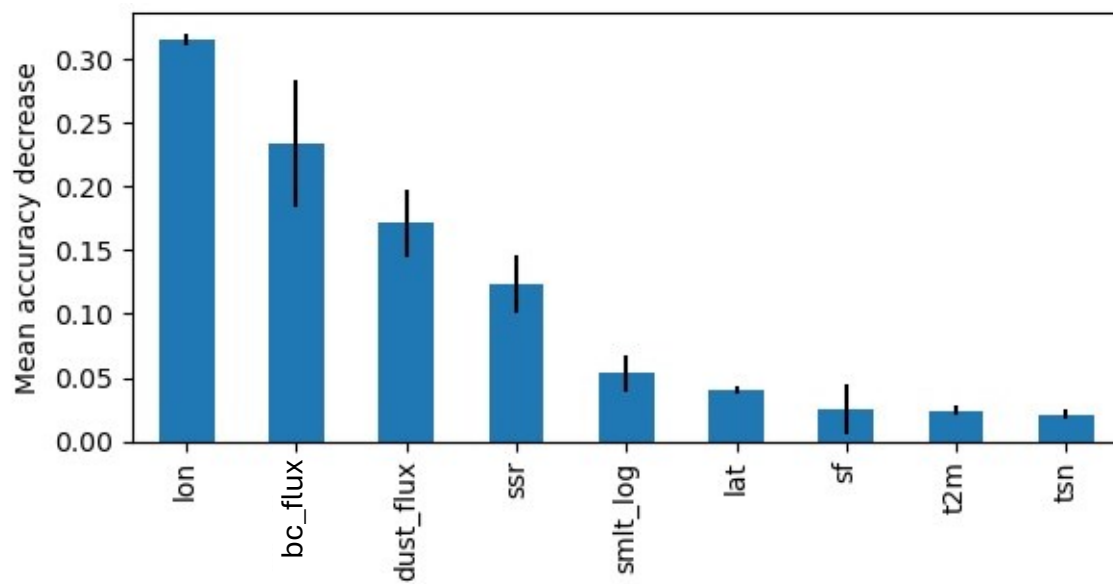
Figure F.18: Permutation feature importance for the XGBoost on the annual model 2023

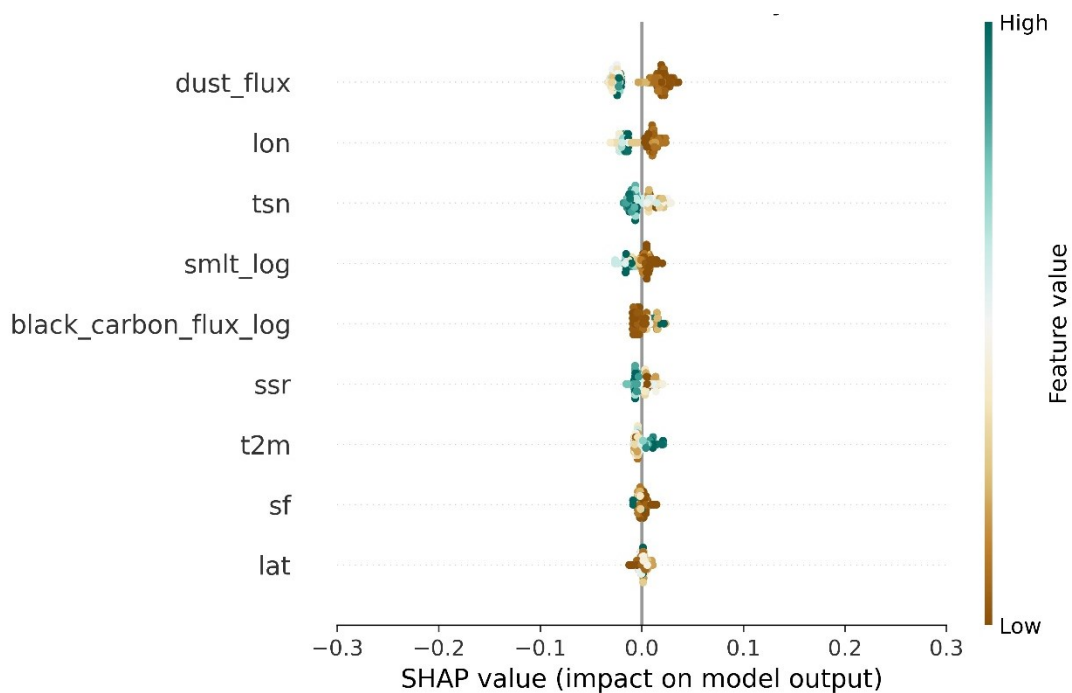## 6.7   Appendix G: Annual model SHAP Value
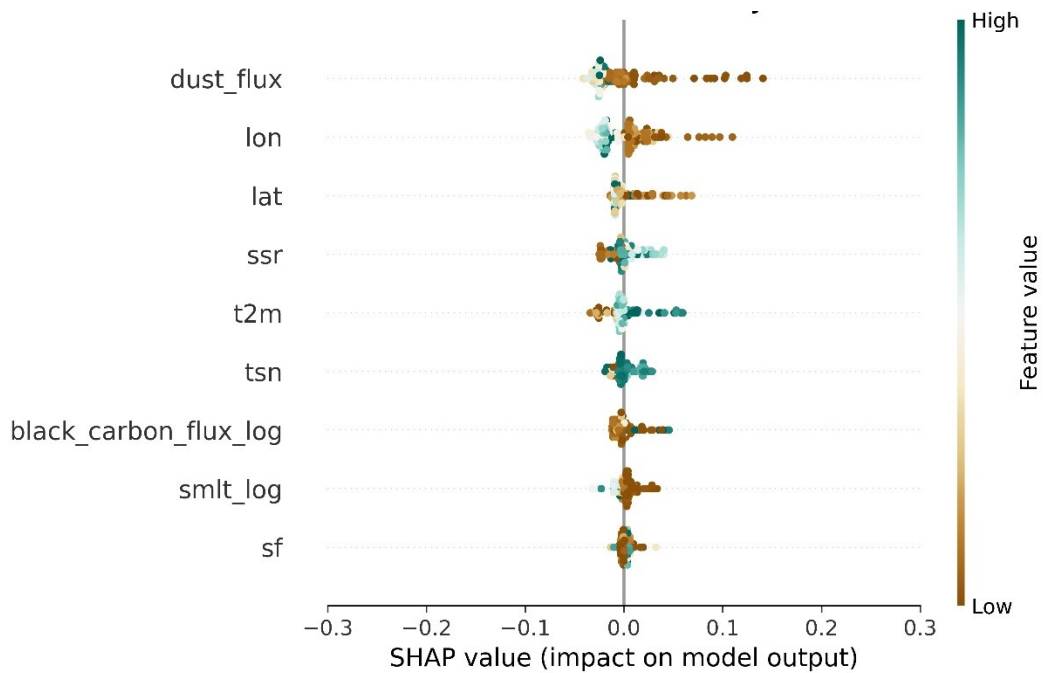
Figure G 1: SHAP Values for the random forest on the annual model 2015
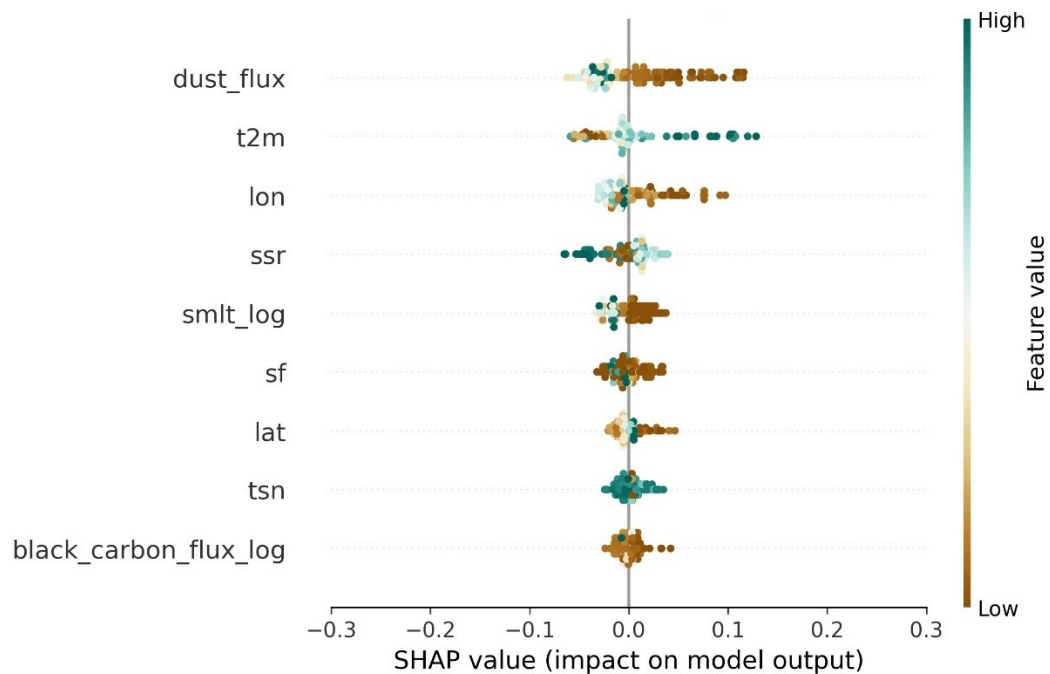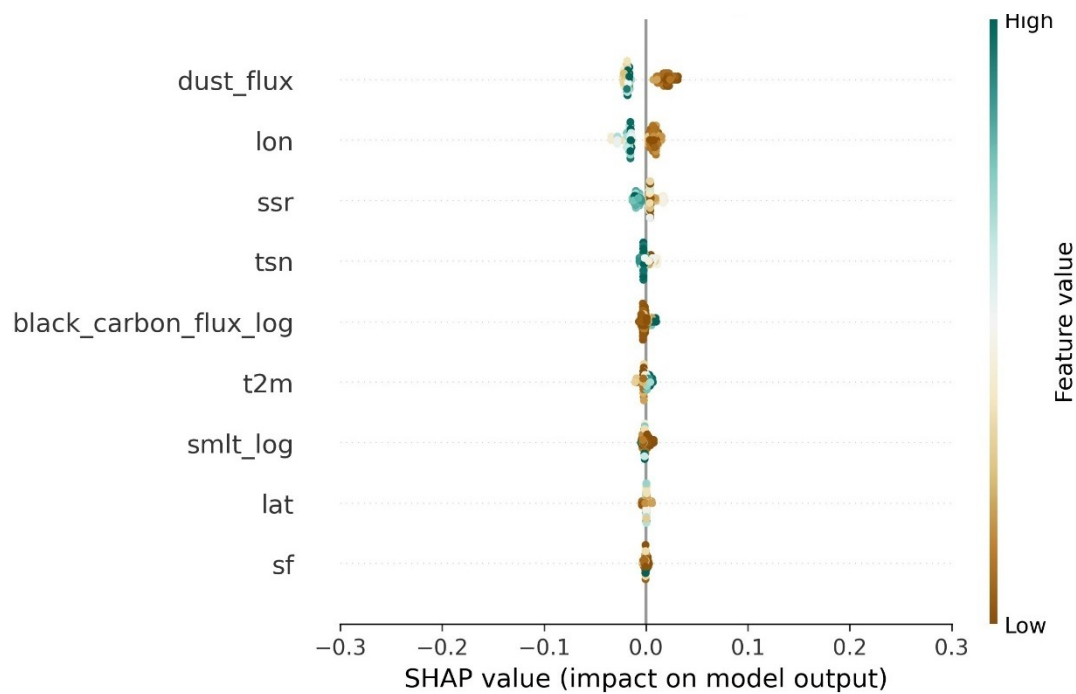

Figure G 2: SHAP Values for the XGBOOST on the annual model 2015
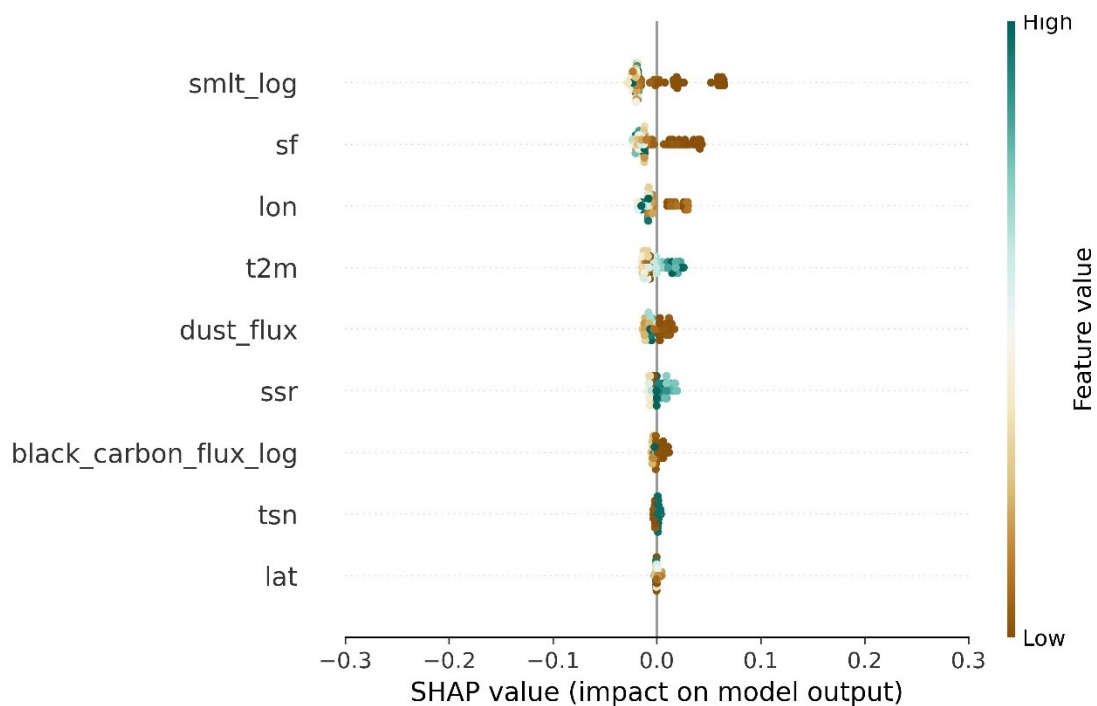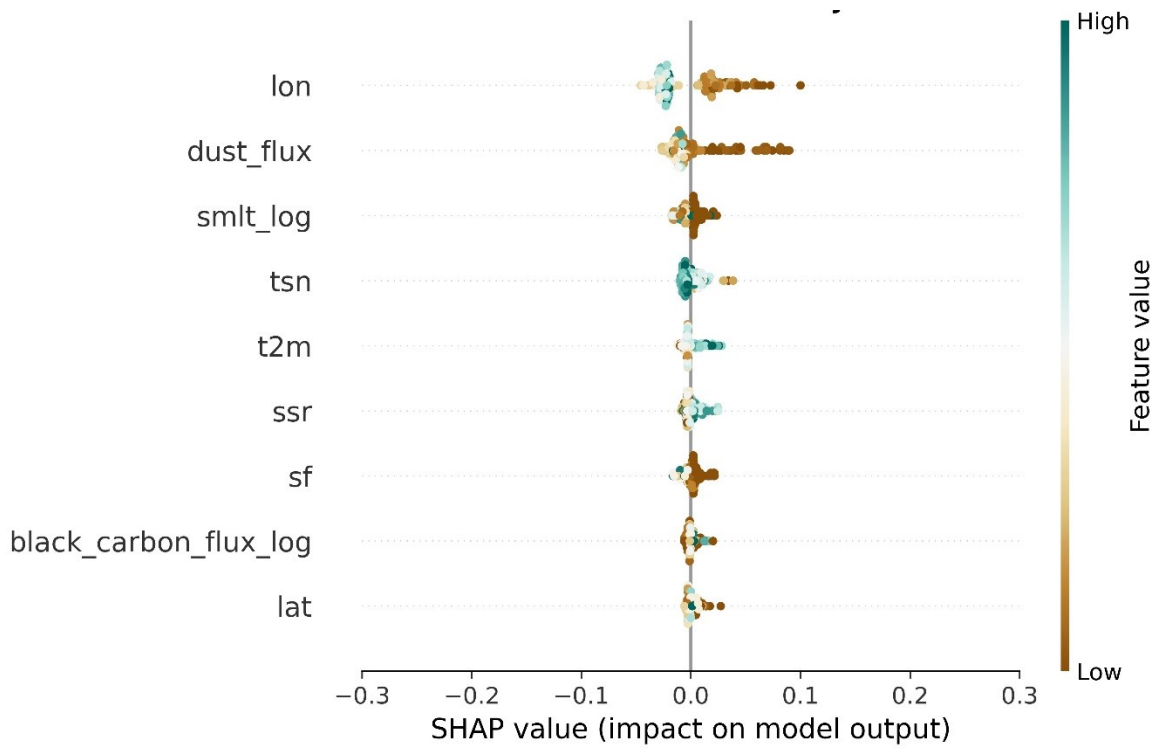
Figure G 3: SHAP Values for the random forest on the annual model 2016
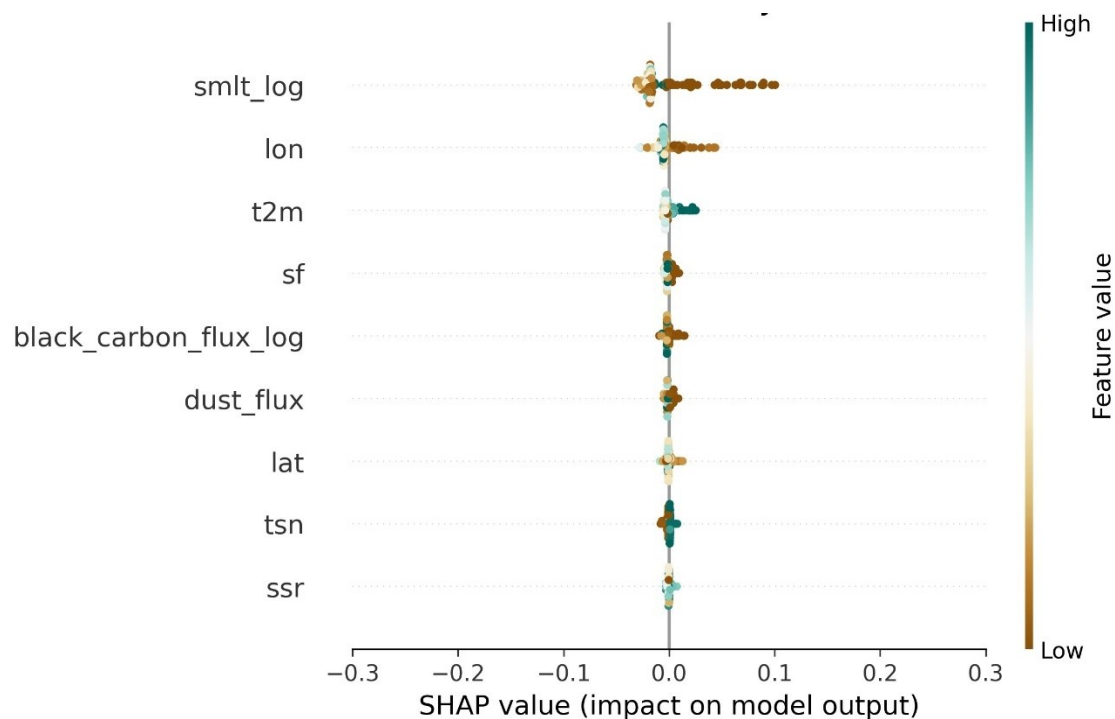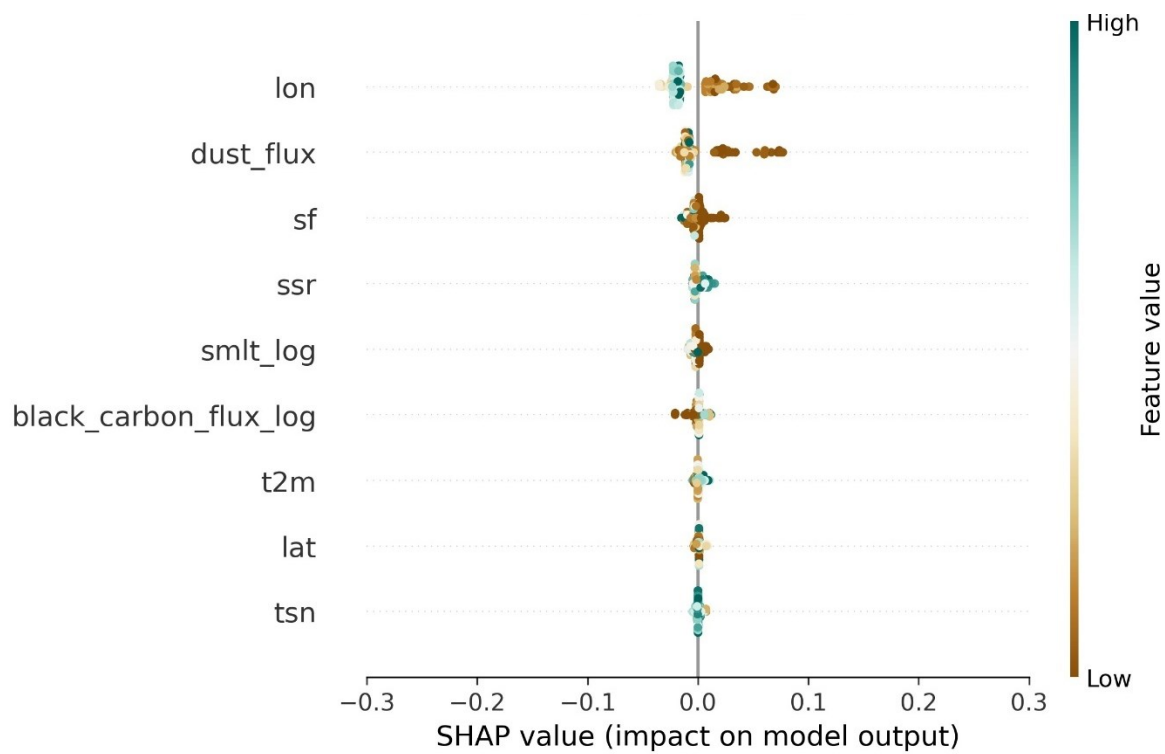

Figure G 4: SHAP Values for the XGBOOST on the annual model 2016
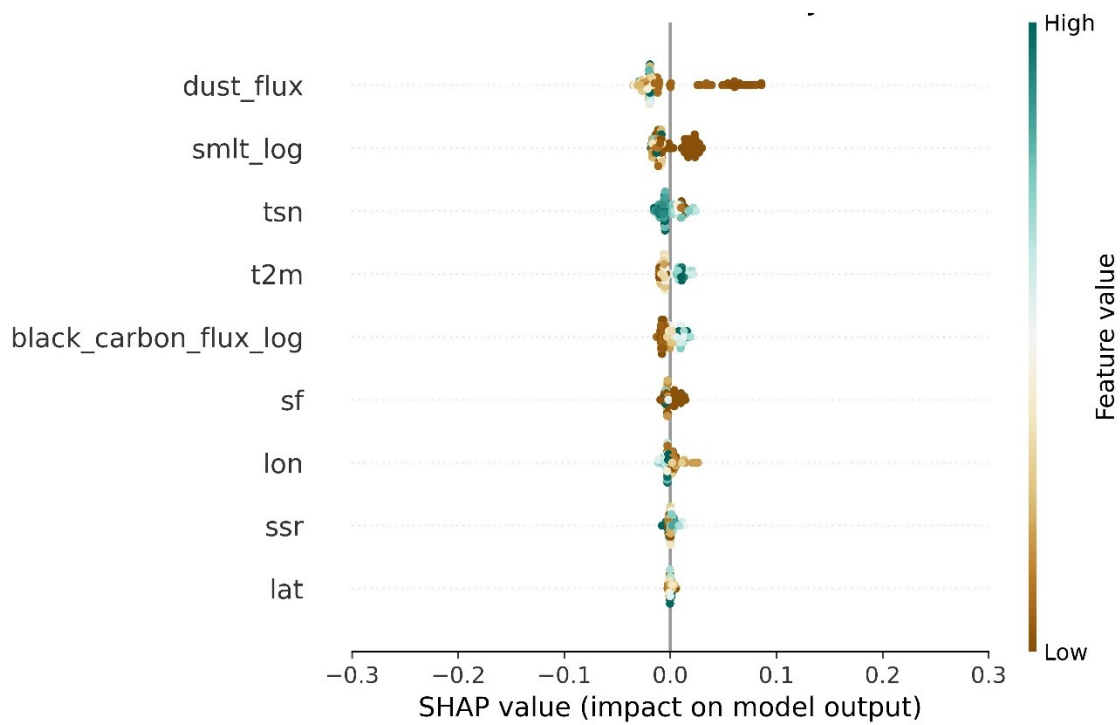
Figure G 5: SHAP Values for the random forest on the annual model 2017
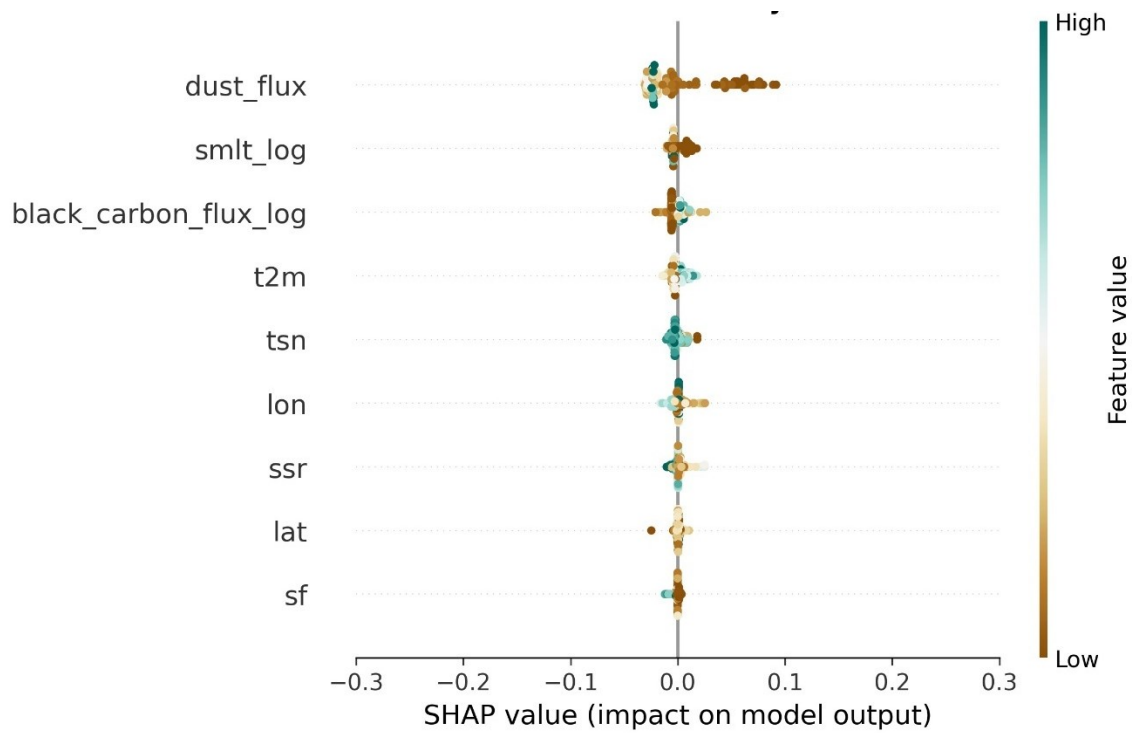
Figure G 6: SHAP Values for the XGBOOST on the annual model 2017
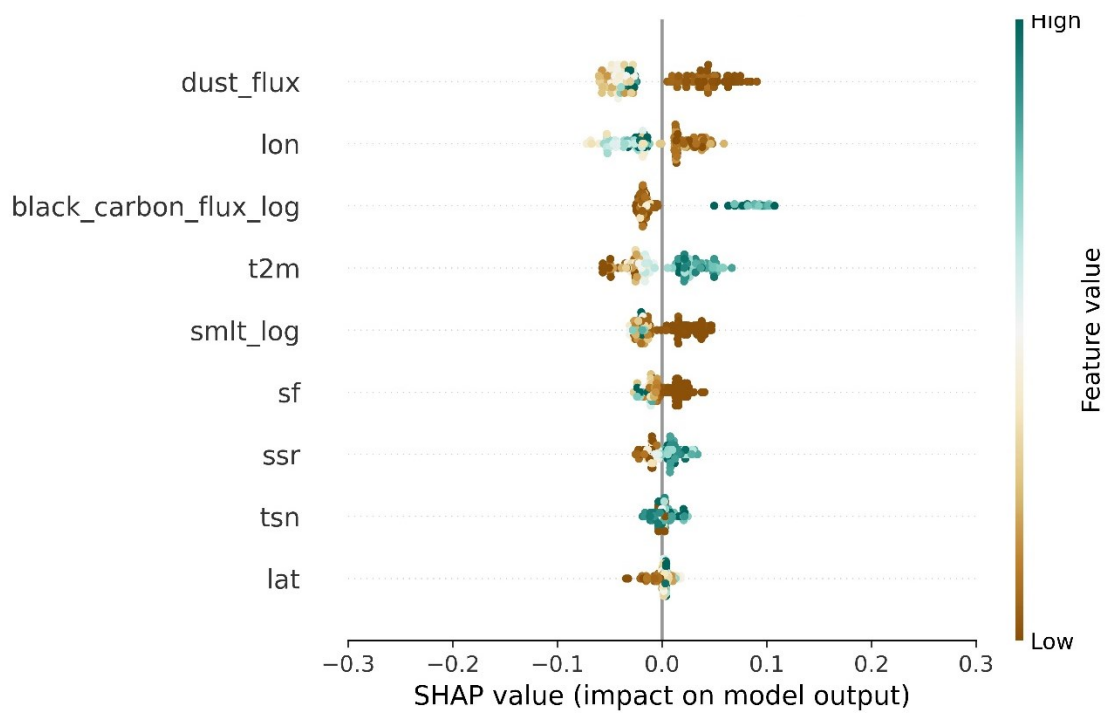
Figure G 7: SHAP Values for the random forest on the annual model 2018
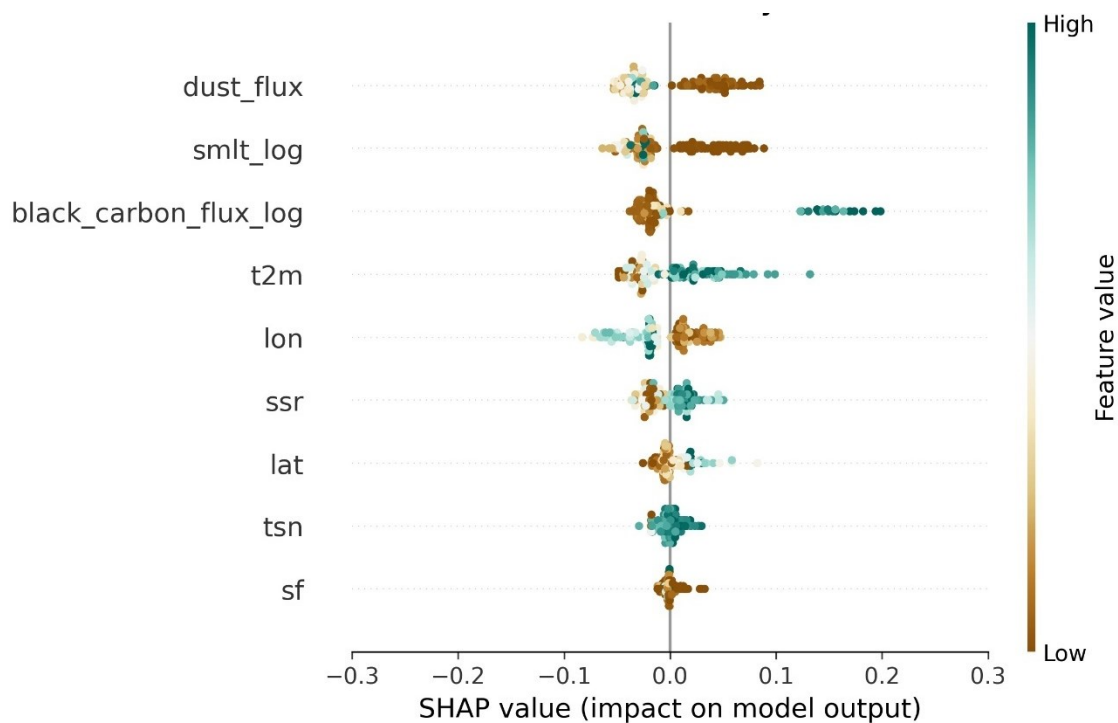
Figure G 8: SHAP Values for the XGBOOST on the annual model 2018
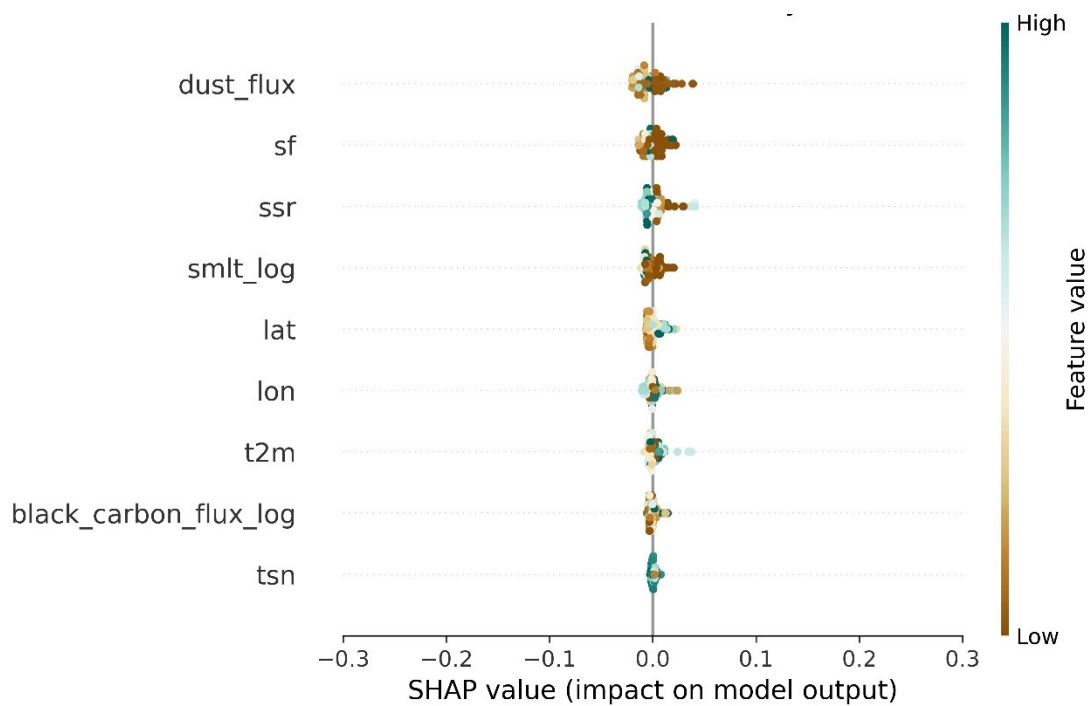
Figure G 9: SHAP Values for the random forest on the annual model 2019
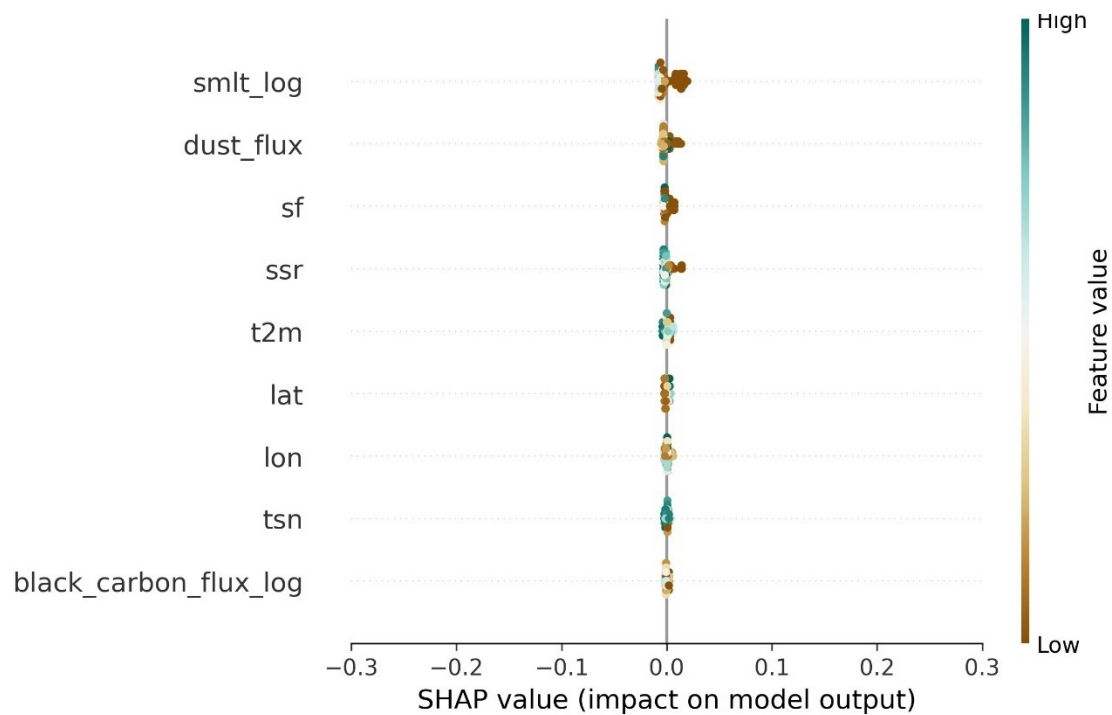
Figure G 10: SHAP Values for the XGBOOST on the annual model 2019

Figure G 11: SHAP Values for the random forest on the annual model 2020

Figure G 12: SHAP Values for the XGBOOST on the annual model 2020

Figure G 13: SHAP Values for the random forest on the annual model 2021

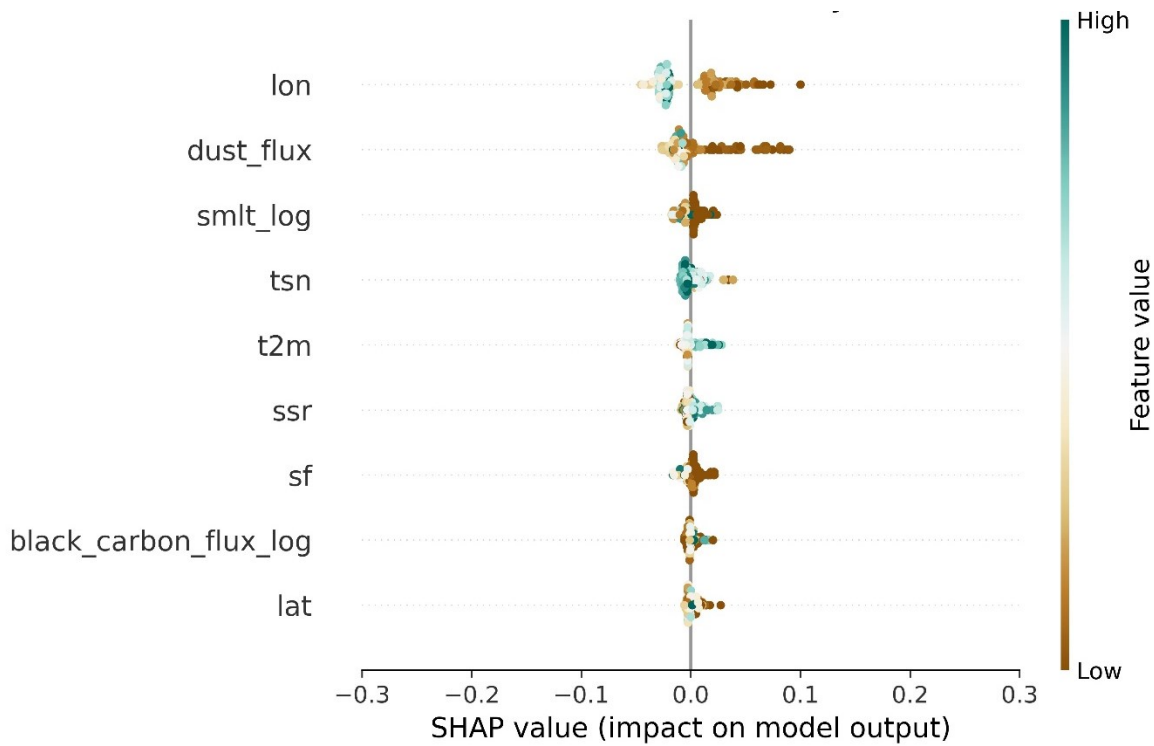**Figure G 14**: SHAP Values for the random forest on the annual model 2021

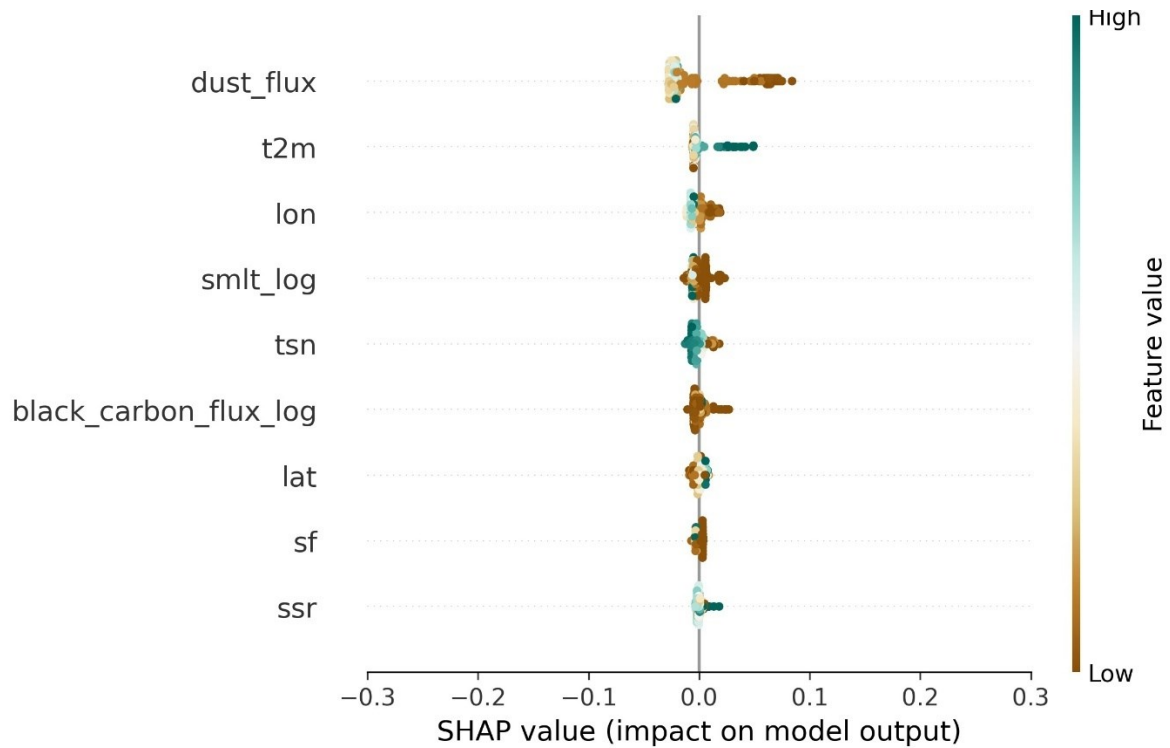**Figure G 15**: SHAP Values for the random forest on the annual model 2022

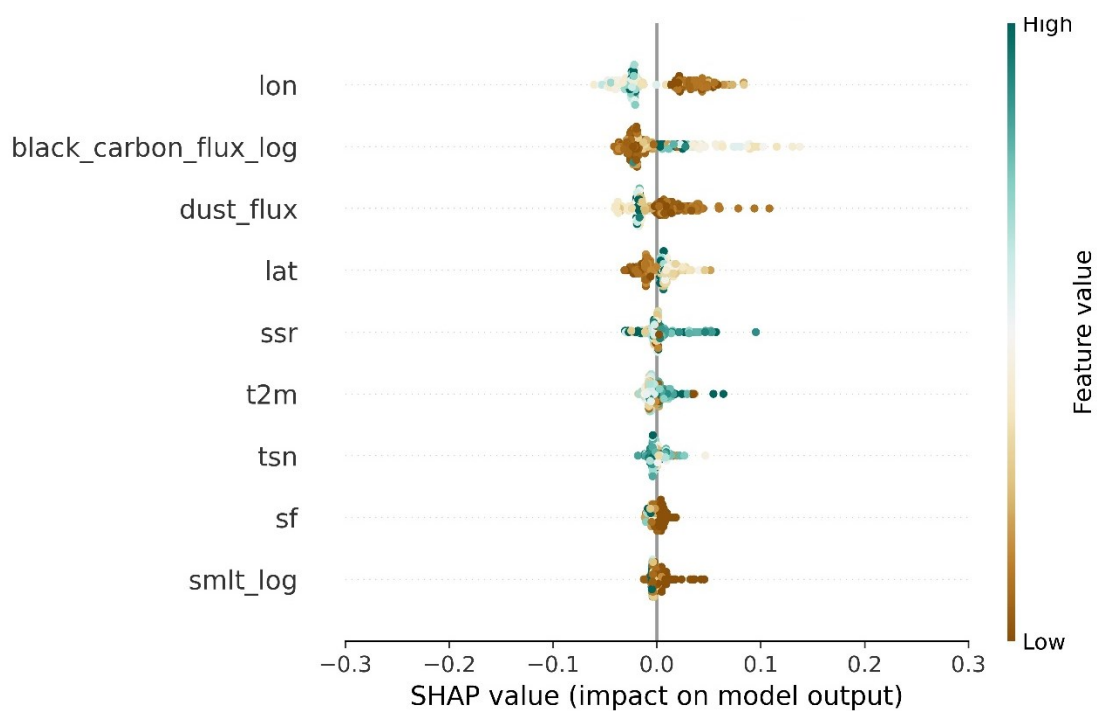**Figure G 16**: SHAP Values for the XGBOOST on the annual model 2022

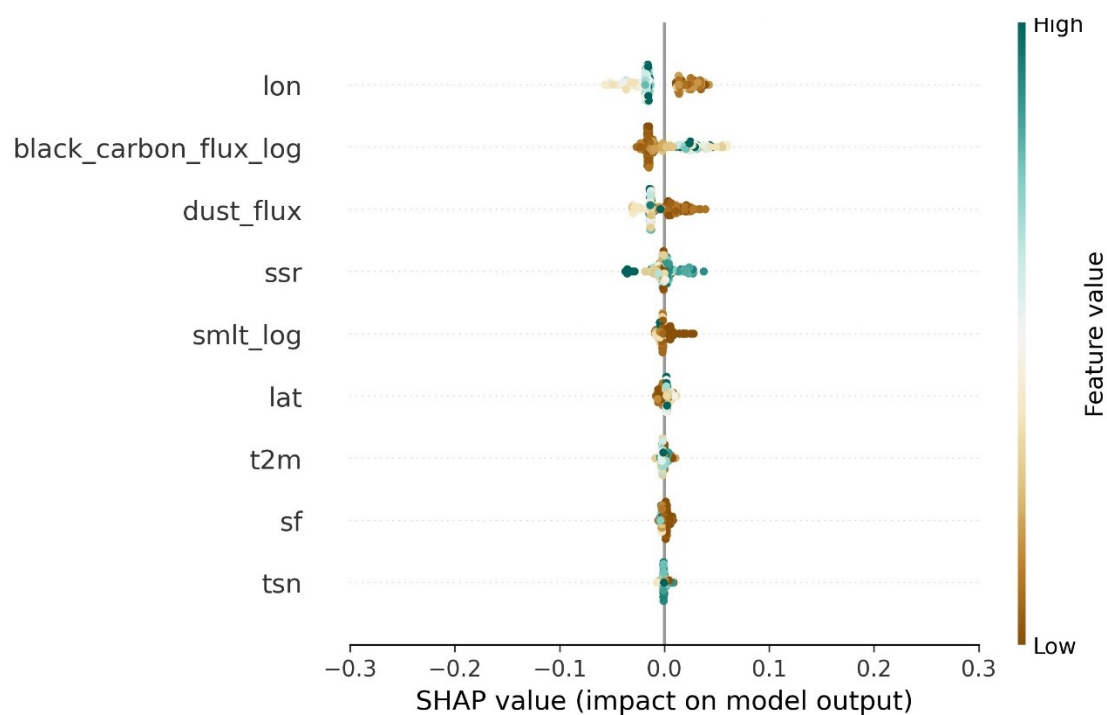**Figure G 17**: SHAP Values for the random forest on the annual model 2015

Figure G 18: SHAP Values for the random forest on the annual model 2015